REPORT DOCUMENTATION PAGE

Form Approved
OMB No. 0704-0188

1. AGENCY USE ONLY (Leave blank)	2. REPORT DATE	3. REPORT TYPE AND DATES COVERED
	Nov. 30, 1994	Annual Report, Oct.1,1993-Nov.30,1994

4. TITLE AND SUBTITLE

Strengthening of NiAl Matrix Composites

5. FUNDING NUMBERS

N00014-94-10118

6. AUTHOR(S)

R.J. Arsenault

7. PERFORMING ORGANIZATION NAME(S) AND ADDRESS(ES)

University of Maryland
College Park, MD 20742-2115

8. PERFORMING ORGANIZATION REPORT NUMBER

MML-1-1994

9. SPONSORING/MONITORING AGENCY NAME(S) AND ADDRESS(ES)

Office of Naval Research
800 North Quincy St.
Arlington, VA 22217

10. SPONSORING/MONITORING AGENCY REPORT NUMBER

11. SUPPLEMENTARY NOTES

12a. DISTRIBUTION/AVAILABILITY STATEMENT

Unlimited

12b. DISTRIBUTION CODE

13. ABSTRACT *(Maximum 200 words)*

The significant result is that the observed strengthening due to various types reinforcements (Al_2O_3 and TiB_2) with same size is almost identical. The smaller size reinforcement 5μm vs 150μm produces greater strengthening. Also, the strengthening due to Al_2O_3 whiskers, which have long ℓ/d (length to diameter) ratios of 10 to 100 is no greater than particulate Al_2O_3 and TiB_2 of approximately the same size, which is a further indication that a load transfer mechanism is not applicable for these composites.

A detailed examination of the data still suggests that the thermally-activated-rate controlling mechanism is the stress assisted motion of jogged screw dislocations. The specific details of the process are now be worked out to be able to obtain the proper stress and temperature dependence of the activation parameters. The strengthening observed in the composites at both high and low temperatures is due to an increase in the internal stress. This internal stress is independent of test temperature and stress.

14. SUBJECT TERMS	15. NUMBER OF PAGES
Discontinuous Intermetallic Matrix Composites, Al_2O_3/NiAl, TiB_2/NiAl, Internal Stress Strengthening	83
	16. PRICE CODE N/A

17. SECURITY CLASSIFICATION OF REPORT	18. SECURITY CLASSIFICATION OF THIS PAGE	19. SECURITY CLASSIFICATION OF ABSTRACT	20. LIMITATION OF ABSTRACT
Unclassified	Unclassified	Unclassified	N/A

STRENGTHENING OF NiAl MATRIX COMPOSITES

Prepared by

R.J. Arsenault

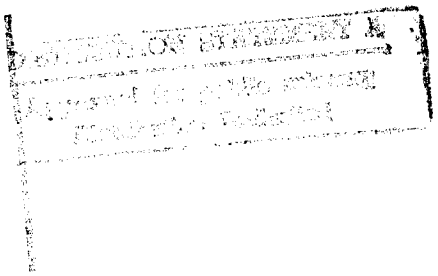

ANNUAL REPORT
N00014-94-10118

Prepared for

Office of Naval Research
800 North Quincy St.
Arlington, VA 22217

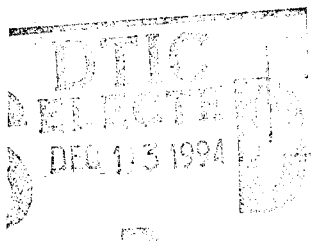

November 1994

Metallurgical Materials Laboratory
Dept. of Materials and Nuclear Engineering
University of Maryland, College Park, MD 20742-2115

Executive Summary

The significant result is that the observed strengthening due to various types reinforcements (Al_2O_3 and TiB_2) with same size is almost identical. The smaller size reinforcement 5μm vs 150μm produces greater strengthening. Also, the strengthening due to Al_2O_3 whiskers, which have long ℓ/d (length to diameter) ratios of 10 to 100 is no greater than particulate Al_2O_3 and TiB_2 of approximately the same size, which is a further indication that a load transfer mechanism is not applicable for these composites.

A detailed examination of the data still suggests that the thermally-activated-rate controlling mechanism is the stress assisted motion of jogged screw dislocations. The specific details of the process are now be worked out to be able to obtain the proper stress and temperature dependence of the activation parameters. The strengthening observed in the composites at both high and low temperatures is due to an increase in the internal stress. This internal stress is independent of test temperature and stress.

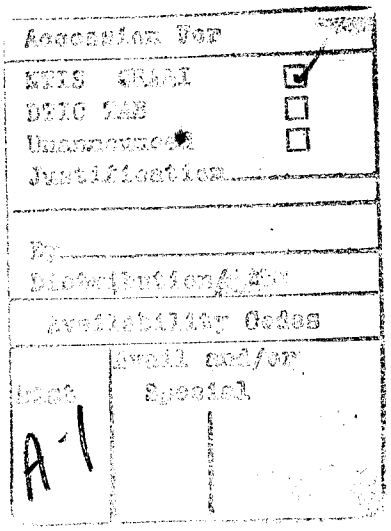

TABLE OF CONTENTS

I Introduction

In previous investigations of the strengthening of NiAl due to additions of particulate Al_2O_3, AlN and TiB_2, the results suggested that differences in strengthening occurred depending upon the particular type of reinforcement addition. In order to examine this possibility in detail, this required the production of composites with various types and size of reinforcements and matrix grain sizes. The composites were produced by powder metallurgy techniques and hot pressing at 1673 K at 25 MPa for 1 hour. Compression testing was conducted from 300 to 1400 K. Figure 1 is plot of yield strength vs temperature for several different combinations of particle size and grain size.

The significant result is that the observed strengthening due to various types reinforcements (Al_2O_3 and TiB_2) with same size is almost identical. The smaller size reinforcement 5μm vs 150μm produces greater strengthening. Also, the strengthening due to Al_2O_3 whiskers, which have long ℓ/d (length to diameter) ratios of 10 to 100 is no greater than particulate Al_2O_3 and TiB_2 of approximately the same size, which is a further indication that a load transfer mechanism is not applicable for these composites.

In Fig.1, it is a little difficult to recognize the change in the yield strength as a function of reinforcement at higher temperatures. Figure 2 is a plot of yield strength vs particle size and type at 1273 K and a strain rate of 10^{-4} sec^{-1}. As in the low temperature region the strengthening due to Al_2O_3 whiskers is no greater than that 5 μm Al_2O_3 particles.

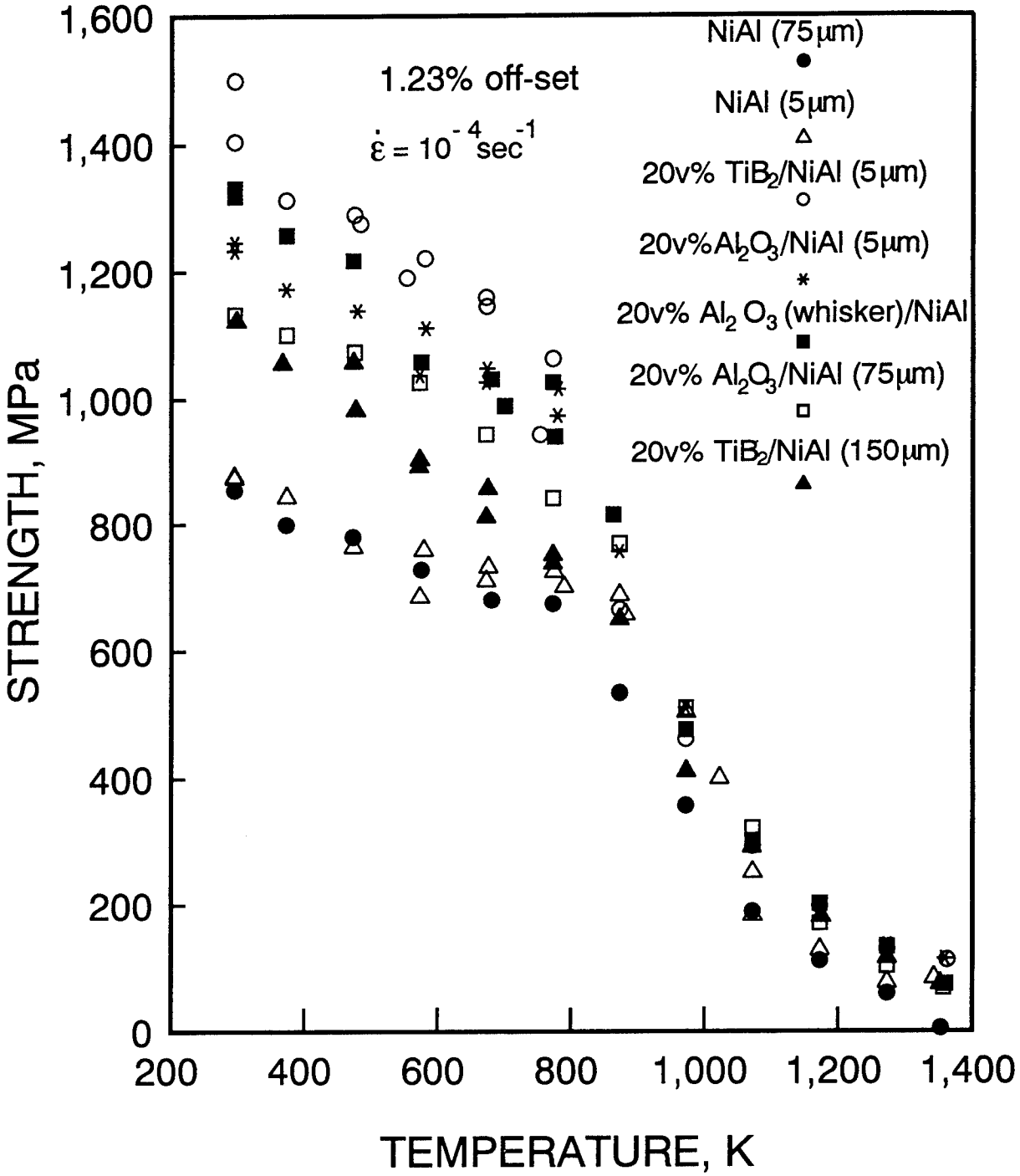

Fig.1 Yield strength at a 1.23% off-set as a function of temperature for various type and sizes of reinforcements.

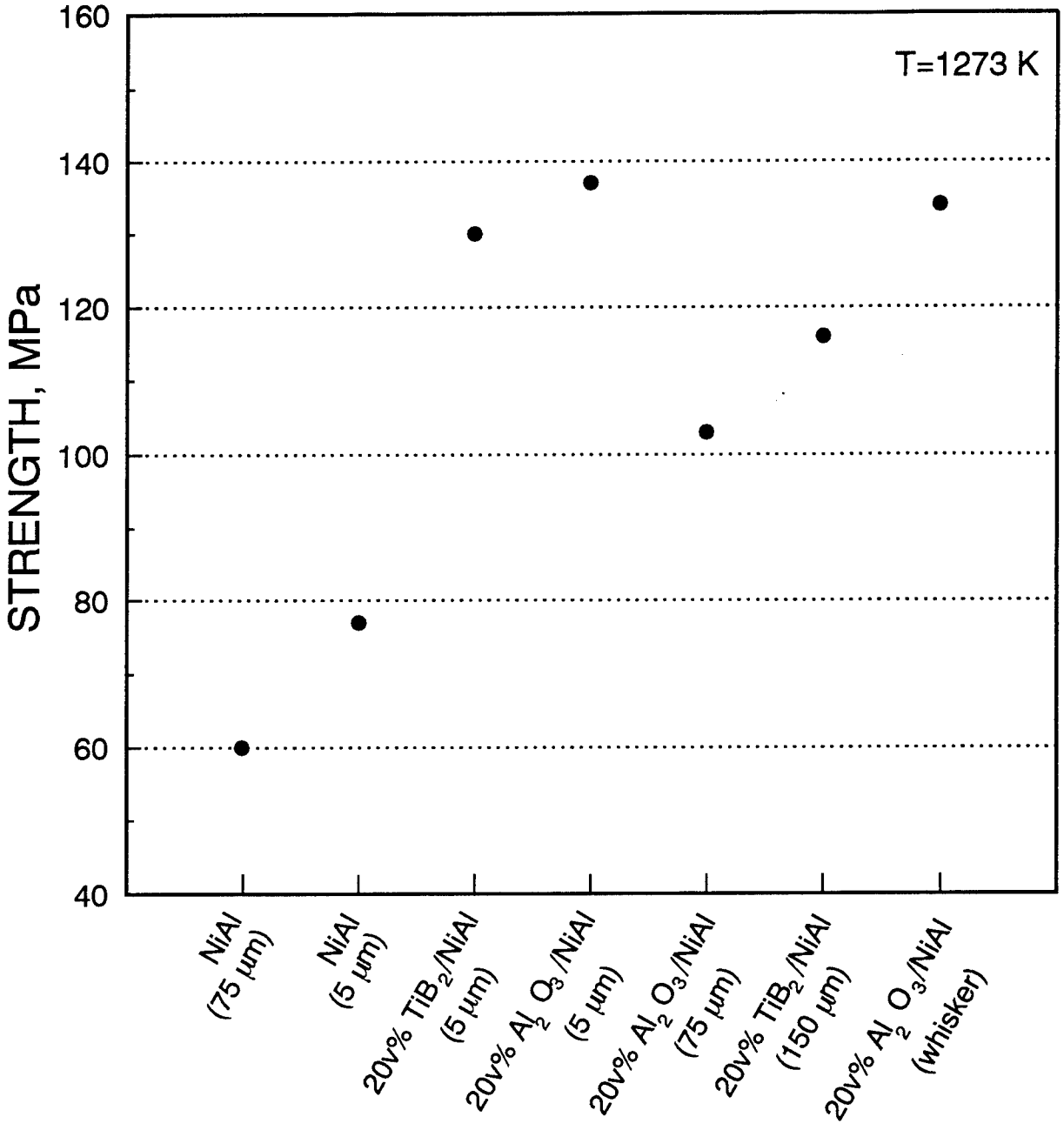

Fig.2 Yield strength as function of particle size and type of reinforcement.

The data convincingly disproves that the prior speculation that the reinforcement type had on effect the strengthening. The data also suggest that an increase in strengthening could occur due to a decrease in reinforcement particle size. There is an indication of this effect in data in the paper by L. Wang et al. [Mater. Sci. & Eng. A177 (1994) 83], in which cyro-milled NiAl produced small AlN particles within the NiAl matrix.

A detailed examination of the data still suggests that the thermally-activated-rate controlling mechanism is the stress assisted motion of jogged screw dislocations [L. Wang, K. Xu and R.J. Arsenault, Intermetallic Matrix Composites III, ed. by J.A. Graves, R.R. Bowman and J.J. Lewandowski, MRS, vol. 350, 1994, p.237]. The specific details of the process are now be worked out to be able to obtain the proper stress and temperature dependence of the activation parameters. The strengthening observed in the composites at both high and low temperatures is due to an increase in the internal stress. This internal stress is independent of test temperature and stress. The detail mechanism by which the reinforcement particles increase the internal stress is not clear at the present time.

Additional investigations have been underway related to interfaces in composites, both continuous filament and discontinuous composites. These investigations were undertaken to obtain an understanding of the strengthening mechanisms in these composites. Interface structures in a continuous Al_2O_3 filament reinforced NiAl composite were investigated by transmission electron microscopy. There appeared to be an intimate bond between the NiAl matrix and the Al_2O_3 filaments. Simulation of TEM diffraction contrast images based upon a three dimensional finite element analysis was employed to investigate the nature of the residual strains in regions along the interface. The

simulations suggested that radial residual strains within the Al_2O_3 filaments were randomly distributed along the interface. These strains were believed to be related to dislocation nucleation in the NiAl which results from the relaxation of the thermally generated residual stresses.

The following are: a list publications, a list of presentations and a selected few publications.

II. List of Publications
(papers published and submitted, book chapters and invited reviews)

1. A COMPARISON OF INTERFACIAL ARRANGEMENTS OF SiC/Al COMPOSITES
   R.J. Arsenault and J. Romero
   Submitted for publication

2. INTERFACES IN METAL AND INTERMETALLIC MATRIX COMPOSITES
   Composites, 25, 1994, 540

3. DISLOCATION IN CONTINUOUS FILAMENT REINFORCED W/NiAl AND AL_2O_3/NIAL COMPOSITES
   L. Wang, R.R. Bowman and R.J. Arsenault
   Submitted for publication

4. INTERFACES IN CONTINUOUS FILAMENT REINFORCED AL_2O_3/NiAl COMPOSITES
   L. Wang, K. Xu, R.R. Bowman and R.J. Arsenault
   Accepted for publication in Met. Trans.

5. STRENGTHENING OF DISCONTINUOUS REINFORCED NiAl COMPOSITES
   L. Wang, N. Beck and R.J. Arsenault
   Mat. Sci. & Eng., A177, 1994, 83

6. ANOMALOUS PENETRATION OF Al INTO SiC
   J.C. Romero and R.J. Arsenault
   Accepted for publication in Acta Met.

7. THE ATHERMAL STRENGTHENING OF DISCONTINUOUSLY REINFORCED NIAL COMPOSITES
   L. Wang, K. Xu and R.J. Arsenault
   Intermetallic Matrix Composites III, ed. by J.A. Graves, R.R. Bowman and J.J. Lewandowski, MRS, vol. 350, 1994, p.237

8. STRENGTHENING OF NIAL AT HIGH TEMPERATURES
   L. Wang and R.J. Arsenault
   Strength of Materials, Japan Institute of Metals, ed. by H.Oikawa, K. Maruyama, S. Takeuchi and M. Yamaguchi, 1994, p.745

9. INTERFACE IN INTERMETALLIC MATRIX COMPOSITES
   K. Xu, L. Wang and R.J. Arsenault
   High Performance Composites, Ed. by K.K. Chawla, P. Liaw and S. Fishman, TMS, 1994, p.155.

10. INTERFACE IN CONTINUOUS FILAMENT COMPOSITES
    Proceedings of 8th CIMTEC-World Ceramics Congress & Forum on New Materials, Florence, Italy, June, 1994, Ed. by P. Vincenzini

11. PLASTIC FLOW IN SIC/AL COMPOSITES - STRENGTHENING AND DUCTILITY
    N. Shi and R.J. Arsenault
    Annual Reviews of Materials Science, 1994, p.321.

III. List of Presentation

1. Institut für Werkstoffkurde und Werkstofftechnik, Technische Universität Clausthal, 1994, "Strengthening Mechanisms in Discontinuous Intermetallic Matrix Composites"

2. 12th U.S. National Congress of Applied Mechanics, 1994, "Differences in Plastic Relaxation due to Reinforcement Size and Shape", K. Xu, N. Shi and R.J. Arsenault

3. TMS/ASM Composite Materials - High Performance Composites, 1994, "Interfaces in Metal and Intermetallic Matrix Composites"

4. DeVivo Lecturer in Materials Science at the Barrett Institute of Chemical Analysis and Materials Science. Northeastern University, 1994, "Strengthening and Deformation of Discontinuous Metal Matrix Composites"

5. ASM Annual Meeting, 1994, "Interfaces in Continuous Filament Reinforced Al_2O_3/NiAl Composites", L. Wang, K. Xu, R.R. Bowman and R.J. Arsenault

6. ICSMA 10, Sendai, Japan, 1994, "Strengthening of NiAl at High Temperatures"

7. MRS Spring Meeting, 1994, "The Athermal Strengthening of Discontinuously Reinforced NiAl Composites"
   L. Wang and R.J. Arsenault

8. 16th Annual DMMC Meeting, 1994, "Interfaces in Continuous Filament Al_2O_3/NiAl Composites"

9. 16th Annual DMMC Meeting, 1994, "Strengthening of NiAl Composites"

IV. Publications (A selected few)

1. STRENGTHENING OF DISCONTINUOUS REINFORCED NiAl COMPOSITES
   L. Wang, N. Beck and R.J. Arsenault
   Mat. Sci. & Eng., A177, 1994, 83

2. THE ATHERMAL STRENGTHENING OF DISCONTINUOUS REINFORCED NiAl COMPOSITES
   L. Wang, K. Xu and R.J. Arsenault
   Intermetallic Matrix Composites III, ed. by J.A. Graves, R.R. Bowman and J.J. Lewandowski, MRS, vol. 350, 1994, p.237

3. STRENGTHENING OF NiAl AT HIGH TEMPERATURES
   L. Wang and R.J. Arsenault
   Strength of Materials, Japan Institute of Metals, ed. by H.Oikawa, K. Maruyama, S. Takeuchi and M. Yamaguchi, 1994, p.745

4. INTERFACES IN METAL AND INTERMETALLIC MATRIX COMPOSITES
   Composites, 25, 1994, 540

5. INTERFACE IN CONTINUOUS FILAMENT COMPOSITES
   Proceedings of 8th CIMTEC-World Ceramics Congress & Forum on New Materials, Florence, Italy, June, 1994, Ed. by P. Vincenzini

6. PLASTIC FLOW IN SiC/Al COMPOSITES - STRENGTHENING AND DUCTILITY
   N. Shi and R.J. Arsenault
   Annual Reviews of Materials Science, 1994, p.321

Strengthening of discontinuous reinforced NiAl composites

L. Wang, N. Beck and R. J. Arsenault

Metallurgical Materials Laboratory, Department of Materials and Nuclear Engineering, University of Maryland, College Park, MD 20742-2115 (USA)

(Received May 12, 1993; in revised form July 19, 1993)

Abstract

Considerable strengthening was observed in cryomilled NiAl, which is stronger than XD™ processed TiB_2/NiAl composites, in the temperature range 300–1273 K. The cryomilled NiAl contained AlN and Al_2O_3 particle aggregates, mainly along grain boundaries, before extrusion. After extrusion the aggregates were broken into submicrometer clusters. The volume fraction of clusters can be as high as 30 vol.%. The actual particle size of the AlN within the cluster is in the range of nanometers to tens of nanometers. The strengthening due to the reinforcements was observed as a result of an increase in the athermal component of the yield stress at low temperatures and this caused high temperature strengthening owing to microstructure stabilization by the reinforcements. The strengthening in the temperature range 300–1273 K is believed to be related to grain size refinement and effective pinning of grain boundaries.

1. Introduction

Recent experimental data indicate that there are at least two different phenomena contributing to the strengthening of NiAl through the addition of discontinuous reinforcements. First, the high-temperature strength of NiAl can be enhanced two- to three-fold by adding a small amount (2–4 wt.%) of small particles (approximately 50 nm in size) such as TiB_2, HfC, and HfB_2 [1, 2]. The strengthening behavior in these dispersion-hardened NiAl materials was found to be similar to that of oxide dispersion-strengthened (ODS) Ni-based alloys. The grain size was found to be unstable in compression in the temperature range 1200–1300 K. It has been observed in HfC reinforced NiAl, that the larger the grain size, the stronger the composites at high temperatures [2]. Surprising results were obtained during the mechanical alloying of NiAl with Y_2O_3 in liquid nitrogen environment, a process called cryomilling, a method used to disperse the Y_2O_3 in the NiAl [3, 4]. A considerable amount of AlN (approximately 10 vol.%), in addition to the small volume fraction of Y_2O_3, was found in these cryomilled composites. The strengthening rate for AlN reinforcement was found to be considerably higher than for other discontinuous reinforcements. Preliminary microstructure investigations revealed that the AlN particles were not uniformly dispersed, but were distributed non-homogeneously mainly along grain boundaries.

The second phenomenon is related to the strengthening of NiAl through the addition of discontinuous reinforcements with considerably larger volume fractions (20–30 vol.%) of relatively large (approximately 1 μm) particulates such as TiB_2 particulates. The high-temperature strength of NiAl has increased two- to three-fold and the modulus is enhanced [5–7]. The behavior of the mechanism for this second type of strenghthening is still unclear. Although strengthening through grain size refinement has been observed in monolithic NiAl at high temperatures, it is unlikely that very small grains (less than 5 μm) would be stable at temperatures above 1200 K and introduce significant strengthening [8]. The grain size or the subgrain size of these composites is extremely small (1–3 μm) [9–11], which would generally result in lack of elevated-temperature strength. One important difference, however, between dispersion-hardened NiAl and the NiAl reinforced with micrometer-size particulates is that the grain size of the latter, though small, is stable at elevated temperatures (1200–1300 K) [9–11].

Questions concerning the high-temperature strengthening of NiAl arise from the previous investigations. What is the strengthening mechanism or mechanisms when the reinforcements are not dispersoids? How important is the matrix grain size in the strengthening

0921-5093/94/$7.00
SSDI 0921-5093(93)09403-6

of NiAl? This paper is a report of some results of recent investigations of various kinds of discontinuous reinforced NiAl composites intending to cast some insight on the strengthening mechanisms of these composites.

2. Materials and experimental methods

Five kinds of composite were used in the current investigations: monolithic NiAl; XD™ processed 0, 10 and 27 vol.% TiB_2/NiAl; cryomilled NiAl composites. The XD™ processed nickel aluminide reinforced with 0, 10, and 27 vol.% TiB_2 was obtained from Martin Marietta Laboratories. Details of this process can be found elsewhere [5, 6]. Subsequent processing included canning in steel plus extrusion at about 1473 K at an extrusion ratio of 8:1. The measured volume fractions of the TiB_2 particulates are approximately 0, 10, and 27 vol.% corresponding to the nominal volume fractions respectively. All other composites were prepared by a four-step, powder processing route involving milling, cold isostatic pressing (CIP), hot isostatic pressing (HIP), and extrusion. Two types of milling were coupled: milling in a rotating ball mill and cryomilling. Cryomilling is a high intensity ball-milling process performed in liquid nitrogen. All materials in this study were cryomilled at Exxon Research and Engineering Laboratory under the direction of M. J. Luton. Nickel aluminide powders (50 at.% Ni, 50 at.% Al), $-150+325$ mesh, were purchased from CERAC Inc., Milwaukee, WI. The unreinforced NiAl material was produced by ball milling for 22 h, CIP, HIP and extruded at 1373 K at an extrusion ratio of 36:1. The cryomilled NiAl composite was produced by cryomilling followed by CIP, HIP (4 h), and extruded at 1473 K at an extrusion ratio of 9:1. CIP conditions in all cases were 770 MPa for 15 min. HIP conditions were 210 MPa at 1473 K for 2 h.

The composites were ground into cylindrical samples with a height-to-diameter (h/d) ratio of 2 and diameter of approximately 4.7–5 mm for compression tests. The cylindrical axis of the sample was parallel to the extrusion direction. The compression tests were conducted on an Instron universal testing machine equipped with high-temperature vacuum chamber. All the tests were conducted at a constant cross-head speed, and in a vacuum of approximately 10^{-4} Torr. The compressive yield stress and flow stress were measured as a function of temperature from 300 K to 1273 K, with a strain rate of 10^{-4} s^{-1}. The yield stress was taken as the stress at 0.002 true plastic strain. Activation volumes V^* were measured as a function of shear stress τ, in the temperature range approximately 300–1273 K, using the method of changing cross-head speed, which follows

$$V^* = kT\left(\frac{\partial \ln \dot{\gamma}}{\partial \tau}\right)$$

where $\dot{\gamma}$ is the shear strain rate and k, T are Boltzman's constant and temperature respectively. One half of the true compressive flow stress σ was taken as the shear stress τ in the calculation of the activation volume.

Samples for transmission electron microscopy (TEM) investigations were cut into 3 mm discs with a thickness of approximately 0.5 mm by electrical discharge machining. Deformed samples for the investigation of dislocation structures were cut both perpendicular to and about 45° away from the loading axis. Discs were thinned by lightly grinding both sides with #400 SiC grinding paper to remove the debris, and then dimple grinding both sides of the sample until the thickness at the center reached 0.07–0.1 mm. Dimple grinding was performed using 10–30 μm diamond paste mixed with polishing oil under a load of less than 30 g. After completion of the above procedure, most of the samples were electrolytically polished with a standard twin-jet electropolishing device using 5% perchloric acid–ethanol solution at 253 K or below until a small hole appeared at the center of the disc. The applied voltage was 50–70 V. Foils, which contain no AlN, in the as-electrolytic-polished condition are suitable for conventional TEM. Cryomilled NiAl foils which contain AlN, and foils for high resolution electron microscopy (HREM) and X-ray energy dispersive spectroscopy (EDS) were prepared in the same way as for conventional TEM except they were also ion milled for 10 min to 1 h as a final procedure to clean the surface. It was found that mechanical polishing of the cryomilled NiAl with water is not appropriate because the AlN can be dissolved in water. Investigations were carried out, using both optical and scanning electron microscopy (SEM) plus digital image analyses (Voyager system by Noran), to determine the average particle sizes and volume fractions. TEM, HREM and EDS analyses were performed using a JEM-2000FX-II analytical electron microscope (AEM).

3. Results and discussion

All five composites exhibit steady state flow or slight strain softening after yielding at a temperature above about 900 K. They can be compressively deformed up to approximately 0.1 plastic strain without fracture at room temperature, and display considerable strain hardening at deformation temperatures of 800 K or below, as shown in Fig. 1. As expected, the yield stress

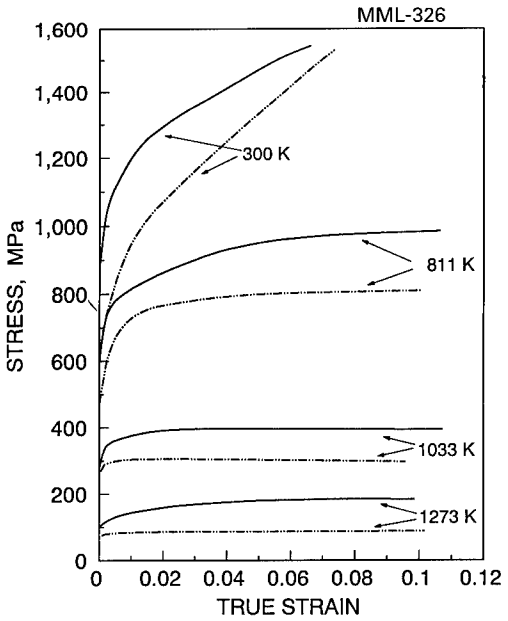

Fig. 1. Stress-strain curves of the Al/NiAl (——) and the 27vol.%TiB_2/NiAl (· − · − ·) composites deformed at different temperatures.

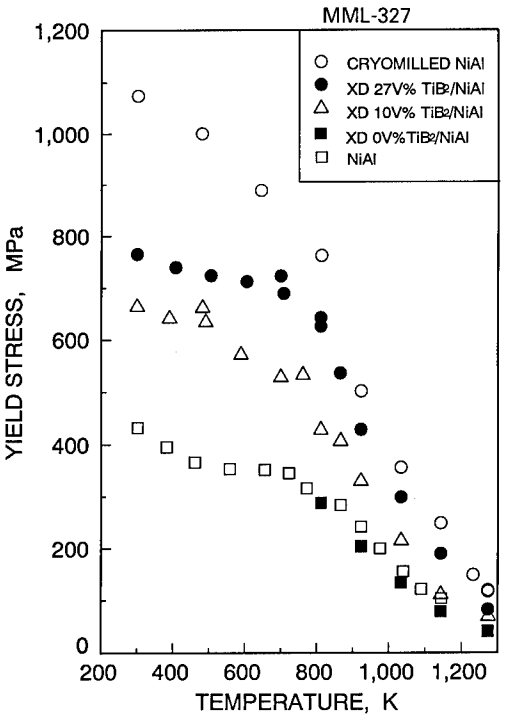

Fig. 2. Temperature dependence of yield stresses of monolithic NiAl and the NiAl matrix composites.

of the monolithic NiAl exhibits typical temperature dependent behavior as common metals and alloys do, as shown in Fig. 2. In both the low temperature (below 500 K) and the high temperature (above 700 K) ranges, this behavior can be described as the yield stress decreasing as the temperature increases, indi-

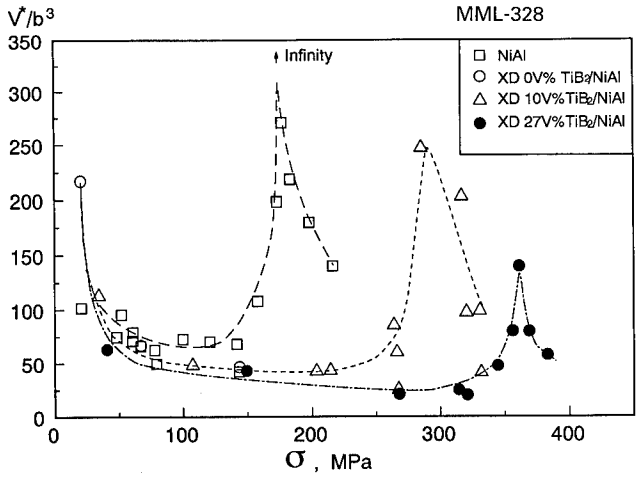

Fig. 3. Activation volumes of monolithic NiAl and 0, 10, and 27vol.% TiB_2/NiAl composites as function of yield shear stress in the temperature range 300–1273 K.

cating that the deformation of these composites is thermally activated in these temperature ranges; there is an intermediate temperature range (500–700 K) in which the yield stress is relatively independent of temperature, *i.e.* an athermal state of deformation is clearly defined in this temperature range. The temperature dependent behavior of all other composites more or less duplicated this behavior of the monolithic NiAl with an obvious but less profound athermal stage. The athermal stress level of the cryomilled NiAl composite is about three times as high as that of the monolithic NiAl, and apparently higher than that of the XD™ processed 27vol.%TiB_2/NiAl composite. It is evident that the overall strengthening of all the composites, over the whole testing temperature range, was initiated by the increase in athermal stress, *i.e.* the athermal component of the strength of these composites. The activation volume measurements also supported the above observations. As shown in Fig. 3, the activation volume displays a peak value at the corresponding athermal stress level for all the monolithic and XD™ processed TiB_2/NiAl composites which indicates the existence of the athermal stress.

The cryomilled NiAl composite contained AlN particles and a relatively small amount of Al_2O_3 particles, which formed an aggregate distributed mainly along the grain boundaries before extrusion. After the extrusion the aggregates are broken into submicrometer clusters, as shown in Fig. 4 which is a SEM image of the cryomilled NiAl composite. The volume fraction of the AlN–Al_2O_3 clusters in the composite is approximately 30 vol.%, measured by the quantitative image analysis system (the Voyager system of Noran). The Ni:Al ratio after *in situ* AlN formation in the cryomilled composites is approximately 53:47. The most

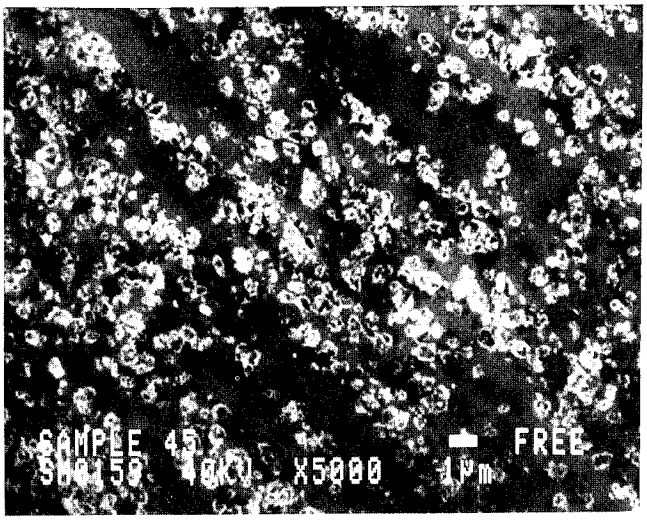

Fig. 4. SEM image of the cryomilled NiAl, extruded condition; the bright particles are clusters of AlN–Al_2O_3.

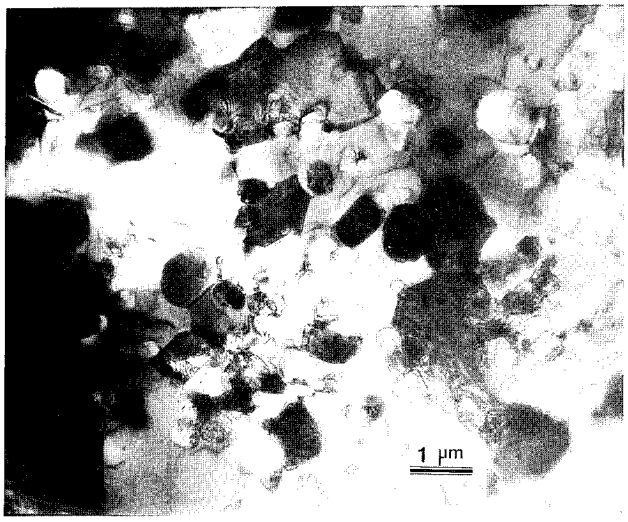

Fig. 6. TEM image of 27vol.%TiB_2/NiAl, extruded condition.

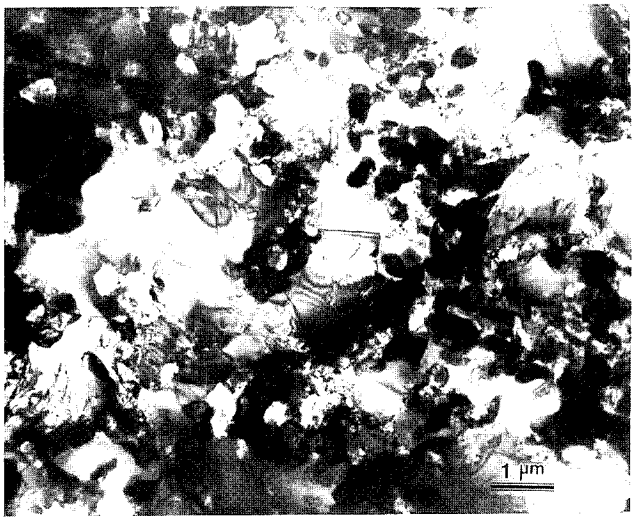

Fig. 5. TEM image of cryomilled NiAl, extruded condition.

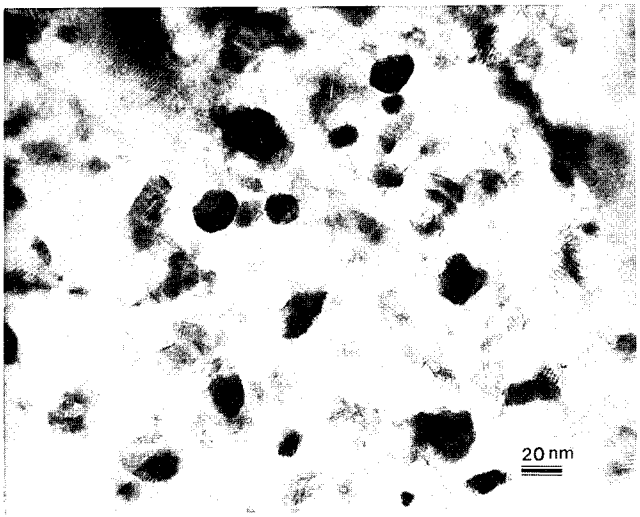

Fig. 7. TEM image of clusters of AlN–Al_2O_3 in the cryomilled NiAl; the actual particle size is in range of nanometers to tens of nanometers.

remarkable change in the microstructure of the matrix, NiAl, resulting from the *in situ* formation of AlN and the addition of TiB_2 is that the grain size has been greatly reduced as shown in Figs. 5 and 6. Compared with the grain size of approximately 20 μm of the monolithic NiAl, the grain size of the cryomilled NiAl and 27vol.%TiB_2/NiAl composites has been reduced to about 1–3 μm. The particle size and grain or subgrain size of both cryomilled NiAl and the 27vol.%TiB_2/NiAl composites are extremely stable during deformation up to a temperature of 1273 K. In most of cases, grain boundaries and subgrain boundaries are not distinctive in the TEM images. TEM investigations revealed that the actual particle size of AlN within the clusters or aggregates is in the range of nanometers to tens of nanometers (Fig. 7). It is important to note that the volume fractions of reinforcements and the grain size of cryomilled NiAl are similar to that of the XD™ processed 27 vol.% TiB_2 reinforced NiAl in the extruded condition. Compared with the TiB_2 particulates, the AlN clusters have a relatively smooth shape, *i.e.* less sharp edges (Figs. 5 and 6). Therefore, the AlN clusters would introduce less stress concentrations during the deformation than TiB_2 particulates.

Dislocation densities in the matrix in extruded composites of cryomilled NiAl and 27vol.%TiB_2/NiAl are extremely low. Deformation at 1273 K only activated one or two ⟨100⟩ slip systems in most of the matrix grains, and the dislocation densities are low for both

composites. At lower deformation temperatures, approximately 1000 K, extensive dislocation reactions and dislocation network formation were observed in both the deformed cryomilled NiAl and 27vol.%TiB_2/NiAl. When the deformation was conducted at about 800 K or below, dislocation densities in the deformed sample were found to be extremely high, and there was no apparent dynamic recovery, in agreement with the considerable amount of work hardening at the lower temperatures.

Based on the above observations, it is proposed that the strengthening resulting from the addition of reinforcements is due to an increase in the athermal component of the yield stress, *i.e.* the reinforcements produce an increase in strength at low temperatures. This increase in strength is simply translated into an increase in strength at higher temperatures owing to stabilization of the microstructures of the composites, which ensures that the mechanism for the increase in athermal strengthening is stable with respect to testing temperature and time of testing, and the mechanism of thermally activated deformation remains the same. One of the most important reasons for the increase in athermal stress is the substantial reduction in the grain or subgrain size. The strengthening through grain size refinement becomes true only under the condition that grain boundary sliding is effectively stopped. At high temperatures, this condition can be fulfilled with the addition of a considerable amount of thermally stable reinforcements such as AlN and TiB_2.

Meanwhile, there remains the experimental observation that the magnitude of the strengthening depends on the type of reinforcement. It has been proposed [12] that the reinforcements themselves actually function as dislocation sources, *i.e.* introducng a softening effect. Therefore, choosing the reinforcements that wll cause less stress concentrations and generate less dislocations during the deformation will optimize the strengthening. For example, smooth shaped particles which have a modulus comparable with that of the matrix materials will be the most effective reinforcements. This might explain why the AlN clusters are a better reinforcement than TiB_2. As a matter of fact, dislocation generations from the TiB_2–NiAl interface were often observed [6–8] in the XD™ processed TiB_2/NiAl composites during the high-temperature deformation. Such an event has never been observed at the AlN–NiAl interface in the cryomilled NiAl composites.

4. Conclusions

From a consideration of the experimental data, the following conclusions were drawn.

(1) The yield strength of all the NiAl matrix composites exhibits typical temperature dependent behavior in the temperature range 300–1273 K, and they can be plastically deformed, in compression, at room temperature. The cryomilled NiAl composite which contains approximately 30 vol.% AlN–Al_2O_3 clusters is stronger than the XD™ processed 27vol.%TiB_2/NiAl composites.

(2) The *in situ* formation of AlN clusters and the addition of TiB_2 greatly reduced the matrix grain size. TEM investigations revealed that the actual particle size of AlN within the clusters or aggregates is in the range of nanometers to tens of nanometers.

(3) Reinforcement causes an increase in the athermal component of the yield stress at low temperatures and this results in high temperature strengthening due to microstructure stabilization. The strengthening obtained in the NiAl matrix composites is believed to be related to the grain size refinement, and the effective resistance of the grain boundaries to sliding due to the pinnng by reinforcements. The most effective reinforcement should be one that reduces stress concentrations in the matrix.

Acknowledgment

The authors wish to acknowledge the continued support of Dr. S. Fishman of the Office of Naval Research. The authors are grateful to M. J. Luton of Exxon Research and Engineering, and to K. Killian and R. K. Everett of the Naval Research Laboratory for assistance in processing of the composites. This work was supported by the Office of Naval Research under grant No. N00014-91-J-1353.

References

1 J. D. Whittenberger, R. Ray, S. C. Jha and S. Draper, *Mater. Sci. Eng., A138* (1991) 83.
2 J. D. Whittenberger, R. Ray, S. C. Jha and S. Draper, *Mater. Sci. Eng., A151* (1992) 137.
3 J. D. Whittenberger, E. Arzt and M. J. Luton, *J. Mater. Res., 5* (1990) 271.
4 J. D. Whittenberger, E. Arzt and M. J. Luton, *J. Mater. Res., 5* (1990) 2819.
5 R. K. Viswanadham, S. K. Mannan and B. Sprissler, *Annu. Rep. Martin Marietta Lab., MML TR 87-66C*, 1987.
6 K. Sharvan Kumar and S. K. Mannan, *Prog. Rep. Martin Marietta Lab., MML TR 87-66C*, 1988.
7 J. D. Whittenberger, R. K. Viswanadham, S. K. Mannan and K. S. Kumar, *J. Mater. Sci., 25* (1990) 35.
8 J. D. Whittenberger, *J. Mater. Sci., 23* (1988) 235.
9 L. Wang and R. J. Arsenault, *Mater. Sci. Eng., A127* (1990) 91.

10 L. Wang and R. J. Arsenault, in D. L. Anton, P. L. Martin, D. B. Miracle and P. McMeeking (eds.), *Intermetallic Matrix Composites, MRS Proc.*, Vol. 194, Materials Research Society, Pittsburgh, PA, 1990, p. 199.
11 L. Wang and R. J. Arsenault, in L. A. Johnson, D. P. Dope and J. O. Stiegler (eds.), *High-Temperature Ordered Intermetallic Alloys IV, MRS Proc.*, Vol. 213, Materials Research Society, Pittsburgh, PA, 1991, p. 1063.
12 J. Friedel, *Dislocations*, Addison-Wesley, Reading, MA, 1964.

THE ATHERMAL STRENGTHENING OF DISCONTINUOUS REINFORCED NiAl COMPOSITES*

L. WANG, K. XU AND R.J. ARSENAULT
Metallurgical Materials Laboratory, Dept. of Materials & Nuclear Engineering,
University of Maryland, College Park, MD 20742-2115

ABSTRACT

An increase in the athermal component of the yield stress at low temperatures is the caused of the high temperature strengthening of discontinuously reinforced NiAl matrix composites. The reinforcements stabilize the microstructure. The strengthening in the temperature range of 300-1273K, is believed to be related to the grain size refinement and effective pinning of grain boundaries. This conclusion was obtained from analysis of data from AlN, TiB_2 and Al_2O_3/NiAl particulate composites.

INTRODUCTION

Recent experimental data indicates that there are at least two different phenomena contributing to the strengthening of NiAl through the addition of discontinuous reinforcements. First, the high-temperature strength of NiAl can be enhanced 2-3 fold by adding a small amount (2-4 wt%) of small particles (~50 nm in size), such as TiB_2, HfC, and HfB_2 [1,2]. The strengthening behavior in these dispersion hardened NiAl materials was found similar to that of the oxide dispersion strengthened (ODS) Ni-based alloys. The grain size was found unstable in compression in the temperature range of 1200-1300 K. It has been observed, in HfC reinforced NiAl, that the larger the grain size, the stronger the composites at high-temperatures [2]. Surprising results were obtained, during the mechanical alloying of NiAl with Y_2O_3 in the liquid nitrogen environment, a process called cryomilling, in order to disperse the Y_2O_3 into the NiAl [3,4]. A considerable amount of AlN (~10 vol%), in addition to the small volume fraction of Y_2O_3, was found in these cryomilled composites. The strengthening rate for AlN reinforcement was found to be considerably higher than other discontinuous reinforcements. Preliminary microstructure investigations revealed that the AlN particles were not uniformly dispersed, but non-homogeneously distributed mainly along grain boundaries.

The second phenomenon is related to the strengthening of NiAl through the addition of discontinuous reinforcements with considerably larger volume fractions (20-30 vol%) of relatively large (~1 μm) particulates, such as TiB_2 particulates. The high-temperature strength of NiAl has increased 2-3 fold and the modulus is enhanced [5-7]. The behavior or the mechanism for this second type of strengthening is still unclear. Although strengthening through the grain size refinement has been observed in monolithic NiAl at high temperatures, it is unlikely that very small grains (< 5μm) would be stable at temperatures above 1200K and introduce significant strengthening [8]. The grain size or the subgrain size of these composites are extremely small (1-3 μm) [9-11], which would generally result in lack of elevated-temperature strength. One important difference, however, between dispersion hardened

* This research was supported by the Office of Naval Research under grant No. N00014-94-10118.

NiAl and the NiAl reinforced with micron-size particulates is that the grain size of the latter, though small, is stable at elevated temperatures (1200-1300 K) [9-11].

Questions concerning the high-temperature strengthening of the NiAl arise from the previous investigations. What is the strengthening mechanism or mechanisms when the reinforcements are not dispersoids? And how important is the matrix grain size in the strengthening of NiAl? This paper is a report of some results of recent investigations of various kinds of discontinuous reinforced NiAl composites intending to cast some insight of the strengthening mechanisms of these composites.

MATERIALS AND EXPERIMENTAL METHODS

Five kinds of composites were used in the current investigations. They are: monolithic NiAl, XD^{TM} processed 0, 10, 27 V% TiB_2/NiAl, and cryomilled NiAl composites. The XD^{TM} processed nickel aluminide reinforced with 0,10, and 27 Vol% TiB_2 was obtained from Martin Marietta Laboratories. The details of this process can be found elsewhere [5,6]. Subsequent processing included canning in steel plus extrusion at ~1473 K at an extrusion ratio of 8:1. The measured volume fraction of the TiB_2 particulates is ~0, 10, and 27 Vol% corresponding to the nominal volume fractions respectively. All other composites were prepared by a four-step, powder processing route involving milling, cold isostatic pressing (CIP), hot isostatic pressing (HIP), and extrusion. Two types of milling were coupled; milling in a rotating ball mill and cryomilling. Cryomilling is a high intensity ball-milling process performed in liquid nitrogen. All materials in this study were cryomilled at Exxon Research and Engineering Laboratory under the direction of M.J. Luton. Nickel aluminide powders (50 at%Ni:50 at%Al), -150 +325 mesh, were purchased from CERAC, Inc. of Milwaulkee, WI. The unreinforced NiAl material was produced by ball milling 22 hours, CIP, HIP and extrusion at 1373 K and an extrusion ratio of 36:1. The cryomilled NiAl composite was produced by cryomilling followed by CIP, HIP (4 hours), and extrusion at 1473 K and an extrusion ratio of 9:1. CIP conditions in all cases were 770 MPa for 15 minutes. HIP conditions were: 1473 K, 210 MPa, 2 hours.

The composites were ground into cylindrical samples with height-to-diameter (h/d) ratio of 2 and diameter of 4.7~5 mm for compression tests. The cylindrical axis of the sample is parallel to the extrusion direction. The compression tests were conducted on an Instron universal testing machine equipped with high-temperature vacuum chamber. All the tests were conducted at a constant cross-head speed, and in a vacuum of ~10^{-4} torr. The compressive yield stress and flow stress were measured as a function of temperature from 300 K to 1273 K, and with a strain rate of 10^{-4} sec^{-1}. The yield stress was taken as the stress at 0.002 true plastic strain. Activation volumes, V*, were measured as a function of shear stress, τ, in the temperature range of 300 ~ 1273 K, by using the method of changing the strain rate, which follows

$$V^* = kT\left(\frac{\partial \ln \dot{\gamma}}{\partial \tau}\right)$$

where $\dot{\gamma}$ is the shear strain rate and kT are Boltzman's constant and temperature, respectively. One half of the true compressive flow stress (σ) was taken as the shear stress (τ) in the calculation of the activation volume.

RESULTS AND DISCUSSION

All the five composites exhibit steady state flow or slight strain softening after yielding at temperature above ~900 K, and can be compressively deformed up to ~0.1 plastic strain without fracture at room temperature, and displays a considerable strain hardening at the deformation temperatures of 800 K or below, as shown in Fig. 1. As expected, the yield stress of the monolithic NiAl exhibits a typical temperature dependent behavior as common metals and alloys do, as shown in Fig. 2. This behavior can be described as, in both the low temperature (< 500 K) and the high temperature range (>700 K), the yield stress decreases as the temperature increases, indicating that the deformation of these composites is thermally activated in these temperature ranges; and there exists an intermediate temperature range (500-700 K) in which the yield stress is relatively independent of temperature, i. e. an athermal state of the deformation is clearly defined in this temperature range. The temperature dependent behavior of all other composites more or less duplicated this behavior of the monolithic NiAl with an obvious but less profound athermal stage. The athermal stress level of the cryomilled NiAl composite is about three times as high as that of the monolithic NiAl, and apparently higher than that of the XD^{TM} processed 27 Vol% TiB_2/NiAl composite. It is evident that the overall strengthening of all the composites, in the whole testing temperature range, were initiated by the increase of the athermal stress, i.e., athermal component of the strength of these composites. The activation volume measurements also supported the above observations. As shown in Fig.3, the activation volume displays a peak value at the corresponding athermal stress level for all the monolithic and XD^{TM} processed TiB_2/NiAl composites which indicates the existence of the athermal stress.

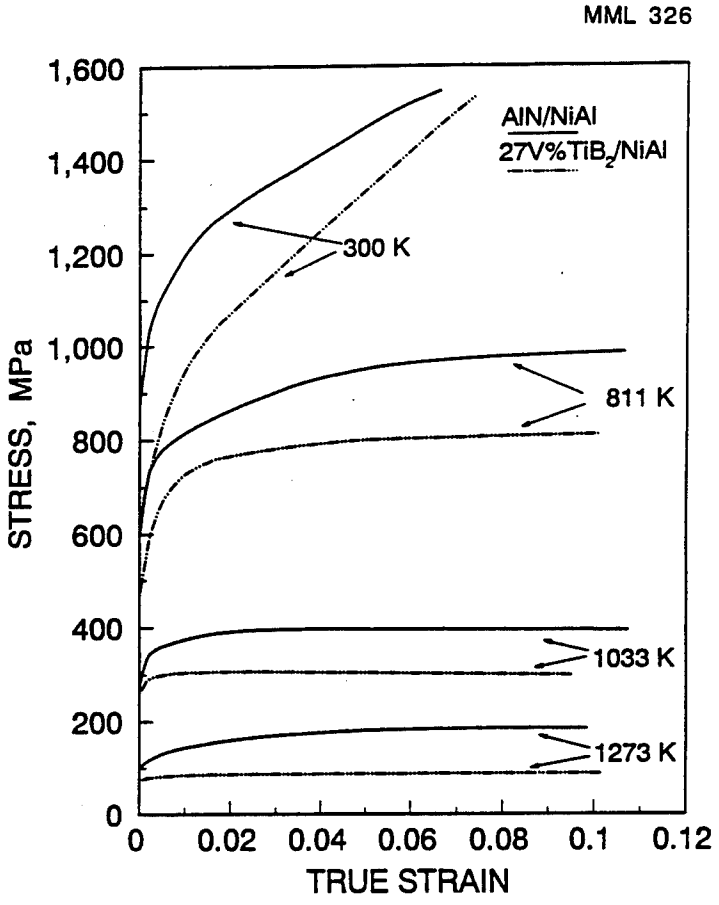

Fig.1
Stress-strain curves of the Al/NiAl and the 27 V% TiB_2/ NiAl composites deformed at different temperatures.

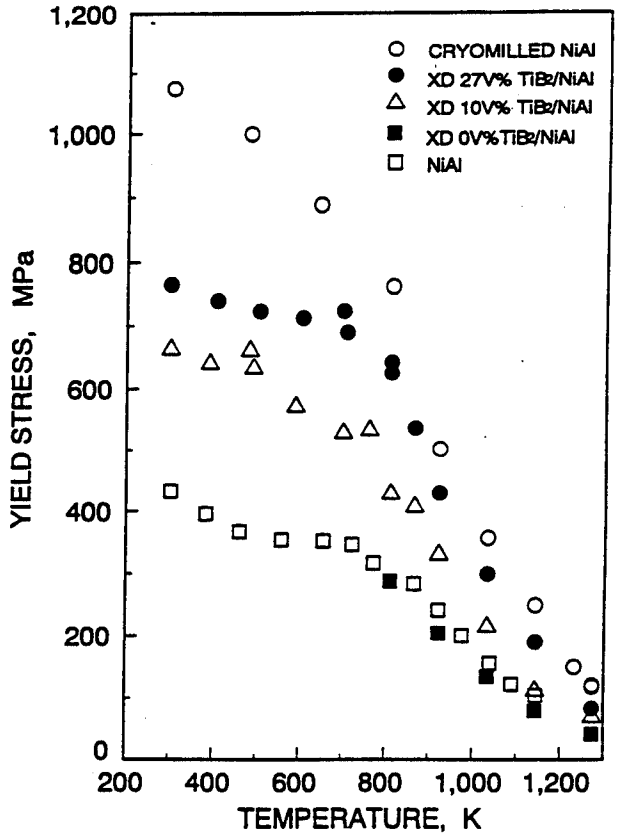

Fig.2
Temperature dependent of yield stresses of monolithic NiAl and the NiAl matrix composites.

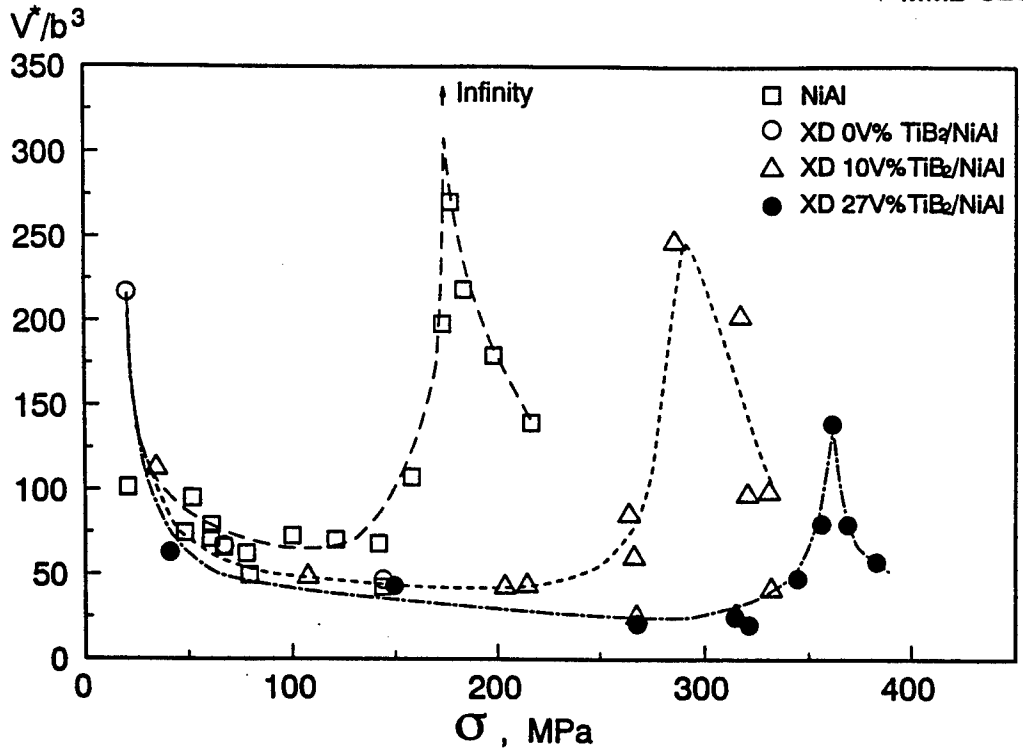

Fig.3 Activation volumes of monolithic NiAl and 0, 10, and 27 V% TiB_2/NiAl composites as function of yield shear stress in the temperature range of 300 - 1273 K.

Based on the above observations and the previous TEM observations of primarily screw dislocation [12], it is proposed that the strengthening, resulting from the reinforcements addition, is due to an increase in the athermal component of the yield stress, i.e., the reinforcements produce an increase in strength at low temperatures. This increase in strength is simply translated into an increase in strength at higher temperatures due to the stabilization of the microstructures of the composites which ensures that the mechanism for the increase in the athermal strengthening is stable with respect to testing temperature and time of testing, and the mechanism of thermally activated deformation remains the same. One of the most important reason for the increase of the athermal stress is due to the substantial reduction of the grain or subgrain size. The strengthening through the grain size refinement becomes true only under the condition that the grain boundary sliding must have been effectively stopped. At high temperatures, this condition can be fulfilled with the addition of a considerable amount of thermally stable reinforcements, such as AlN and TiB_2.

If we make the assumption that the reinforcement only produces an increase in the athermal component of the yield stress and the thermal activated process is the motion of jogged screw dislocations, then the following equation can be derived for the time necessary to make a thermally "jump"

$$t_i = K\left(\frac{\sigma_i^2 - \sigma^{*2}}{2\sigma_i\sigma^*}\right)e^{\frac{Q_a}{RT}}$$

where K is a constant, σ_i is the athermal stress, σ^* is the instantaneous effective stress, the apparent activation energy is as follows:

$$Q_a = Q_{SD} - \frac{\partial n}{\partial\left(-\frac{1}{RT}\right)}\ln\frac{\sigma_a}{\sigma_i}$$

where Q_{SD} is activation energy of self diffusion of NiAl, n is the stress exponent which is a function of temperature, σ_a is the applied stress and RT are the gas constant and temperature respectively. If it assumed that athermal stress varies with a periodicity corresponding to the subgrain or grain size, then a computer simulation investigation of the total time required to traverse the grain can be obtained and then the average dislocation velocity. Finally it is possible to obtain a plot of stress vs temperature which can be compared to the experimental data. The comparison was found to be quite good.

CONCLUSIONS

From a consideration of the experimental data, the following conclusions were drawn:

1. Reinforcements causes an increase in the athermal component of the yield stress at low temperatures and this results in the high temperature strengthening due to microstructure stabilization by the reinforcement. The strengthening obtained in the NiAl matrix composites is believed to be related to the grain size refinement, and the effective resistance of the grain boundaries to sliding due to the pinning by reinforcements. The most effective reinforcement should be the one that reduces stress concentrations in the matrix.

2. The yield strength of all the NiAl matrix composites exhibit typical temperature dependent behavior in a temperature range of 300-1273 K, and can be plastically deformed, compressively, at room temperature.

ACKNOWLEDGEMENT

The authors wish to acknowledge the continued support of Dr. S. Fishman of the Office of Naval Research. The authors are grateful to M.J. Luton of Exxon Research & Engineering, and to K. Killian and R.K. Everett of the Naval Research Laboratory for assistance in processing of the composites.

REFERENCES

1. J.D. Whittenberger, R. Ray, S.C. Jha, and S. Draper, Mater. Sci. Eng., **A138**, 83(1991).
2. J.D. Whittenberger, R. Ray, S.C, Jha, and S. Draper, Mater. Sci. Eng., **A151**, 137(1992).
3. J.D. Whittenberger, Eduart Arzt, and M.J. Luton, J. Mater. Res., **5**, 271(1990).
4. J.D. Whittenberger, Eduart Arzt, and M.J. Luton, J. Mater. Res., **5**, 2819(1990).
5. R. K. Viswanadham, S. K. Mannan, and B. Sprissler, Annual Report of Martin Marietta Lab., MML TR 87-66C, 1987.
6. K. Sharvan Kumar, and S. K. Mannan, Progress Report of Martin Marietta Lab., MML TR 87-66C, 1988.
7. J. D. Whittenberger, R. K. Viswanadham, S. K. Mannan, and K. S. Kumar, J. Mater. Sci. **25**, 35(1990).
8. J.D. Whittenberger, J. Mater. Sci., **23**, 235(1988).
9. L. Wang and R.J. Arsenault, Mater. Sci. Eng., **A127**, 91(1990).
10. L. Wang and R. J. Arsenault, in *Intermetallic Matrix Composites*, edited by D. L. Anton, P. L. Martin, D.B. Miracle and P. McMeeking, (MRS Proc. 194, 1990) p.199.
11. L. Wang and R. J. Arsenault, in *High-Temperature Ordered Intermetallic Alloys IV*, MRS Proc. (Eds. L.A. Johnson, D.P. Dope, and J.O. Stiegler), (MRS Proc. **213**, 1991) p. 1063.
12. L. Wang and R. J. Arsenault, Mater. Sci. and Eng., **A127**, 91(1990).

Oikawa et al. (eds), Strength of Materials

Strengthening of NiAl at High Temperature*

L. WANG and R. J. ARSENAULT

Metallurgical Materials Laboratory, Dept. of Materials & Nuclear Engineering, University of Maryland, College Park, MD 20742-2115

Abstract

An increase in the athermal component of the yield stress at low temperatures is the caused of the high temperature strengthening of discontinuously reinforced NiAl matrix composites. The reinforcements stabilize the microstructure. The strengthening in the temperature range of 300-1273K, is believed to be related to the grain size refinement and effective pinning of grain boundaries. This conclusion was obtained from analysis of data from AlN, TiB_2 and Al_2O_3/NiAl particulate composites.

1. INTRODUCTION

The high-temperature strength of NiAl has increased 2-3 fold and the modulus is enhanced [1-3] through the addition of discontinuous reinforcements with large volume fractions (20-30 vol%) of relatively large (~1 μm) particulates, such as TiB_2 particulates. The behavior or the mechanism for this second type of strengthening is still unclear. Although strengthening through the grain size refinement has been observed in monolithic NiAl at high temperatures, it is unlikely that very small grains (< 5μm) would be stable at temperatures above 1200K and introduce significant strengthening [4]. The grain size or the subgrain size of these composites are extremely small (1-3 μm) [5-7], which would generally result in lack of elevated-temperature strength. One important difference, however, between dispersion hardened NiAl and the NiAl reinforced with micron-size particulates is that the grain size of the latter, though small, is stable at elevated temperatures (1200-1300 K) [5-7].

Questions concerning the high-temperature strengthening of the NiAl arise from the previous investigations. What is the strengthening mechanism or mechanisms when the reinforcements are not dispersoids? And how important is the matrix grain size in the strengthening of NiAl? This paper is a report of some results of recent investigations of various kinds of discontinuous reinforced NiAl composites intending to cast some insight of the strengthening mechanisms of these composites.

2. MATERIALS AND EXPERIMENTAL METHODS

Five kinds of composites were used in the current investigations. They are: monolithic NiAl, XD^{TM} processed 0, 10, 27 V% TiB_2/NiAl, and cryomilled NiAl composites. The XD^{TM} processed nickel aluminide reinforced with 0,10, and 27 Vol% TiB_2 was obtained from Martin Marietta

* This research was supported by the Office of Naval Research under grant No. N00014-94-10118.

Laboratories. The details of this process can be found elsewhere [1,2].

The composites were ground into cylindrical samples with height-to-diameter (h/d) ratio of 2 and diameter of 4.7~5 mm for compression tests. The cylindrical axis of the sample is parallel to the extrusion direction. The compression tests were conducted on an Instron universal testing machine equipped with high-temperature vacuum chamber. All the tests were conducted at a constant cross-head speed, and in a vacuum of ~10^{-4} torr. The compressive yield stress and flow stress were measured as a function of temperature from 300 K to 1273 K, and with a strain rate of 10^{-4} sec^{-1}. The yield stress was taken as the stress at 0.002 true plastic strain. Activation volumes, V*, were measured as a function of shear stress, τ, in the temperature range of 300 ~ 1273 K, by using the method of changing the strain rate.

3. RESULTS AND DISCUSSION

All the five composites exhibit steady state flow or slight strain softening after yielding at temperature above ~900 K, and can be compressively deformed up to ~0.1 plastic strain without fracture at room temperature, and displays a considerable strain hardening at the deformation temperatures of 800 K or below. As expected, the yield stress of the monolithic NiAl exhibits a typical temperature dependent behavior as common metals and alloys do, as shown in Fig. 1. This behavior can be described as, in both the low temperature (< 500 K) and the high temperature range (>700 K), the yield stress decreases as the temperature increases, indicating that the deformation of these composites is thermally activated in these temperature ranges; and there exists an intermediate temperature range (500-700 K) in which the yield stress is relatively independent of temperature, i. e. an athermal state of the deformation is clearly defined in this temperature range. The temperature dependent behavior of all other composites more or less duplicated this behavior of the monolithic NiAl with an obvious but less profound athermal stage. The athermal stress level of the cryomilled NiAl composite is about three times

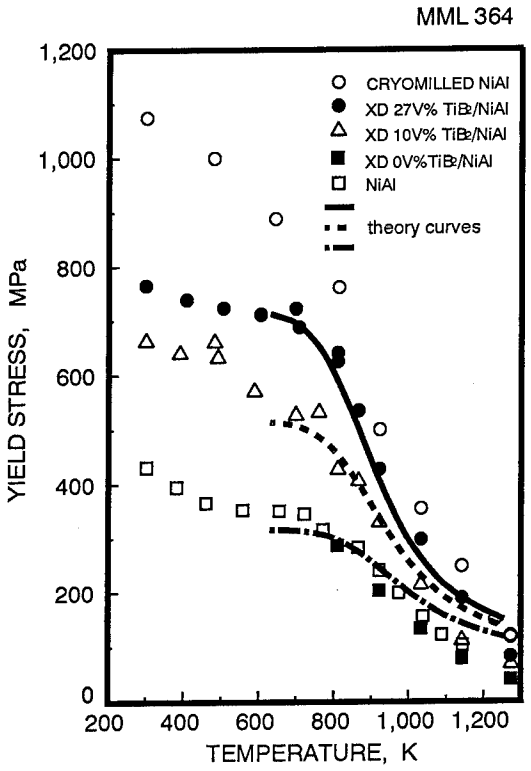

Fig. 1
Temperature dependent of yield stresses of monolithic NiAl and the NiAl matrix composites.

as high as that of the monolithic NiAl, and apparently higher than that of the XD^{TM} processed 27 Vol% TiB_2/NiAl composite. It is evident that the overall strengthening of all the composites, in the whole testing temperature range, were initiated by the increase of the athermal stress, i.e., athermal component of the strength of these composites. The activation volume measurements also supported the above observations. As shown in Fig.2, the activation volume displays a peak value at the corresponding athermal stress level for all the monolithic and XD^{TM} processed TiB_2/NiAl composites which indicates the existence of the athermal stress.

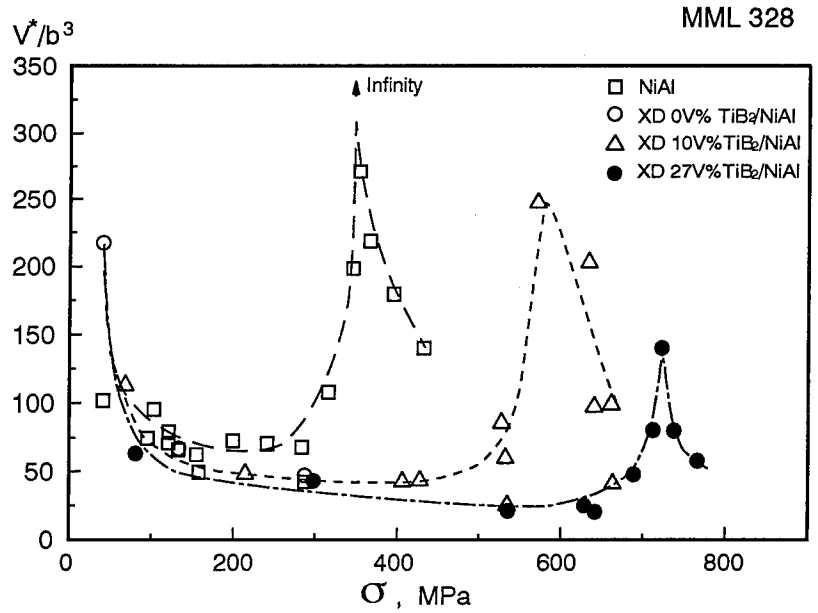

Fig. 2 Activation volumes of monolithic NiAl and 0, 10, and 27 V% TiB_2/NiAl composites as function of the tensile yield stress in the temperature range of 300 - 1273 K.

Based on the above observations and the previous TEM observations of primarily screw dislocation [8], it is proposed that the strengthening, resulting from the reinforcements addition, is due to an increase in the athermal component of the yield stress, i.e., the reinforcements produce an increase in strength at low temperatures. This increase in strength is simply translated into an increase in strength at higher temperatures due to the stabilization of the microstructures of the composites which ensures that the mechanism for the increase in the athermal strengthening is stable with respect to testing temperature and time of testing, and the mechanism of thermally activated deformation remains the same. One of the most important reason for the increase of the athermal stress is due to the substantial reduction of the grain or subgrain size. The strengthening through the grain size refinement becomes true only under the condition that the grain boundary sliding must have been effectively stopped. At high temperatures, this condition can be fulfilled with the addition of a considerable amount of thermally stable reinforcements, such as AlN and TiB_2.

If we make the assumption that the reinforcement only produces an increase in the athermal component of the yield stress and the thermally activated process is the motion of jogged screw dislocations, then the following equation can be derived for the time necessary to make a thermally "jump"

$$t_i = K\left(\frac{\sigma_i^2 - \sigma^{*2}}{2\sigma_i\sigma^*}\right)e^{\frac{Q_a}{RT}} \quad (1)$$

where K is a constant, σ_i is the athermal stress, σ^* is the instantaneous effective stress and the apparent activation energy is as follows:

$$Q_a = Q_{SD} - \frac{\partial n}{\partial\left(-\frac{1}{RT}\right)}\ln\frac{\sigma_a}{\sigma_i} \quad (2)$$

where Q_{SD} is activation energy of self diffusion of NiAl, n is the stress exponent which is a function of temperature, σ_a is the applied stress and RT are the gas constant and temperature respectively. If it assumed that athermal stress varies with a periodicity corresponding to the subgrain or grain size, then a computer simulation investigation of the total time required to traverse the grain can be obtained and then the average dislocation velocity. Finally it is possible to obtain a plot of stress vs temperature which can be compared to the experimental data. The comparison was found to be quite good, the solid lines in Fig. 1 are theoretically predicted curves.

4. CONCLUSIONS

From a consideration of the experimental data, the following conclusions were drawn:

1. The yield strength of all the NiAl matrix composites exhibit typical temperature dependent behavior in a temperature range of 300-1273 K, and can be plastically deformed, compressively, at room temperature.
2. Reinforcements causes an increase in the athermal component of the yield stress at low temperatures and this results in the high temperature strengthening due to microstructure stabilization by the reinforcement.

ACKNOWLEDGEMENT

The authors wish to acknowledge the continued support of Dr. S. Fishman of the Office of Naval Research. The authors are grateful to M.J. Luton of Exxon Research & Engineering, and to K. Killian and R.K. Everett of the Naval Research Laboratory for assistance in processing of the composites.

REFERENCES

(1) R. K. Viswanadham, S. K. Mannan, and B. Sprissler, *Annual Report of Martin Marietta Lab.*, MML TR 87-66C, (1987).
(2) K. Sharvan Kumar, and S. K. Mannan, *Progress Report of Martin Marietta Lab.*, MML TR 87-66C, (1988).
(3) J. D. Whittenberger, R. K. Viswanadham, S. K. Mannan, and K. S. Kumar, *J. Mater. Sci.*, **25**(1990), p.35.
(4) J.D. Whittenberger, *J. Mater. Sci.*, **23**(1988), p.235.
(5) L. Wang and R.J. Arsenault, *Mater. Sci. Eng.*, **A127**(1990), p.91.
(6) L. Wang and R. J. Arsenault, in *Intermetallic Matrix Composites*, edited by D. L. Anton, P. L. Martin, D.B. Miracle and P. McMeeking, *MRS Proc.*, 194(1990) p.199.
(7) L. Wang and R. J. Arsenault, in *High-Temperature Ordered Intermetallic Alloys IV*, MRS Proc. Ed. by L.A. Johnson, D.P. Dope, and J.O. Stiegler, MRS Proc., **213**(1991), p. 1063.
(8) L. Wang and R. J. Arsenault, *Mater. Sci. and Eng.*, **A127**(1990), p.91.

Interfaces in metal- and intermetallic-matrix composites

R.J. ARSENAULT

(University of Maryland, USA)

Received 14 September 1993; revised 14 March 1994

It is well known that the nature of the interface between reinforcement and matrix has a very important role in determining the mechanical properties of composites. However, there are other unusual and important aspects of the interface. An intriguing observation concerning particulate TiB_2/NiAl composites is the lack of dislocation generation after cooling from high temperature (1673 K) annealing. The predicted thermal residual stress is very large and this stress should be relieved by dislocation generation. It is possible that an interface layer exists between the TiB_2 and NiAl that can act as a stress absorber. Also, in the case of continuous filament Al_2O_3/NiAl there can be differences in the bond strength between the filament and the matrix. Experimental and theoretical results indicate that the interface between SiC and Al is non-coherent. There is no layer at the interface between Al_2O_3 or TiB_2 and NiAl that can act as a stress absorber. Continuous filament Al_2O_3/NiAl was degraded by graphite decorations at the interface. An unusual diffraction modulation was observed in the Al_2O_3 filament, and this could be modelled by finite element analysis.

Key words: *interfaces; particulate SiC/Al; particulate Al_2O_3/NiAl; particulate TiB_2/NiAl; continuous filament Al_2O_3/NiAl; adhesion energy calculations; $(112)_{Al} \| (0001)_{\alpha\text{-}SiC}$; semicoherent interface; diffraction modulations*

In the case of discontinuously reinforced metal- and intermetallic-matrix composites where the mechanism accounting for the observed strengthening is based on work hardening of the matrix and stability of the substructure, we need to ask why the nature of the interface has an effect, especially since load transfer does not account for the strengthening. Let us consider strengthening due to work hardening of the matrix. The generation and motion of dislocations are due to relaxation of the thermal residual stress which results from the difference between the coefficients of thermal expansion (ΔCTE) upon cooling from the processing or annealing temperature (ΔT). If we begin with a composite at room temperature in which the discontinuous reinforcement is completely debonded from the matrix (but with no gap between reinforcement and matrix), heat it to some higher temperature (there is a ΔCTE) and cool it again to room temperature, there will be no work hardening of the matrix and no generation and motion of dislocations. If we consider a case where the composite is at a high temperature and there is intimate contact (with no gap and no bond) between the reinforcement and the matrix, subsequent cooling of the composite to room temperature will result in dislocation generation. However, upon reheating to the same high temperature, the dislocations will anneal out and a gap will exist; i.e., the hole in the matrix will be larger than the size of the reinforcement. Upon cooling to room temperature there will be no dislocation generation, i.e., no work hardening of the matrix. Therefore, in order to have work hardening of the matrix, it is necessary to have some degree of bonding between the reinforcement and the matrix.

In intermetallic-matrix composites reinforced with particles, the strengthening is due to the stabilizing effect of the reinforcement on the grain size and substructure. The influence of the degree of bonding on the stabilizing effect has not been clearly delineated as yet.

In continuous filament composites, the need for bonding between the reinforcement and matrix is obvious, for this is the strengthening mechanism. However, the degree of bonding is important.

In this review three specific interface systems will be considered: particulate SiC/Al, particulate TiB_2 or Al_2O_3/NiAl and continuous filament Al_2O_3/NiAl.

Table 1. Calculated results for the bridge position shown in Fig. 1

First layer of SiC	Position	E (Hartree)	E_{Al} (Hartree)	E_{SiC} (Hartree)	ΔE (eV)	$\lvert\Delta E/\text{atom}\rvert$ (eV/atom)	ν (eV Å^{-2})
C	Bridge	−118.6012	−26.7335	−91.6031	−7.20	0.51	0.157
Si	Bridge	−117.2636	−26.7335	−90.2001	−8.98	0.64	0.196

PARTICULATE SiC/Al

Although several experimental investigations[1,2] based on macromechanics have reported that the SiC/Al bond is good, no basic understanding of the mechanism of this bonding exists. The reasons for this are twofold. First, the nature and composition of the interface are not fully known. For example, three hypotheses[3–5] have been put forward concerning the interface between SiC and an Al matrix: (1) there is an SiO_2 layer at the interface; (2) there is an Al_4C_3 film at the interface; and (3) there is nothing at the interface, i.e., the interface is simply formed by two surfaces of SiC and Al. Secondly, even if one ignores the uncertainty in the composition at the interface, the problem is too complicated for a theoretical study at the atomic level due to reduced symmetry and the large number of atoms per unit cell.

To illustrate this problem further, let us enumerate some of the possibilities one needs to explore for a fundamental understanding of the bonding at the interface.

1) The interface can be formed by SiC and Al surfaces of different crystallographic orientations.
2) SiC has two different structures, α and β. Particulates have the α-structure, whereas whiskers are in the β-phase. Furthermore, there are six different polymeric structures for α-SiC.
3) The interface can be formed between C and Al layers of Si and Al layers.
4) The atoms at the interfaces formed by all orientations of SiC and Al surfaces do not constitute a commensurate structure since there is a lattice mismatch at the interface; this is also referred to as a lack of coherence. The unit cell, therefore, contains a rather large number of atoms, thus making any *ab initio* studies of bond energies virtually impossible.
5) One would expect the atoms at the interface to reconstruct.

An intermediate-neglect of differential-overlap (INDO) method was used to study adhesion at SiC/Al interfaces[6]. Although semi-empirical and semi-quantitative, this study represented the first attempt at understanding the bonding at the SiC/Al interface from an atomic viewpoint. By minimizing the total energy of the cluster, we can determine the equilibrium separation between adjacent layers at the interface and its adhesion energy. Calculations were repeated for different crystallographic orientations as well as for varying atomic composition at the interface.

In the cluster model of Li *et al.*[6], the energy necessary to create the interface is defined by[7]:

$$\Delta E = (E_{Al} + E_{SiC}) - E$$

where E_{Al} and E_{SiC} are the total energies of the Al and SiC clusters, respectively, and E is the total energy of the Al/SiC composite. This is calculated by varying the distance between cleaved surfaces of Al and SiC and E corresponds to the minimum in this energy. The cleaved basal plane of SiC could contain either Si or C atoms. The results of ΔE/atom and $\nu = \Delta E/(A_{SiC} + A_{Al})$ are presented in Table 1 for the clusters shown in Fig. 1, where A_{SiC} and A_{Al} are the cross-sectional areas of the two approaching surfaces.

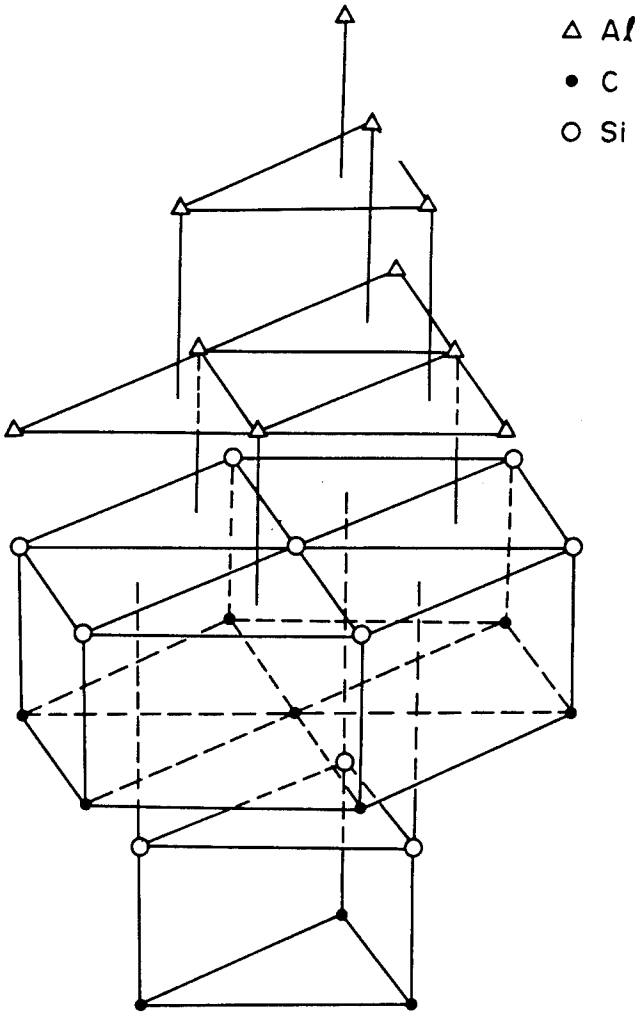

Fig. 1 Cluster model of (111) Al parallel to (0001) α-SiC in what is called the bridge position

In Table 1 the results indicate that the bond between Si and Al is slightly stronger than the bond between C and Al. However, Rao and Jena[8] performed a first principle dimmer calculation and showed that the bond strength between C and Al is greater than that between Si and Al.

Several other interface configurations were considered for α-SiC and β-SiC was also examined. The results indicate that the bonding of the side surface of β-SiC whiskers is larger than that of the basal plane of α-SiC.

The effect of reconstruction at the interface on the adhe-

sion was also examined. Note that SiC is a high strength covalent solid with a melting point of 3373 K. Its coefficient of thermal expansion is very small. It is, therefore, safe to assume that at the processing temperature of the composite (~873 K) the lattice constants of SiC remain relatively unchanged. We therefore studied the effect of reconstruction by changing the atomic spacings in an Al (111) plane from 2.86 to 3.07 Å to match with a (0001) plane of α-SiC. The effect of reconstruction is to enhance the adhesive energy significantly, as can be seen from the results presented in Table 2.

The following conclusions can be drawn from the investigation of Li *et al.*[6]. The bond strength between SiC and Al could possibly be two to three times stronger than the bond between Al and Al. The adhesive energy between the side surface $(2\bar{1}\bar{1})$ of β-SiC fibre and Al is larger than that between the cleavage surface (0001) of α-SiC particle and Al. Also, there is a further increase in the adhesive energy if the interface is reconstructed, i.e., a set of misfit dislocations is introduced.

Based on the theoretical prediction that the interface between the (0001) plane of α-SiC should be parallel to the (111) plane of Al and there should be a set of misfit dislocations at the interface, a high resolution-electron microscopy (HREM) investigation was undertaken.

The samples were first checked for their chemical stability; these results revealed the interfaces to be rather planar and clean of any precipitates. (The composite was heated to 953 K to ensure that the matrix was in the liquid state.) The concentration gradients obtained were sharp at the interface and this indicated that no interdiffusion or penetration had developed at the observed interfaces. A linescan profile taken across these interfaces is shown in Fig. 2. The profile is the same across any crystallographic orientation. The interfaces were then tilted and checked to make sure there were no traces of any Al layer lying across the boundary (i.e., on top of the SiC) that would interfere with the HREM images. Once this had been accomplished, the sample was oriented so that the electron beam was *perpendicular* to the $[11\bar{2}0]$ direction of the SiC and the [110] direction of the Al matrix. This was done with the basal planes of the SiC being parallel to the length of the interface so that the orientation of the (111) planes of Al at the interface could then be obtained in relation to the SiC basal planes. In order to obtain the necessary HREM images, it was required to concentrate on very thin regions of the samples and to orient the sample in such a way that the useful diffraction conditions were obtained in both the matrix and the particle. This was sometimes difficult; the different ion milling rates of the components created a step at the interface so that not all the interfaces were useful even if the required diffraction conditions were met.

The results show that there is a difference in orientation

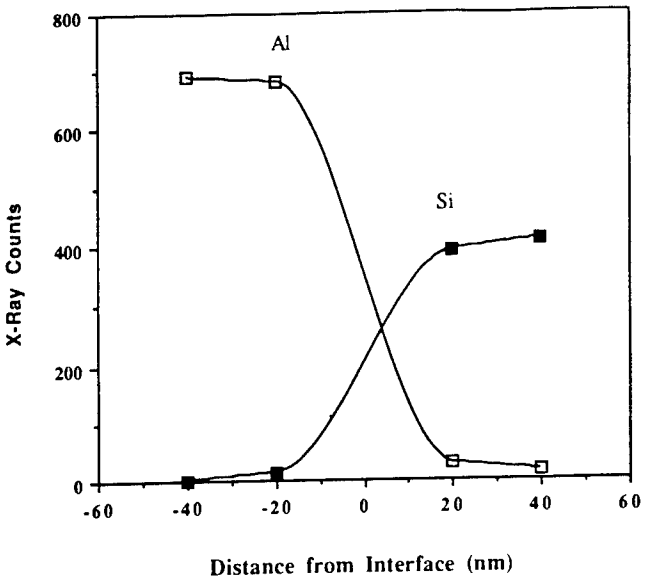

Fig. 2 Linescan profile across the interface. This shows the interface to be very stable and free of any segregation

between these adjoining planes, such that the (111) planes of the Al are oriented at 20° to the (0001) planes of the SiC, see Fig. 3. These results are somewhat different to those obtained by Weimin *et al.*[9]. Their work also revealed clean and continuous interfaces with few if any dislocations at the interface, but the (111) Al planes were oriented at 70° to the basal planes of the SiC while the basal planes were perpendicular to the interfacial axis (in our case, the basal planes are parallel to the interface).

Fig. 3, which was typical, shows four general observations. First, the interface is clean, rather planar and continuous. Second, not all interfaces contain an amorphous layer so that a continuous lattice matching is possible between the matrix and the reinforcement across the interface. Third, the (111) Al planes are oriented at 20° to the basal planes of the SiC. Last, there is no evidence of any dislocations being generated at the interface solely due to the bonding of the lattices.

On the other hand, as shown in Fig. 4, a few of the interfaces actually had a thick (~5 nm) amorphous layer, although the SiC surface was again quite planar in appearance and the matrix planes still showed the same 20° orientation relationship as when there was actual contact at the interface. Some of the interfaces observed in this investigation could not be resolved, which had been attributed in the past to the presence of a 1 nm amorphous layer although this might also be due to the 'edge' or 'step' effect at the interface. A lot of the interfaces, though, did not appear to have such layers and were rather clean and sharp.

The next step was to observe the interfacial structure through an observation of the interface across the same

Table 2. Calculated results for reconstructed Al (111) ||α-SiC (0001)

First layer of SiC	Position	E (Hartree)	E_{Al} (Hartree)	E_{SiC} (Hartree)	ΔE (eV)	$\lvert\Delta E/\text{atom}\rvert$ (eV/atom)	ν (eV A^{-2})
C	Bridge	−118.5581	−26.6335	−91.6031	−8.75	0.62	0.191
Si	Bridge	−117.2244	−26.6335	−90.2001	−10.58	0.75	0.231

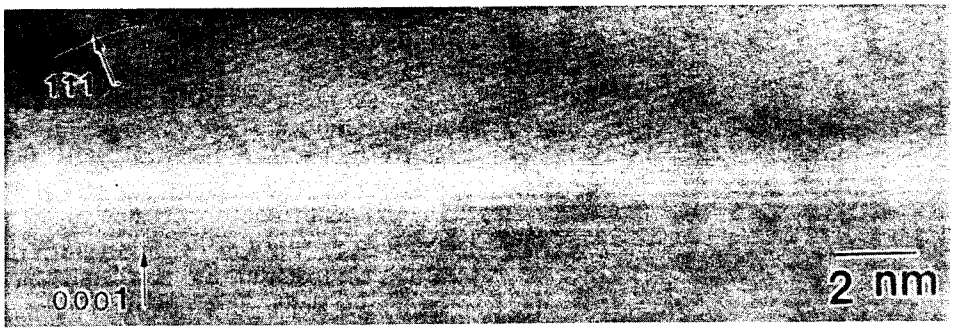

Fig. 3 Clean and planar interface. Such an interface does not show the presence of any dislocations. No amorphous layer can be observed. The (111) planes are aligned at 20° to the SiC basal planes so that the (112) Al planes are parallel to the basal planes

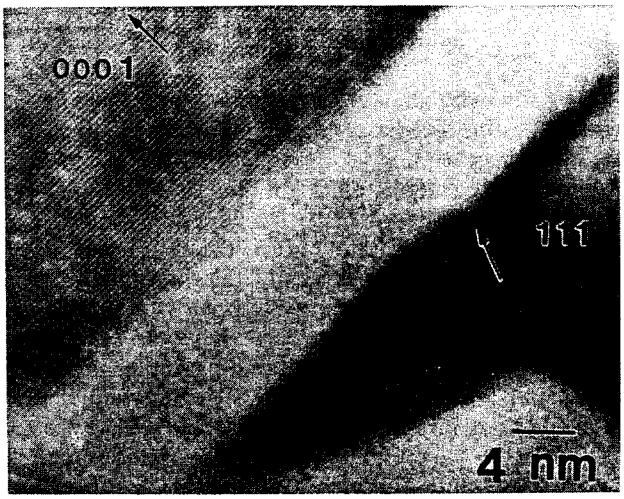

Fig. 4 Amorphous layer at the boundary of some interfaces; such an interfacial layer was not observed at all interfaces. Notice how the matrix still has the same orientation as shown in Fig. 3 in which no amorphous layer was seen

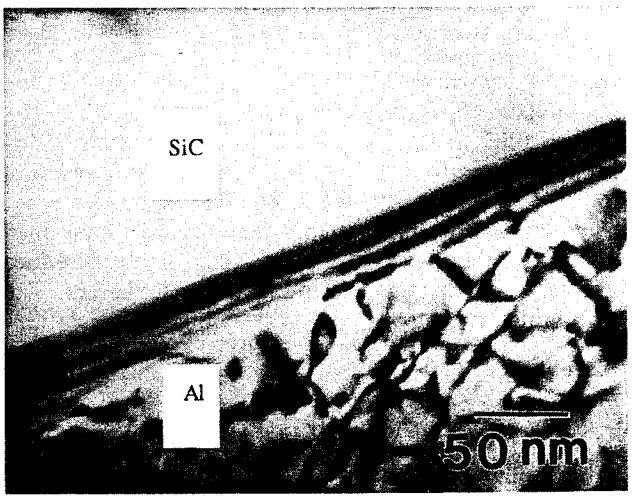

Fig. 5 Conventional image across the interface. No specific pattern can be deduced from this figure as to the existence of dislocations

particle by continuously changing the tilt angle. As can be seen in Fig. 5, no interfacial dislocations can be observed on the tilted side of the SiC. These surfaces show no regular dislocation distribution and no distinctive periodic pattern. Since the SiC/Al interface is an incoherent interface, no specific information can be gathered from a diffraction pattern along the interface. There was, then, no dislocation pattern to speak of and in fact most of the interfaces showed no change as the sample was tilted. The SiC surface appears once again to be very clean and devoid of any precipitates. Use of the weak beam technique also showed no evidence of the existence of dislocations at the interface.

In all the reported cases so far, where the matrix was molten, the (111) Al planes have been seen to align themselves either perpendicular or at 70° to the interfacial axis when the SiC basal planes are perpendicular to the interfacial axis or at 20° to the interfacial axis if the SiC basal planes are parallel to the interfacial axis, which is the case observed in this investigation. The crystallographic relationship obtained in the investigation by Romero and Arsenault[10] is then given by:

$$[11\bar{2}0] \parallel [110] , (0001) \parallel (112)$$

Next, a stereoprojection of the $(11\bar{2}0)$ and (110) poles of the SiC and Al, respectively, was prepared in order to obtain the other crystallographic relationships possible in the SiC–Al system. Once these stereoprojections were obtained, the (110) Al plot was superimposed onto the SiC plot with the (111) Al pole on top of the (0001) SiC pole. This set-up was then rotated by 20° (since this was the experimentally obtained condition) and the new alignment was checked to see which poles from Al and SiC coincided with each other. As can be seen in Fig. 6, not only do the (112) Al planes coincide with the (0001) SiC planes (which is the relationship observed in this investigation), but the following variant relationship can also be observed:

$$[11\bar{2}0] \parallel [110] , (01\bar{1}0) \parallel (111)$$

This appears to be similar to what has been reported by Carim[11], who found the relationship to be $[11\bar{2}0] \parallel [110]$, $(1\bar{1}01) \parallel (557)$; note, though, that this is not a low index relationship. A closer examination of the work by Weimin *et al.*[9] seems to imply that the (111) Al planes observed in their work are aligned parallel to the $(01\bar{1}0)$ planes of the SiC. Since the (111) Al planes are at 70° to the interfacial axis, a different set of (111) planes (which are at 70° to each other) must then be lying parallel to the interfacial axis, while the basal planes in that work are aligned perpendicular to the interfacial axis. Note, then,

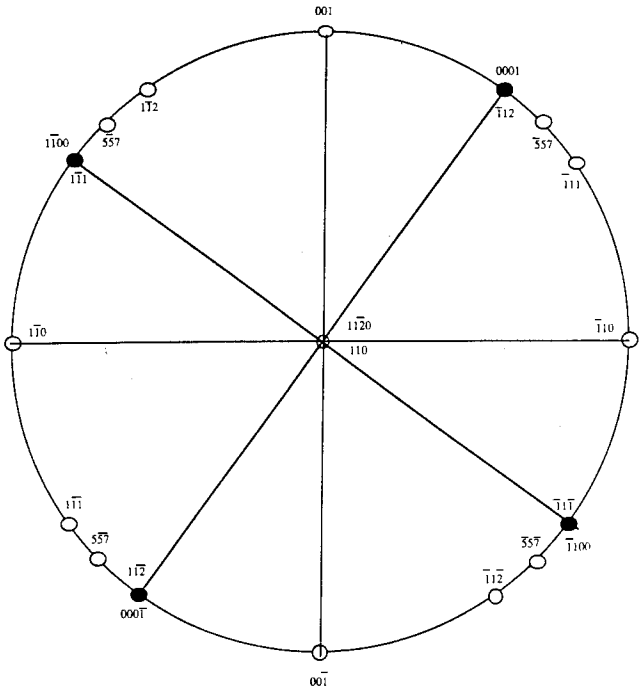

Fig. 6 Stereoplots of Al and SiC along the [11$\bar{2}$0] and [110] directions showing the crystallographic orientation relationships that are possible in this system. The black circles represent those poles that are coincident for both systems. The SiC plot has been tilted by 20° with respect to that of the Al pole (after the (111) pole was placed on top of the (0001) pole)

that this is the variant of the relationship obtained by the stereoprojections mentioned above.

Van Den Burg and De Hosson[12] reported a preferred orientation between the (0001) planes of SiC and the (111) planes of Al. Of course, it must be noted that there has been no consistency in the way these different research groups prepared their respective samples. For example, the three groups that have shown a consistent result (i.e., Romero and Arsenault[10], Weimin *et al.*[9] and Carim[11]) studied composites in which the Al matrix was in the liquid state during the production of the composite and these samples were either cast from the melt or annealed into the liquidus region of the matrix for extended periods of time. On the other hand, the work of Van Den Burg and De Hosson[12] and Radmilovic *et al.*[13] considered samples prepared via a powder metallurgy route. These two last groups have obtained different results. For example, Radmilovic *et al.*[13] studied the interface of an SiC/6061-Al composite and no orientation relationship of any kind was obtained. It was specifically stated that the (0001) and (111) planes were not crystallography oriented with respect to each other across the interface axis. This is in contrast to the work of Van Den Burg and De Hosson[12], in which a (0001) || (111) relationship was observed in an SiC/6061-Al composite. On the other hand, an SiC/2014-Al composite prepared by Van Den Burg and De Hosson[12], also via powder metallurgy, obtained no relationship of any kind across the interface; this is in contrast to the work of Carim[11], who found a ($\bar{1}\bar{1}$01) || (557) relationship in a similar SiC/2014-Al composite that was cast from the melt. Thus, it can be seen that as long as the matrix is in the liquid state during preparation of the composite, a consistent result (i.e., the present investigation) is obtained by different research groups. On the other hand, when the matrix is in the solid state (i.e., powder metallurgy by Van Den Burg and De Hosson[12] and Radmilovic *et al.*[13]), inconsistent results are obtained. These inconsistent results are not only different from one alloy matrix to another, but also differ from those results obtained by other groups using the same alloy matrix. The difference is probably due to the use of a powder compaction route in the fabrication of the composite: during compaction, the powders come in contact with the reinforcement in a random manner and are bonded together at high temperature with this random orientation across the interface (i.e., there is no preferred orientation between the matrix and the reinforcement). On the other hand, when the matrix is in the liquid state, this restriction is removed and it is now possible for the matrix to readjust itself across the interface with the reinforcement along a consistent crystallographic orientation (i.e., the lowest energy arrangement).

The reason why the (111) Al planes are not bonded parallel to the SiC basal planes (as expected from the work of Li *et al.*[6]), even though they have a stacking similar to the basal planes, might then be due to the large interfacial dislocation density that would be generated at the interface. In order to reduce the interfacial strain energy, the matrix planes would then adopt an orientation that would present a more open structure to the SiC basal planes. Such a procedure would be accomplished by the (111) Al planes bonding, either perpendicular or at a given angle, to the SiC. This would then allow more open planes, such as the (112), to bond parallel to the SiC basal planes. As the orientation angle changes, Al matrix planes with higher Miller indices would begin to appear. These higher index planes would generate a greater disordered interfacial structure which might then result in a deleterious increase of the interfacial energy. Thus, it is seen that it is not necessary to generate dislocations in the matrix along the interface in order for the bond between Al and SiC to be strong. The interface between Al and SiC can be rather planar, clean, devoid of any inherent dislocations and incoherent and yet the bonding between the matrix and the reinforcement is very strong.

From the data generated in the HREM investigation, the following conclusions can be drawn. The (112) Al planes bond parallel to the (0001) SiC planes. Inherent interfacial dislocations expected due to the bonding between the (111) Al planes and the (0001) SiC planes were not generated. This was probably due to the more open structure of the (112) Al planes which served to reduce the interfacial energy. The interface is incoherent. The SiC/Al interface has a specific crystallographic relationship defined by: [11$\bar{2}$0] || [110], (0001) || (112).

PARTICULATE TiB_2 AND Al_2O_3/NiAl

An intriguing observation concerning TiB_2/NiAl composites is the lack of dislocation generation upon cooling from high temperature (1673 K) annealing[14,15]. The predicted thermal residual stress is very large and this stress should be relieved by dislocation generation[16]. It is possible that an interface layer exists between the TiB_2 and NiAl that can act as a stress absorber[16].

Initially, an investigation was undertaken to determine if any crystallographic orientation relationships existed between the reinforcement (including α-Al_2O_3) and matrix materials. Although, in some cases, one or two lower indexed crystal planes of α-Al_2O_3 or TiB_2 phases can be aligned with that of the matrix phase, no consistent crystallographic orientation relationships were found between the reinforcements and the matrix phase. In other words, there was a random crystallographic orientation relationship between the particles and the matrix. (These composites were made by a powder metallurgy process.)

However, despite the differences between their crystal structures and their random crystallographic orientation relationships, there are some interesting aspects of interfaces between Al_2O_3 and NiAl. In some cases, it seems that one or two disordered atomic layers exist on the α-Al_2O_3 side, as shown in Fig. 7. It is possible that this observation is an image effect. However, it has been proposed that a disordered region occurs to obtain atomically well-matched interfaces where, crystallographically, there is a large level of atomic mismatch[17]. Unfortunately, there are at least two difficulties preventing us from carrying out computer image simulations to interpret the observations. The first difficulty is that the crystal orientations between NiAl and α-Al_2O_3 are random. As a consequence of this, there is a second difficulty: a lack of theoretical models for interface structures. There are too many possible ways to construct the interface. Since the observed disordered layer is apparently in α-Al_2O_3 which has a higher elastic modulus than NiAl[18–20], it makes the interpretation even more difficult except we believe that elastic anomalies[21,22] of α-Al_2O_3 occur at the interface region.

In the case of the lower indexed planes of α-Al_2O_3 aligned with that of the matrix, semicoherent interfaces were observed. For instance, Fig. 8 shows a semicoherent interface where the {110} planes of NiAl aligned with {110} planes of α-Al_2O_3. By using a hard sphere model of the interface structure, the distance between misfit dislocations is[23]:

$$D = d_1 d_2/(d_1 - d_2)$$

where d_1 and d_2 are the interplanar distances for reinforcement and the matrix, respectively. The interplanar distances of the (110) planes in NiAl and (110) planes in α-Al_2O_3 are 0.288 and 0.3479 nm, respectively. Calculated $D = 1.673$ nm, which is just about six times greater than the interplanar distance of (110) planes in NiAl. In Fig. 8, six of the (110) planes in NiAl are aligned with five of the (110) planes in α-Al_2O_3 with one misfit dislocation on the matrix side. This agrees with the calculated value very well. Coherent or semicoherent interfaces between TiB_2 and NiAl were not observed via HREM. At the TiB_2/NiAl interface, there exists a very thin layer (maybe a different crystal structure, but too thin to obtain a micro-

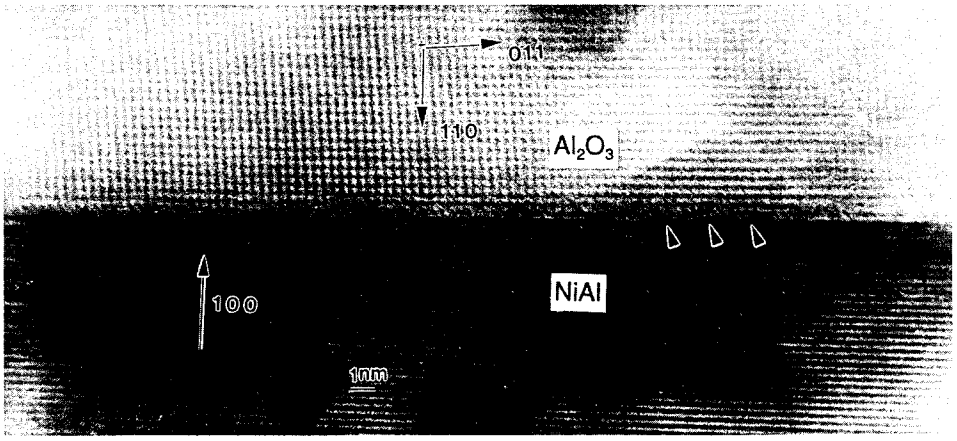

Fig. 7 HREM micrograph of α-Al_2O_3/NiAl interface. Arrows indicate the disturbed interface

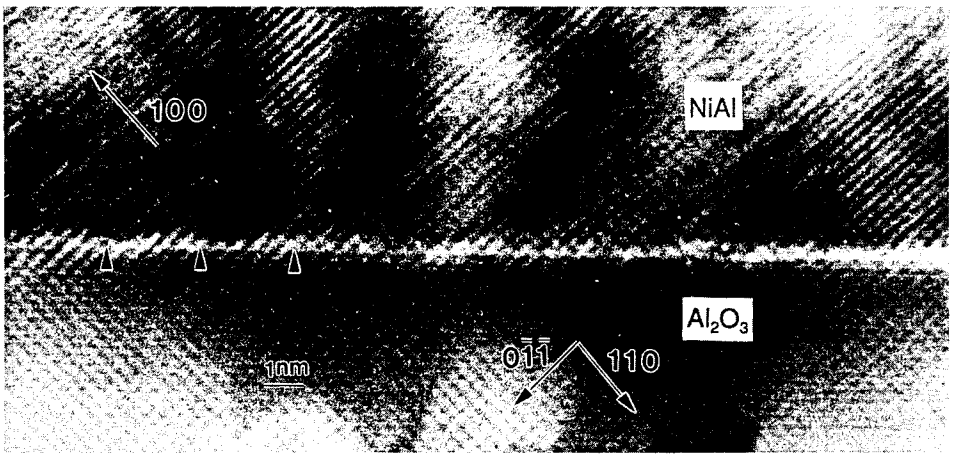

Fig. 8 HREM micrograph of α-Al_2O_3/NiAl interface. Arrows indicate the misfit dislocations in the NiAl

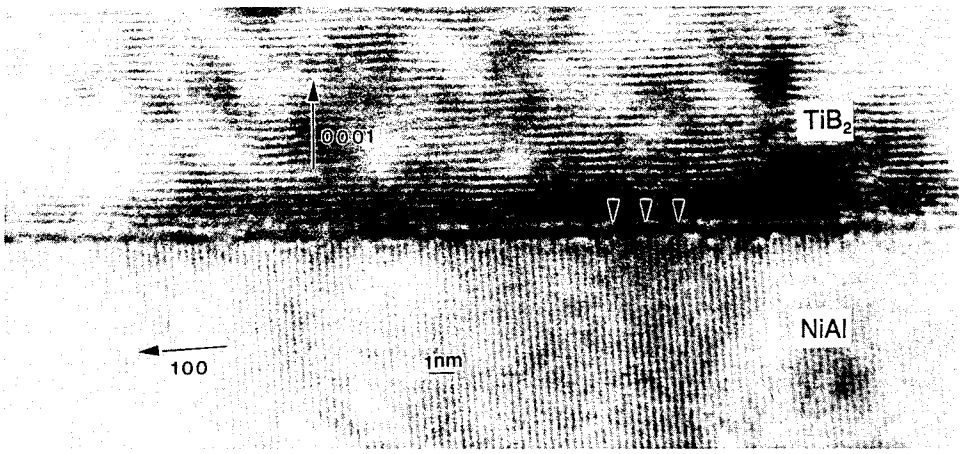

Fig. 9 HREM micrograph of TiB_2/NiAl interface. Arrows indicate the silicon segregated layer

diffraction pattern) of atoms that had a different lattice spacing, as shown in Fig. 9. The thickness of this layer was about 0.6 nm when the observation was made along the basal plane of TiB_2.

The results discussed above indicate that the interface layer at the TiB_2/NiAl interface is very thin (0.6 nm). Therefore, it is not thick enough to absorb the thermal residual stress, but there is a possibility that the thermal residual stress is relaxed by the diffusion of atoms having a larger atomic radius than the matrix atoms in the interface region. This relaxation would occur because the matrix is in hydrostatic tension[15] and the oversized atoms would reduce the stress. The possibility of segregation was investigated by X-ray energy dispersion spectroscopy (EDS) analysis.

The results of EDS investigations indicate that an interface layer does not exist at the Al_2O_3/NiAl interface. The Si segregation layer at the TiB_2/NiAl interface is too thin to act as a shock absorber of the thermal residual stress.

From the investigation of Wang and Arsenault[24] several conclusions can be drawn. No consistent crystallographic orientation relationships have been found between the NiAl matrix and TiB_2 or α-Al_2O_3 particles, although in some cases one or two low indexed crystallographic planes of TiB_2 or α-Al_2O_3 might be aligned with those of NiAl. Silicon segregation has been found in the TiB_2/NiAl interface region. No coherent or semicoherent interfaces have been observed between the TiB_2 and NiAl, and the Si layer is too thin to absorb any of the thermal residual stress. There is a strong tendency for the formation of semicoherent interfaces between α-Al_2O_3 and NiAl. No segregation has been found at these interfaces.

CONTINUOUS FILAMENT Al_2O_3/NiAl

In a further attempt to understand the lack of dislocation generation from the TiB_2 or Al_2O_3 particles as a result of the ΔCTE effect, an investigation of continuous filament Al_2O_3 in an NiAl matrix was undertaken. It was found that dislocation generation due to the ΔCTE effect did occur in the continuous filament Al_2O_3/NiAl composite. The results of this investigation are discussed elsewhere[25].

An unusual observation is that diffraction contrast on the Al_2O_3 filament side is not homogeneous, but rather modulated randomly along the clean interface, as shown in Fig. 10(a)[26]. The wavelength of the modulation is around 0.1 μm. The modulated diffraction contrast disappears at the region where the foil thickness becomes less than a two-beam extinction distance with operating diffraction vector of $g=300$, i.e., $\sim$ 95 nm. Different operating diffraction conditions were applied to produce different two-beam diffraction contrast images of the interface area, as shown in Figs 10(b)–10(d). According to an analysis of these images, two important features have been found. First, minimum diffraction contrast is obtained when the diffraction vector is almost parallel to the interface (Fig. 10(d)); second, the pattern of the dark or bright area of the image always tends to be parallel to the diffraction vector (Figs 10(b) and 10(c)). There is no precipitation or any other second phase involved in this interphase region. Therefore, it is likely that this modulated diffraction contrast may be caused by an inhomogeneous distribution of strains which originate at the interface.

In order to understand the nature of the strains at the interface producing the diffraction contrasts, a finite element analysis was undertaken to simulate a number of cases of strains originating at interfaces, from which transmission electron microscopy (TEM) diffraction contrast images were calculated. The calculated TEM diffraction contrast images are shown in Fig. 11. These images were calculated using the same diffraction conditions and foil thickness as those of the experimental images (Fig. 10). It turns out that only the simple normal loading model can duplicate all the major features of the experimental images. The contrast is localized around the loading area (in a range of $\sim$0.1 μm from interface), which indicates that the residual strains were concentrated at that region. Furthermore, changes of the location of the loading area in the depth direction (z-direction) will not drastically change the basic features of the calculated diffraction contrast images.

Radial residual strains within the Al_2O_3 are inhomogeneously distributed along the interface. It is believed that the random modulation of the radial residual strains in the Al_2O_3 filament along the interface is caused by the plastic deformation of NiAl, i.e., dislocation generation in NiAl.

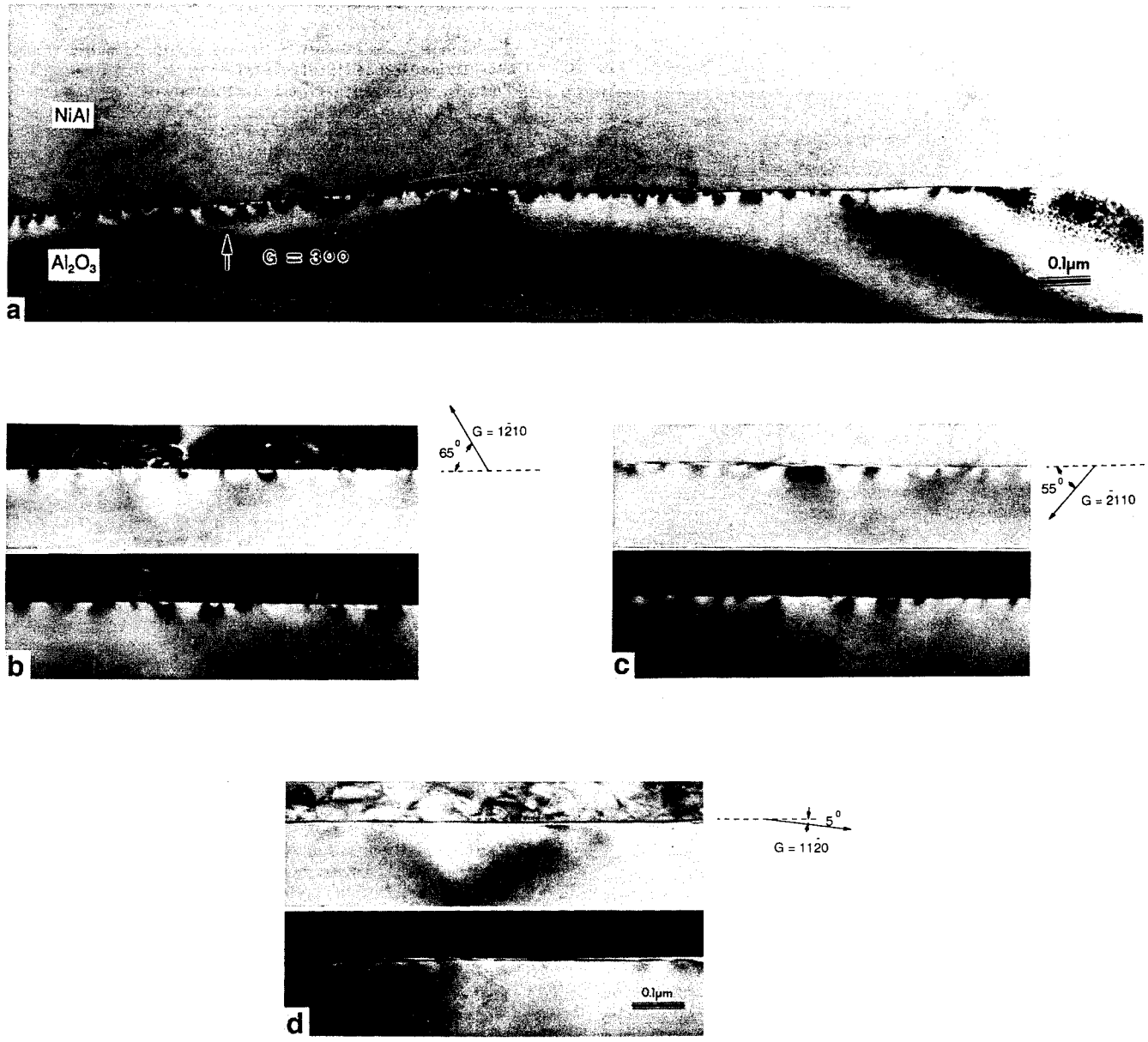

Fig. 10 TEM micrographs of clean interface between the single crystal Al_2O_3 filament and NiAl matrix, after 10 thermal cycles: (a) the inhomogeneous diffraction contrast observed along the interface on the Al_2O_3 filament side; (b)–(d) bright (top) and dark (bottom) field images of the interface with different operating diffractions, $t = 1.3\ \xi_g$ with $G = \{11\bar{2}0\}$

CONCLUSIONS

From the investigation of Li *et al.*[6], the following conclusions can be drawn. The bond strength between SiC and Al could possibly be two to three times stronger than the bond between Al and Al. The adhesive energy between the side surface $(2\bar{1}\bar{1})$ of β-SiC fibre and Al is larger than that between the cleavage surface (0001) of α-SiC particle and Al. Also, there is a further increase in the adhesive energy if the interface is reconstructed, i.e., a set of misfit dislocations is introduced.

From the data generated in the HREM investigation, the following conclusions can be drawn. The (112) Al planes bond parallel to the (0001) SiC planes. Inherent interfacial dislocations, expected due to the bonding between the (111) Al planes and the (0001) SiC planes, were not generated. This was probably due to the more open structure of the (112) Al planes which served to reduce the interfacial energy. The interface is incoherent. The SiC/Al interface has a specific crystallographic relationship defined by: $[11\bar{2}0] \parallel [110]$, $(0001) \parallel (112)$.

From the investigation of Wang and Arsenault[24] several conclusions can be drawn. No consistent crystallographic orientation relationships have been found between the NiAl matrix and TiB_2 or α-Al_2O_3 particles, although in some cases one or two low indexed crystallographic planes of TiB_2 or Al_2O_3 might be aligned with those of NiAl. Silicon segregation has been found in the TiB_2/NiAl interface region. No coherent or semicoherent interfaces have been observed between the TiB_2 and NiAl, and the Si layer is too thin to absorb any of the thermal residual stress. There is a strong tendency for the formation of semicoherent interfaces between α-Al_2O_3 and NiAl. No segregation has been found at these interfaces.

Radial residual strains within the continuous filament Al_2O_3 are inhomogeneously distributed along the inter-

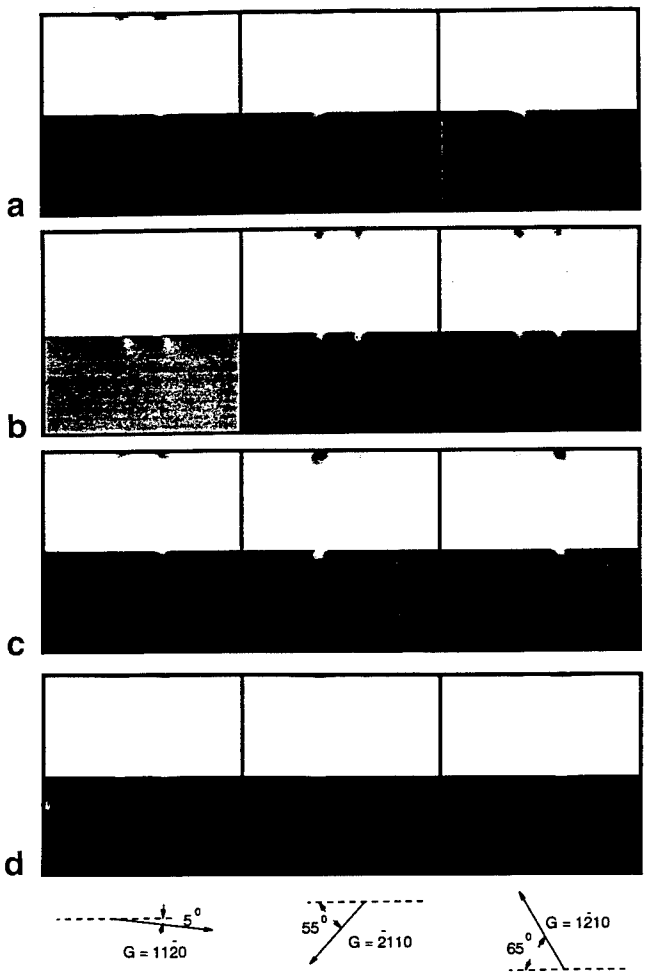

Fig. 11 Bright field (top) and dark field (bottom) diffraction contrast image simulations of the finite element model under different diffraction conditions, $w=1.0$ and $t=1.3\ \xi_g$: (a) concentrated shear load; (b) concentrated normal load; (c) both shear and normal; (d) surface contraction

face. It is believed that the random modulation of the radial residual strains in the Al_2O_3 filament along the interface is caused by the plastic deformation of NiAl, i.e., dislocation generation in NiAl.

ACKNOWLEDGEMENTS

The author wishes to acknowledge the support from the following individuals: Drs Steve Fishman, Nick Shi, Len Wang and Juan Romero. Also, continuing support from the Office of Naval Research under grant N00014-91-J-1353 is acknowledged.

REFERENCES

1 **Divecha, A.P., Fishman, S.G. and Karmarkar, S.D.** 'Silicon carbide reinforced aluminum—a formable composite' *J Met* **33** (1986) pp 12–17
2 **Flom, Y. and Arsenault, R.J.** 'Interfacial bond strength in an aluminum alloy 6061–SiC composite' *Mater Sci and Engng* **77** (1986) pp 191–197
3 **Arsenault, R.J. and Pande, C.S.** 'Interfaces in metal matrix composites' *Scripta Met* **18** (1984) pp 1131-1134
4 **Porte, L.** 'Photoemission spectroscopy study of the Al/SiC interface' *J Appl Phys* **60** No 2 (1986) pp 635–638
5 **Nutt, S.R.** in *Interfaces in Metal-Matrix Composites* edited by A.K. Dhingra and S.G. Fishman (The Metallurgical Society, Inc. Warrendale, PA, 1986) p 157
6 **Li, S., Arsenault, R.J. and Jena, P.** 'Quantum chemical study of adhesion at the SiC/Al interface' *J Appl Phys* **64** (1988) pp 6246–6253
7 **Batra, I.P.** 'First-principles calculation of energy of an epitaxial system' *Phys Rev B* **29** (1984) pp 7108–7110
8 **Rao, B.K. and Jena, P.** 'Molecular view of the interfacial adhesion in aluminum–silicon carbide metal-matrix composites' *Appl Phys Lett* **57** (1990) pp 2308–2310
9 **Weimin, S., Pengxing, L. and Geyang, L.** in *Composites: Design, Manufacturing and Application, Proc ICCM/VIII* edited by S. Tsai and G.S. Springer (SAMPE, Covina, CA, 1991) pp 19k3–19k8
10 **Romero, J. and Arsenault,R.J.** 'Interfacial structure of a SiC/Al composite' to be published
11 **Carim, A.H.** 'SiC/Al_4C_3 interfaces in aluminum–silicon carbide composites' *Mater Lett* **12** (1991) pp 153–157
12 **Van Den Burg, M. and De Hosson, J. Th. M.** 'Al–SiC interface structure studied by HREM' *Acta Metall* **40** (1992) pp S281–S287
13 **Radmilovic, V., Thomas, G. and Das, S.K.** 'Microstructure of α-Al base matrix and SiC particulate composites' *Mater Sci and Engng* **A132** (1991) pp 171–179
14 **Wang, L. and Arsenault, R.J.** 'Microstructure of TiB_2/NiAl' *Mater Sci and Engng* **A127** (1990) pp 91–98
15 **Wang, L. and Arsenault, R.J.** 'Dislocations in titanium diboride' *Phil Mag* **63** (1991) pp 121–130
16 **Taya, M. and Arsenault, R.J.** in *Metal Matrix Composites, Thermomechanical Behaviour* (Pergamon Press, Oxford, UK, 1989) pp 23–105
17 **Merkle, K.L.** in *Interfaces Between Polymers, Metals and Ceramics, MRS Symp Proc 153* edited by B.M. Dekoven, A.J. Gellman and R. Rosenberg (Materials Research Society, Pittsburgh, PA, 1989) p 83
18 **Sharvan, K. and Mannan, S.K.** *MML TR 88-66C* (Martin Marietta Laboratories Progress Report, 1988)
19 **Wasilewski, R.J.** 'Elastic constant and Young's modulus of NiAl' *Trans AIME* **236** (1966) pp 455–457
20 *Handbook of Materials Science, Vol 2* edited by C.T. Lynch (CRC Press, Boca Raton, FL, 1974) p 358
21 **Schuller, I.K., Fartash, A. and Grimsditch, M.** 'Elastic anomalies in superlattices' *MRS Bull* **10** XV (1990) pp 33–37
22 **Phillpot, S.R., Wolf, D. and Yip, S.** 'Effects of atomic-level disorder at solid interfaces' *MRS Bull* **10** XV (1990) pp 38–47
23 **Mader, W.** in *Characterization of Defects in Materials, MRS Symp Proc 82* edited by R.W. Siegel, J.R. Weertman and R. Sinclair (Materials Research Society, Pittsburgh, PA, 1987) p 403
24 **Wang, L. and Arsenault, R.J.** 'Interfaces in XD processed TiB_2/NiAl composites' *Met TransA* **22A** (1991) pp 3013–3018
25 **Wang, L., Bowman, R.R. and Arsenault, R.J.** 'Dislocations in continuous filament reinforced W/NiAl and Al_2O_3/NiAl composites' to be published
26 **Wang, L., Xu, K., Bowman, R.R. and Arsenault, R.J.** 'Interfaces in continuous filament reinforced Al_2O_3/NiAl composites' to be published

AUTHOR

The author is with the Metallurgical Materials Laboratory, Department of Materials & Nuclear Engineering, University of Maryland, College Park, MD 20742-2115, USA.

INTERFACES IN CONTINUOUS FILAMENT COMPOSITES

R. J. Arsenault

Metallurgical Materials Laboratory, Dept. of Materials & Nuclear Engineering
University of Maryland, College Park, MD 20742-2115

Interface structures in a continuous Al_2O_3 filament reinforced NiAl composite were investigated by transmission electron microscopy. There appeared to be an intimate bond between the NiAl matrix and the Al_2O_3 filaments. Simulation of TEM diffraction contrast images based upon a three dimensional finite element analysis was employed to investigate the nature of the residual strains in regions along the interface. The simulations suggested that radial residual strains within the Al_2O_3 filaments were randomly distributed along the interface. These strains were believed to be related to dislocation nucleation in the NiAl which results from the relaxation of the thermally generated residual stresses.

1. INTRODUCTION

The use of continuous filaments as composite reinforcements is currently being considered as a means of improving the creep resistance of intermetallics, and there a lot of examples but at present only a specific case will be considered. In particular, it has been demonstrated that single crystal Al_2O_3 filaments are capable of improving both the creep and fatigue resistance of NiAl[1]. The interfacial bond strength, which is strongly dependent upon the processing methods, plays a key role in the control of the mechanical properties of these continuously reinforced composites[1]. The strength of the interfacial bond is important because it strongly influences the thermal residual stresses (TRS) which develops during cooling due to the coefficient of thermal expansion (CTE) mismatch between the filaments and the matrix. In a previous investigation[2] it was found that if an Al_2O_3 /NiAl composite with an as-fabricated interfacial bond strength (measured by push-out testing) in the range of 90-180 MPa was thermally cycled ten times in a temperature range of 373 to 1373 K, matrix cracking occurred. On the other hand, cracks were not observed after identical thermal cycling in those samples which had an interfacial bond strength in a range of 35-120 MPa. Also, the interfacial bond strength of these weakly bonded samples dropped to 5-30 MPa in the post thermal cycled condition. The mechanism responsible for the difference in interfacial bond strength is due to an interfacial graphite islands[3]. It was also confirmed that the NiAl matrix was plastically

deformed as a result of the relaxation of the TRS. Although dislocation densities in the region adjacent to the interface were found to be very high, dislocation generation in the interface region was not necessarily related to the interfacial bond strength since dislocation activity was observed in both weakly and strongly bonded composites.

An electron microscopy investigation was undertaken to determine the interface structures of the single crystal Al_2O_3 filament reinforced NiAl composites. Simulations of TEM diffraction contrast images based upon a three dimensional (3D) finite element method (FEM) analysis were generated to understand the residual strain at regions adjacent to the interface.

2. MATERIALS AND EXPERIMENTAL METHODS

The composites used in this investigation consisted of a stoichiometric NiAl matrix unidirectionally reinforced with six plies of 125 μm diameter, c-axis oriented, continuous, single crystal Al_2O_3 filaments comprising 30 vol.% of the composite, the matrix was fabricated from 50-150 μm diameter vacuum atomized prealloyed powders obtained from Homogeneous Metals, Inc., Clayville, NY. The Al_2O_3 filaments were supplied by Saphiton Inc., Milford, CT. The composites were fabricated using the powder-cloth (P-C) technique[4]. The composites were annealed at 1473 K for 4 hrs followed by furnace cooling. TEM samples of monolithic NiAl were produced via the dimple grinding plus an electro- polishing method. Polishing was performed in a solution of 5% perchloric acid + ethanol at ~253 K with an applied voltage of 50-70 V. The cross-section Al_2O_3/NiAl TEM samples were prepared by dimple grinding plus ion milling as described elsewhere[5].

TEM and X-ray energy dispersive spectra (EDS) analyses were performed on a JEM 2000-FX analytical electron microscope equipped with Noran Voyager system. The foil thickness used in the calculation of the diffraction contrast image was measured by convergent beam electron diffraction (CBED) method[6,7]. An ABAQUS FEM software package was used to simulate the interface strains. The programs used for diffraction contrast simulation of TEM images were written in Interactive Data Language (IDL) running on a Sun work station system.

3. EXPERIMENTAL RESULTS

There were no consistent crystallographic orientation relationships between the filaments and matrix, i.e. the orientations between the filament and matrix were random

as shown in Fig. 1. Neither coherent nor semicoherent interfaces were observed between the filament and matrix. However, HREM investigations of the clean interface indicated that the matrix and filament formed direct contact without noticeable intermediate layer or precipitates, as shown in Fig. 2. It is likely that a randomly direct bond between the Al_2O_3 filament and the NiAl matrix has been achieved on an atomic level at the clean interface.

An unusual observation is that diffraction contrast in the Al_2O_3 filament at the interface was not homogeneous, but rather modulated randomly along the clean interface, as shown in Fig. 1. The wave length of the modulation is around 0.1 μ m. The modulated diffraction contrast disappeared in regions where the foil thickness became less than a two-beam extinction distance with operating diffraction vector of $g=\bar{3}300$, which is less than 95 nm. Different operating diffraction conditions were applied to produce different two-beam diffraction contrast images of the interface area, as shown in Fig. 3(a)-(c). According to an analysis of these images, two important features were observed. First, minimum diffraction contrast was obtained when the diffraction vector was almost parallel to the interface (Fig. 3(c)); second, the shape of the dark and bright areas of the image always tended to parallel the diffraction vector (Fig. 3(a) and (b)). Since there is no precipitation or any other second phase present in this interface region, it is likely that this modulated diffraction contrast is caused by an inhomogeneous distribution of strains which originate at the interface. Also, there was no indication of any interfacial dislocations.

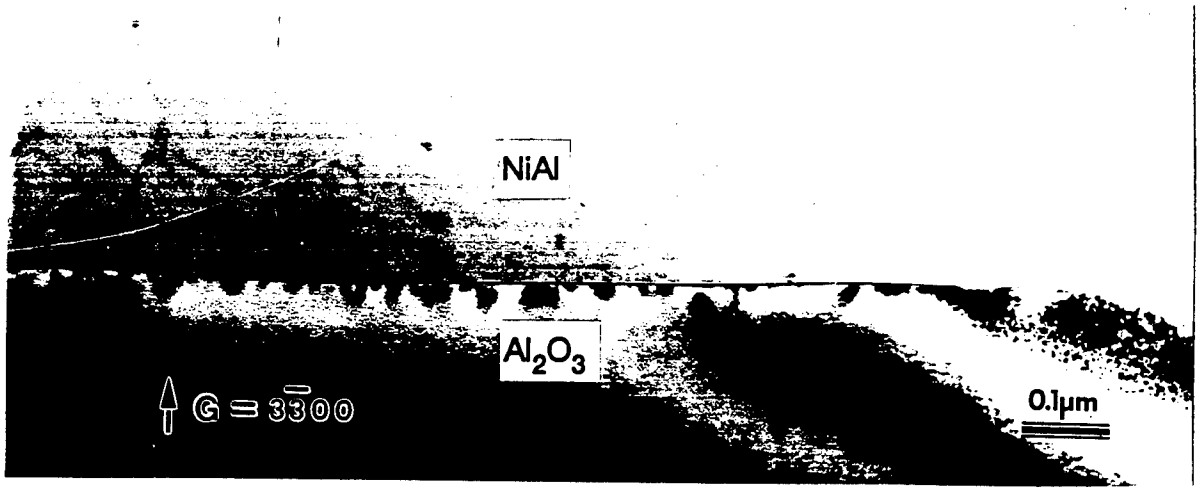

FIGURE 1
TEM micrograph of a clean interface between the single crystal Al_2O_3 filament and NiAl matrix after ten thermal cycles, inhomogeneous diffraction contrast is observed along the interface on the Al_2O_3 filament side.

FIGURE 2
HREM micrograph of the very thin area in Fig. 1.

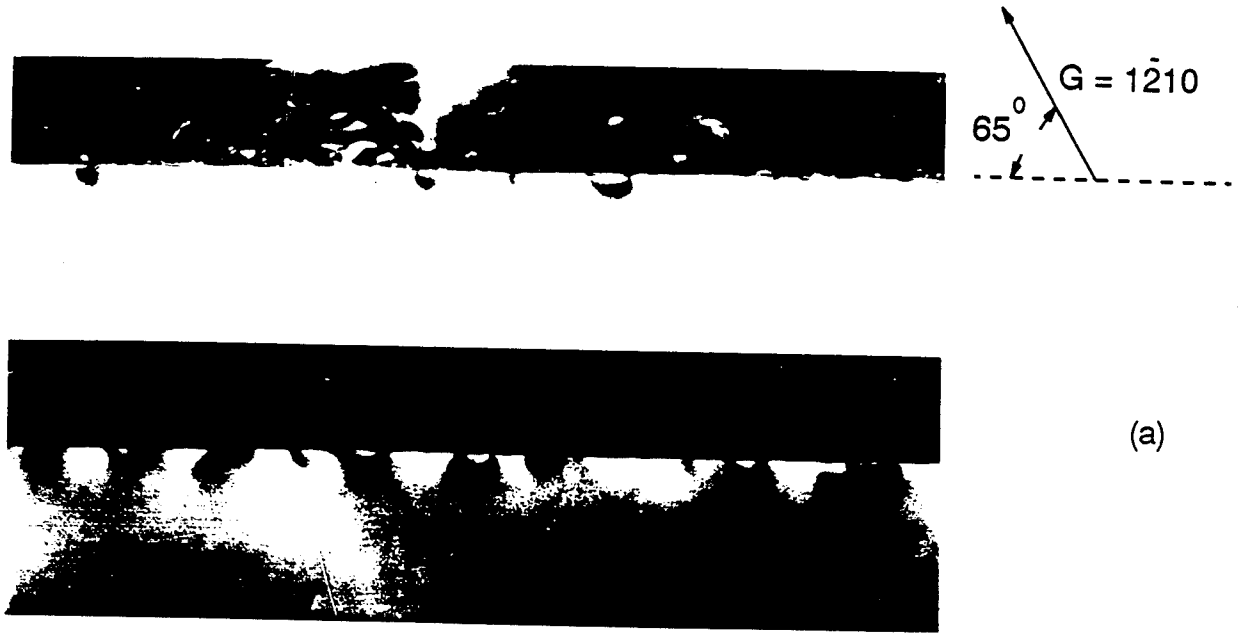

(a)

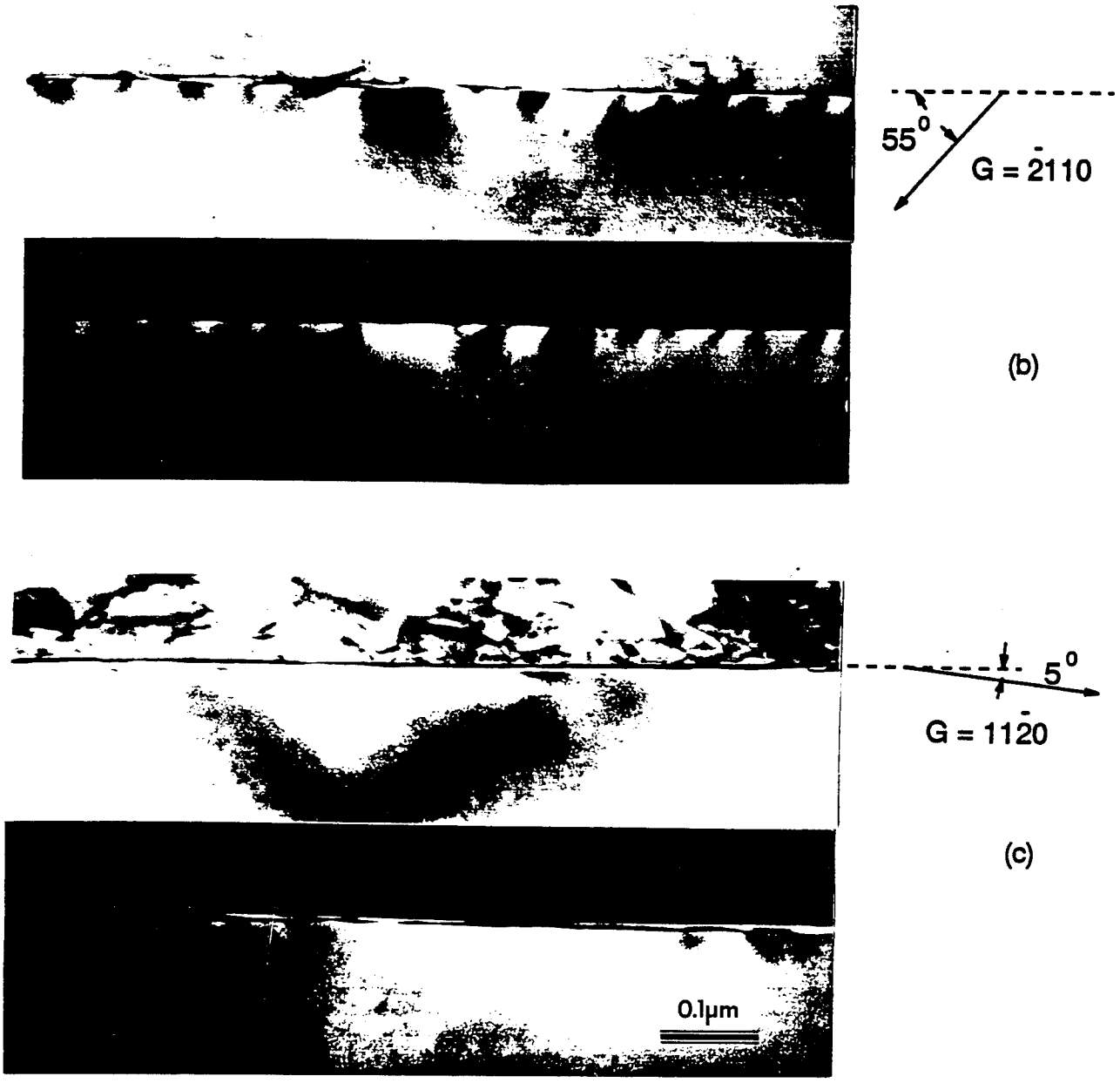

FIGURE 3

TEM micrographs of a clean interface between the single crystal Al_2O_3 filament and NiAl matrix after ten thermal cycles, (a)-(c) bright (top) and dark (bottom) field images of the interface with different operating diffractions, $t=1.3\xi_g$ with $g=11\bar{2}0$.

4. MODELING

To investigate the possible role of interfacial strain on the modulating diffraction contrast described above, an FEM analysis was undertaken to simulate various strain

conditions originating from the interface. From these results TEM diffraction contrast images were then calculated and compared to the observed images.

Since the exact distribution of the randomly modulated strain is unknown, the goal of the current modeling was to reveal the basic character of these inhomogeneous strains along the interface. Comparison was made between the calculated images and the experimental images to see if the main important features of the experimental images described above could be duplicated by a number of simplified models. As shown in Fig. 4, the inhomogeneity of the strains was simulated as concentrated loads or surface tractions which were applied at the interface in an area with a dimension less than an extinction distance (ξ_g). This thickness was chosen since the foil thickness of the region in Fig. 1 was ~ 220 nm, which is ~ $1.3\xi_g$ of $g=11\bar{2}0$. To best fit into the experimental images, the size of the loading area was found to be ~50 nm.

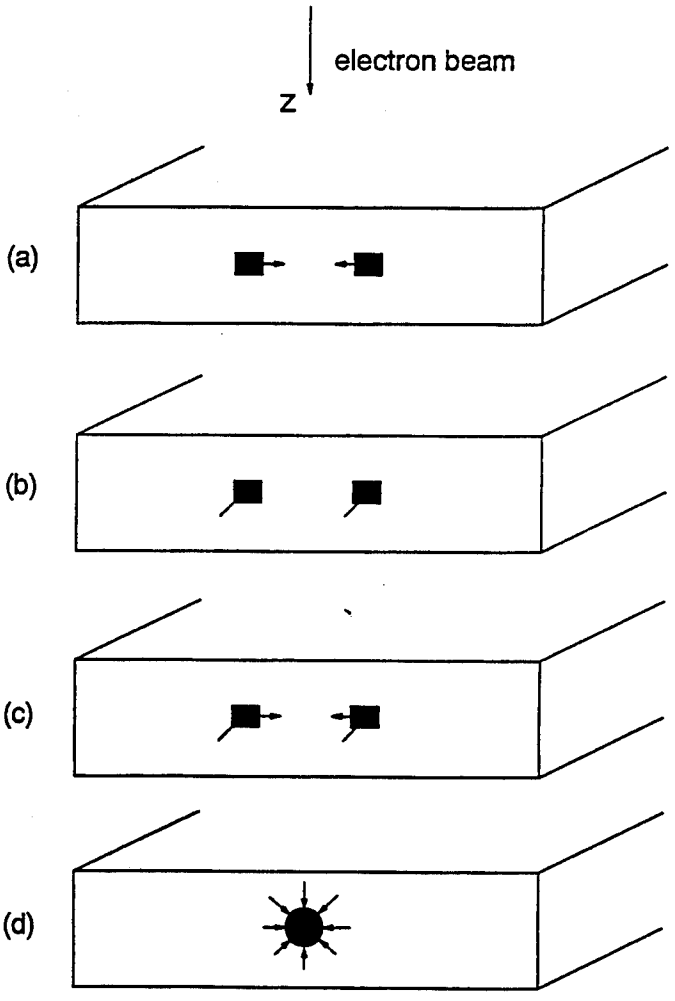

FIGURE 4
Schematic illustrations of FEM models of strains introduced at interface, (a) concentrated shear load, (b) concentrated normal load, (c) both the shear and the normal loading, and (d) surface traction.

Several possible loading configurations were examined. First, a concentrated pure shear load was considered, as shown in Fig. 4(a). The TRS has been partially relaxed due to TEM sample preparation, i.e. the matrix material has been partially removed from the filament surface which could cause a shear stress at the remaining interface region. Second, a normal load was considered, Fig. 4(b), since the TRS will also be in the normal direction if it is not completely relaxed. Fig. 4(c) presents a case of both shear and normal loading. Surface traction, Fig. 4(d), might also be developed during the sample cooling process, if the bond strength of the interface was not homogeneous.

The FEM analyses employed a three dimensional (3D) eight-node linear solid elements and a displacement boundary condition which gave rise to a maximum strain of ~0.001 at the boundary to produce the observed diffraction contrast level. A maximum strain of 0.001 was used throughout the calculations (the corresponding maximum stress was ~ 200 MPa in the Al_2O_3). The diameter of the Al_2O_3 filament is so big (125 μm) that the interface can be approximated as a flat plane on an one-micron scale. According to symmetry, a quarter of the block was considered in all the FEM analyses. An example of the FEM mesh is shown in Fig. 5. Because of to the nature of thin foils used as TEM samples, the boundary conditions of the FEM block were chosen so that the top and bottom surface (plane ABCD in Fig. 5) of the block were free of restrictions, as was the side plane BB'C'C. Following the symmetry requirement, plane AA'D'D and A'B'C'D' were restricted to move in the Y and Z directions, respectively. The interface, which is represented by the plane of ABB'A', had no restrictions whenever there is a normal loading at interface as the boundary condition. In the case of pure shear or surface contraction as the boundary condition, the interface was restricted in the X direction. The plane CC'D'D is totally restricted in the X, Y and Z directions due to the fact that very thin regions of the Al_2O_3 filament in the TEM foils are present only in vicinity of the interface, i.e. the foil thickness soon becomes very thick in the direction towards the center of the filament. Subjected to these boundary conditions, stresses and strains obtained from the FEM analyses are rather localized around the loading area while the top and bottom surface are stress free. Stresses and strains near plane CC'D'D and plane BB'C'C are about 1~2 orders of magnitude smaller than the region close to the loading area. A more elaborate model which includes periodic boundary conditions on the plane of BB'C'C and the matrix constraint is currently being carried out.

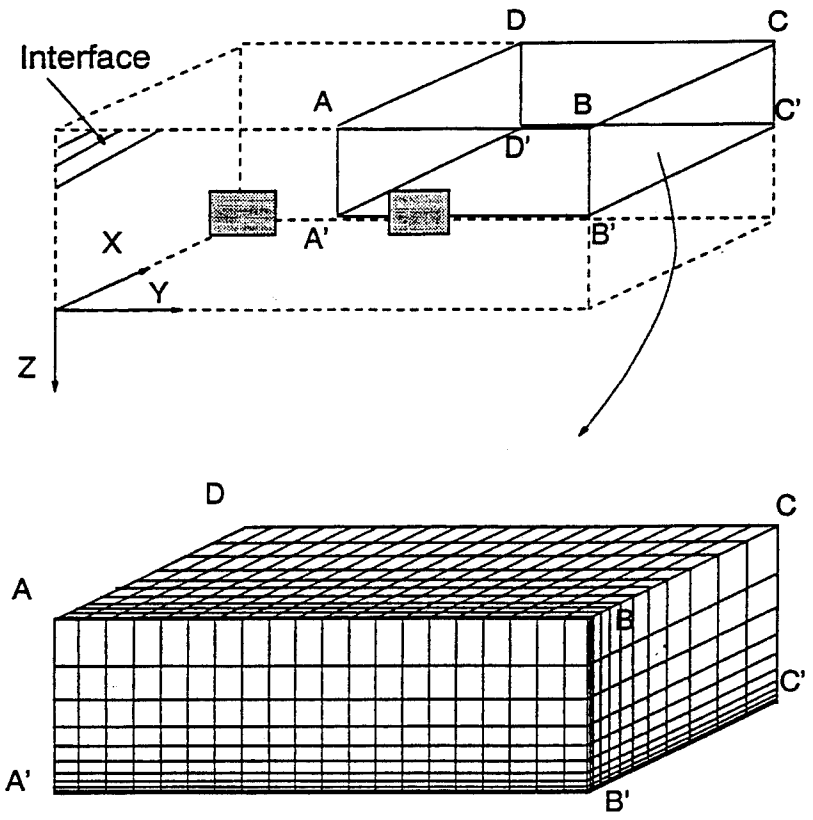

FIGURE 5
An example of the FEM mesh where the 3D 8-node linear solid elements were used in all the FEM analyses. See Table 1 for boundary conditions.

Simulations of diffraction contrast images are based on the dynamical theory of diffraction contrast in the form developed by Howie and Whelan[8]. When two-beam conditions are applied, the amplitude of the transmitted and diffracted beams, i.e. A_0 and A_g, is determined by,

$$\frac{dA_0}{dz} = -\pi a A_0 + \pi(i - a')A_g$$

$$\frac{dA_g}{dz} = -\pi(i - a')A_0 + \pi(-a - 2i(w + \beta'))A_g$$

where

$$\beta' = \frac{d(g.u)}{dz}$$

In these equations, the depth (z) is normalized by the two-beam extinction distance (ξ_g), g is the operating diffraction vector, w is a dimensionless form of the deviation parameter, and u is the displacement field within the sample which causes the diffraction contrast. In the current investigation, u was obtained from the FEM analyses, i.e., the simulated diffraction contrast image was based on the displacement field generated from the FEM analyses. The effect of inelastic scattering was treated phenomenologically by absorption parameters a and a'. Where a is the exponential decay parameter and the a' represents the anomalous absorption. As suggested by Hashimoto et al.[9], and generally adapted by many other investigators, a = a' = 0.1 was used in this investigation.

In the calculation of the diffraction contrast image, the whole FEM block was equally divided into 128 x 128 columns parallel to the electron beam direction. The total image size was 128 x 256 columns, which contains twice as many columns as the FEM block (Fig.5). The advantage of using IDL in the programming is that an integration column-by-column can be avoided. The integration can be done in all the columns simultaneously by matrix operation, i.e., each of the variables in the equations can be represented by a 128 x 128 matrix. Integration of the equations started at $A_0 = 1$ and $A_g = 0$. At each integration step, the displacement matrix from the FEM analyses was inserted into these equations. Displacements between the FEM nodes were linearly interpolated from the nearest neighbor nodes. The integration was terminated at the desired foil thickness. The resulting diffraction contrast matrix was then normalized into a 256 gray level black and white image. Zero intensity was taken as complete darkness in all the simulated images.

The calculated TEM diffraction contrast images corresponding to the loading conditions depicted in Fig. 4 are shown in Fig. 6. These images were calculated using the same diffraction conditions and foil thickness as those of the experimental images (Fig.1). It turns out that only the simple normal loading model (Fig. 6b) can duplicate all the major features of the experimental images. The contrast is localized around the loading area (in a range of ~ 0.1 μm from interface) which indicates that the residual strains are concentrated at that region. Furthermore, changes of the location of the loading area in the depth direction (z-direction) will not drastically change the basic features of the calculated diffraction contrast images.

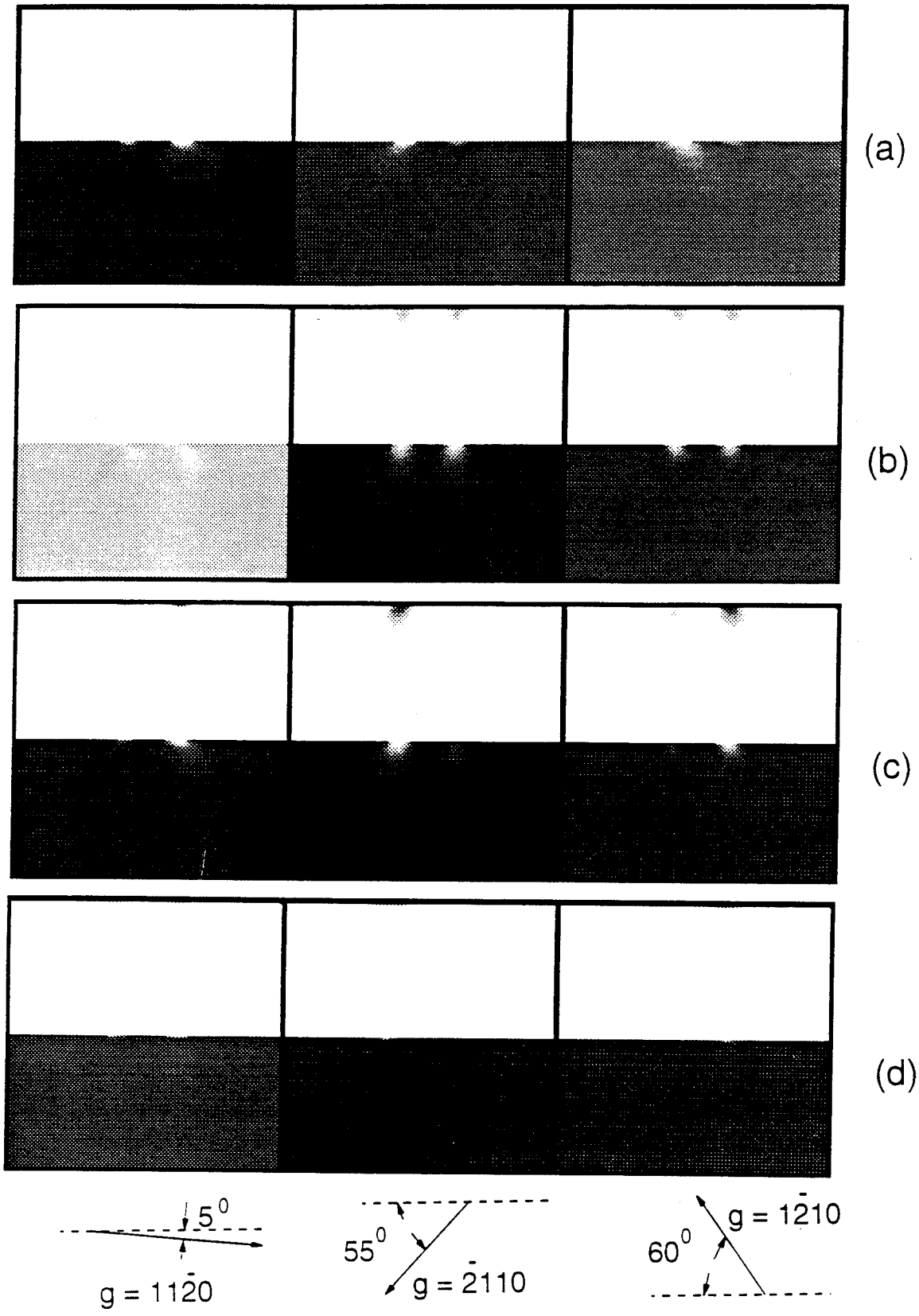

FIGURE 6

Bright filed (top) and dark field (bottom) diffraction contrast image simulations of the FEM model under different diffraction conditions, w=1.0, and t=1.3ξ_g, (a) concentrate shear load, (b) concentrate normal load, (c) both shear and normal, and (d) surface traction.

5. DISCUSSION

The modulated diffraction contrast of the clean interface may be caused by an inhomogeneous distribution of normal residual strain along the interface. The data obtained from the simulation indicates that the magnitude of the strain at interface should be at least ~10^{-3} and localized around the interface in a range of ~0.1 μm. It is unknown why the normal residual strain would modulate along the interface and how it is exactly distributed. One possible reason is that due to the relaxation of TRS the plastic deformation in NiAl is not microscopically homogeneous, i.e. the dislocation generation in NiAl created an inhomogeneous "back stress" towards the filament. Since the filament cannot be plastically deformed, this back stress will build up a considerable elastic strain in the filament. One supporting observation is that the modulated diffraction contrast does disappear in very thin area (less than ~90 nm), i.e. the edge of perforation hole of the TEM sample, where dislocations have escaped from the foil in that area.

Semicoherent interfaces between Al_2O_3 and NiAl have been observed in a XD processed TiB_2/NiAl composite which contained Al_2O_3 particles. In that system low indexed crystallographic planes of both α-Al_2O_3 and NiAl were aligned[10]. The current investigation does not rule out the possibility of the existence of a semicoherent interface between the Al_2O_3 and NiAl, but none were observed. One important difference between the XD-processed TiB_2/NiAl composite and the current composite is that in the current composite dislocation generation due to TRS has occurred. This dislocation generation was not observed in the XD processed TiB_2/NiAl composite. In general, plastic deformation by dislocation motion is considered microscopically inhomogeneous and therefore modulation of strains is expected to occur in all regions of the ceramic-metal interface where the metal phase undergoes plastic deformation and the ceramic phase remains elastic.

6. CONCLUSIONS

From the data generated in the present investigation, the following conclusions can be drawn.

The matrix and filament bonded without any noticeable intermediate layer or precipitates. It is likely that a random direct bond between Al_2O_3 filaments and NiAl matrix was achieved at an atomic level at the clean interfaces. Modulating diffraction contrast

along the interface suggest that radial residual strains within the Al_2O_3 are inhomogeneously distributed along the interface. It is believed that the random modulation of the radial residual strains in the Al_2O_3 filament along the interface is caused by plastic deformation of the NiAl matrix.

7. ACKNOWLEDGEMENTS

The author wishes to acknowledge the assistance of Drs. L. Wang and R.R. Bowmann and Mr. K. Xu. He also wishes to acknowledge the continualy support of Dr. S. Fishman of the Office of Naval Research. The work was supported by the Office of Naval Research under grant N00014-94-10118.

REFERENCES

1) R. R. Bowman, in Intermetallic Matrix Composites II, proceedings of the Materials Research Society Symposium, vol, 273, D.B. Miracle, D.L. Anton, and J.A. Gravees, eds., 1992, p. 145.

2) L. Wang, R. R. Bowman and R. J. Arsenault, to be published.

3) L. Wang, K. Xu, R.R. Bownmann and R.J. Arsenault, to be published.

4) J.W. Pickens, R.D. Noebe, G.K. Watson, P.K. Brindley and S.L. Draper, NASA Technical Memorandum 102060 (1989).

5) R. J. Arsenault, L. Wang and C. R. Feng, Acta Metall. Mater., 39 (1991) 47.

6) S.M. Allen, Phil. Mag. A43 (1981) 325.

7) P.M. Kelly, A. Jostsons, R.G. Blake and J.G. Napier, Phys. Stat. Sol. A31 (1975) 771.

8) A. Howie, and M.J. Whelan, Proc. Roy, Soc. A 263 (1962) 217.

9) H. Hashimoto, A. Howie, and M.J. Whelan, Phil. Mag. 5 (1960) 967.

10) L. Wang and R.J. Arsenault, Metall. Trans. 22A (1991) 3013.

Annu. Rev. Mater. Sci. 1994. 24: 321–57

PLASTIC FLOW IN SiC/Al COMPOSITES—STRENGTHENING AND DUCTILITY

N. Shi

CMS/LANSCE, Los Alamos National Laboratory, Los Alamos, New Mexico 87545

R. J. Arsenault

Metallurgical Materials Laboratory, Department of Materials and Nuclear Engineering, University of Maryland, College Park, Maryland 20742–2115

KEY WORDS: DMMCs, strengthening, ductility, asymmetric, constitutive behavior, failure mechanisms, plastic flow

INTRODUCTION

Composite materials are of interest for structural applications because they have high specific strengths and stiffnesses, and discontinuously reinforced metal matrix composites (DMMCs) have advantages because of their relatively low cost of production. Understanding matrix plastic flow in DMMCs is useful because of the influence of matrix flow characteristics on composite strength and ductility.

The theories of plastic deformation of DMMCs originated from an understanding of dispersion strengthening of a "monolithic" material, where detailed elastic interactions of the field quantities from an array of dislocations and sub-micron particles are considered. The strengthening from incoherent non-shearable dispersoids mainly comes from the inability of dislocations to glide through the particles, in which case the activation of other mechanisms are needed that normally require a higher energy (stress). A well studied case is the Orowan mechanism (1). The strengthen-

0084–6600/94/0801–0321$05.00

ing can also come from a continuity requirement wherein a network of "geometrically necessary dislocations" is generated (2). This is equivalent to the concept of "plastic misfit" used by the continuum mechanicians. A series of early investigations (3) on Cu-SiO_2 brought many fundamental insights that are useful in understanding the plastic deformation of what are now referred to as DMMCs.

A uniqueness of DMMCs that separates them from the dispersion-strengthened alloys is that the size of the second-phase reinforcement is larger in DMMCs. Typically, the average size of the reinforcement particle is of the same order as the dislocation slip distance in the matrix. Therefore, interactions between individual dislocations and the particles become less trackable during deformation. On the other hand, due to a comparable size scale between the matrix microstructure and the reinforcement, the necessary material smoothness required for a continuum analysis is not rigorously satisfied. Therefore, continuum analyses based on phenomenological constitutive models can no longer be applied without careful considerations.

Despite the above uncertainties, with the advent of the finite element method (FEM), continuum modeling of composite mechanical properties using a unit cell model has had great success in recent years. With the unit cell model the particles in a composite are assumed to take the form of a periodic array of particles in an infinite matrix; such an ideal composite may then be divided into an array of self-repeating unit cells. The material smoothness requirement is circumvented by an implicit averaging scheme in which field quantities at a representative location within the unit cell are taken as averages of those at the equivalent locations over all the repeating unit cells. Therefore, any local microstructural perturbation that may otherwise affect the development of the local field quantities is likely to be averaged out at the unit cell level. The mean field model (4), which is based on the Eshelby stress-free transformation theory (5), is another popular method in modeling the mechanical properties of DMMCs. The continuum assumption, in this case, is accurate in a sense that the basic and the smallest geometrical entities are the domains of the matrix and the reinforcements within which the average field quantities are defined.

Despite the size factor, reinforcements in DMMCs in other aspects may have similar effects as dispersoids in dispersion-strengthened solids. For example, extensive matrix metallurgical modifications can occur due to the presence of the inclusions. Therefore, construction of a phenomenological constitutive relationship that adequately describes the behavior of the in situ phases sometimes become difficult. Local microstructure variations may promote early deformation instabilities such as crack initiation and void nucleation during loading. These spatially localized and nonperiodic

events are generally beyond the immediate reach of the aforementioned unit cell and mean field averaging schemes. Therefore, understanding and further enhancement of the performance of DMMCs require a concerted effort from both material scientists and continuum mechanicians. There have been several extensive reviews reflecting this effort (6–9).

In this article, we review recent developments in the understanding of plastic flow in DMMCs and its impact on the strengthening and ductility of DMMCs. We concentrate on, but are not restricted to, SiC/Al DMMCs, and most of the results also apply to other ceramic-reinforced DMMCs. We cover subjects including (*a*) strengthening, (*b*) generation of residual stresses, (*c*) asymmetrical plastic flow and constitutive behavior due to thermal residual stresses (TRS) under tensile and compressive loading, and (*d*) the effect of work hardening of the matrix, localized plastic flow, and reinforcement distribution on the ductility of the composites.

STRENGTHENING

Several sources that may contribute to the strengthening of DMMCs generally include (*a*) reinforcement constraints to matrix plastic flow and/or matrix dislocation motion, (*b*) load partition between phases, and (*c*) thermally induced work hardening.

The effect of particles on the development of matrix plasticity may be revealed by studying the constraints by the particles to either the explicit dislocation motion or the phenomenological matrix plastic flow. In DMMCs, despite the inherent complexity involved with the explicit dislocation interactions from the particle size scale (see Introduction), there have been several attempts using this approach based on simplified models. The Orowan strengthening mechanism has been proposed as an applicable mechanism for DMMCs. Lederich & Sastry (10) and Miller & Humphreys (11) estimated the contribution of the Orowan loops in the strengthening of the SiC/Al DMMCs and argued that these loops could account for the observed strength increases. However, the possible strengthening has been shown to be very small (12).

As another attempt to study the effect of the reinforcement on the matrix plastic flow, Christman et al (13) employed a phenomenological approach by using the unit cell model and performed a comprehensive FEM modeling of the composite elasto-plastic response under static loading. They found that large triaxial stresses were developed as a result of the addition of plastically nondeformable reinforcement, and the strengthening scaled with the magnitude of the triaxial stresses (13, 14). Following Drucker (15), they pointed out that plastic flow in the matrix is "constrained" by a lack of deviatoric stresses. By accounting for the development of triaxial

stresses, they obtained good agreement with the experimental stress–strain relations and suggested that the constrained-plastic flow (15) is the strengthening mechanism for SiC/Al DMMCs. This is further illustrated by McHugh et al (16), who have shown that increasing the reinforcement volume fraction results in increases in the amount of matrix that experiences higher triaxial stresses. However, Shi et al (17) have shown that the matrix triaxiality at the same load level decreased when the plastic relaxation of thermal misfit during the cooling process is considered. This suggests that other contributing factors may be needed in maintaining a similar composite strength.

If load transfer occurs through interfacial shear loading between the ductile matrix and the high strength short fibers, then the stresses in the fiber will be greater than those in the matrix, which leads to strengthening to the composite. This is commonly called the shear lag model and was first analyzed by Cox in the 1950s (18). Later, Nardone & Prewo (19) applied this method to predict the yield strength of a whisker-reinforced SiC/Al composite, with an assumption that the stress at the tip of the whiskers is the same as the matrix yield stress. They found good numerical agreement with a selected set of experimental data. In the shear lag model, emphasis is placed on the stress partitions through interfacial shear load transfer arising from elastic misfit between the matrix and the inclusions. Using a mean field approach, Taya & Arsenault (20), on the other hand, showed that by considering stress partition via elasto-plastic misfit during deformation and ignoring the precise transfer mechanisms (Eshelby model), a more rigorous solution for the load partitions could be obtained. However, the strengthening predicted is much smaller than observed experimentally (6) (Figure 1). Data from a larger population of tested SiC-reinforced Al DMMCs (21) have shown that strength variations observed in the composite cannot be consistently explained by a load transfer mechanism. This suggests that other parameters may also play a role.

Arsenault and co-workers have shown (22, 23) that a high dislocation density in the matrix is induced in SiC/Al composites by plastic relaxation of thermal stresses because of the difference in the coefficients of thermal expansion (ΔCTE) during cooling from annealing or processing temperature (Figure 2). Similar TEM observations of the high matrix dislocation density were also made by other investigators (24–28). Based on the experimental evidence of a high dislocation density, Arsenault proposed that the high matrix dislocation density should account for the observed strengthening (29). To study the postulation of dislocation strengthening, Arsenault & Shi (30) developed a model based on prismatic punching of dislocations, in which the thermal mismatch is assumed to be completely relaxed through dislocation generation. They predicted (30) that the increase in dislocation

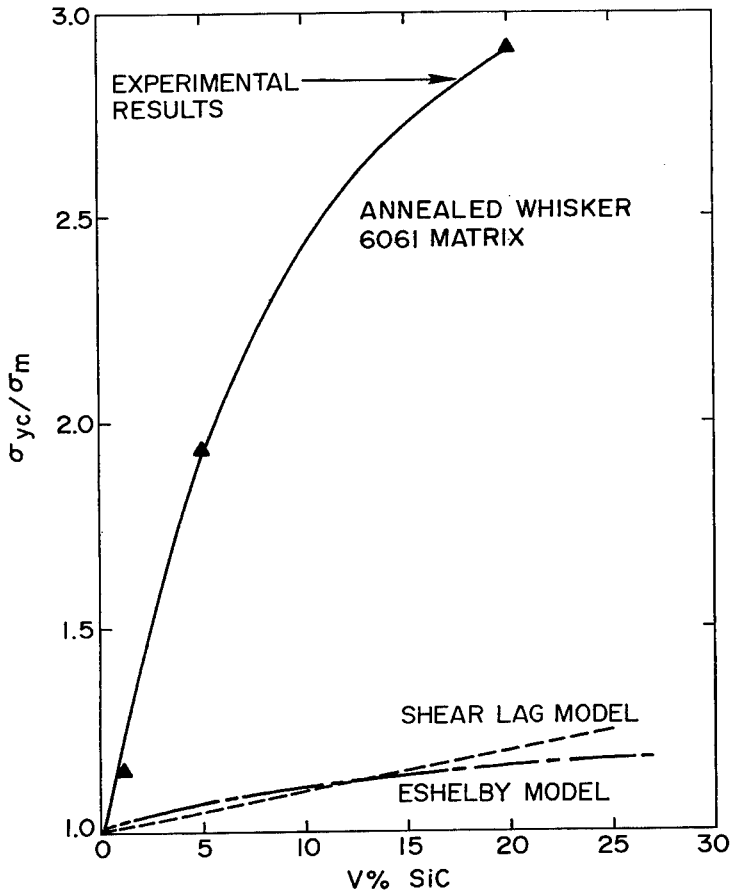

Figure 1 The ratio of the yield stress of 20 vol% composite to that of matrix vs the volume fraction of the whiskers, as estimated from the shear lag and the Eshelby model and compared with experiment (from 20).

density ($\Delta\rho$) due to the thermal mismatch is proportional to

$$\Delta\rho \sim \frac{V_i\varepsilon}{b(1-V_i)}\frac{1}{t}, \qquad 1.$$

where b is the Burger's vector, ε is the thermal misfit strain prior to plastic relaxation, V_i is the reinforcement volume fraction, and t is the smallest reinforcement dimension. Since prismatic punching is the most efficient mode for plastic relaxation of misfit strain, Equation 1 represents a lower limit on the dislocation density that can be used to calculate the flow stress increase from

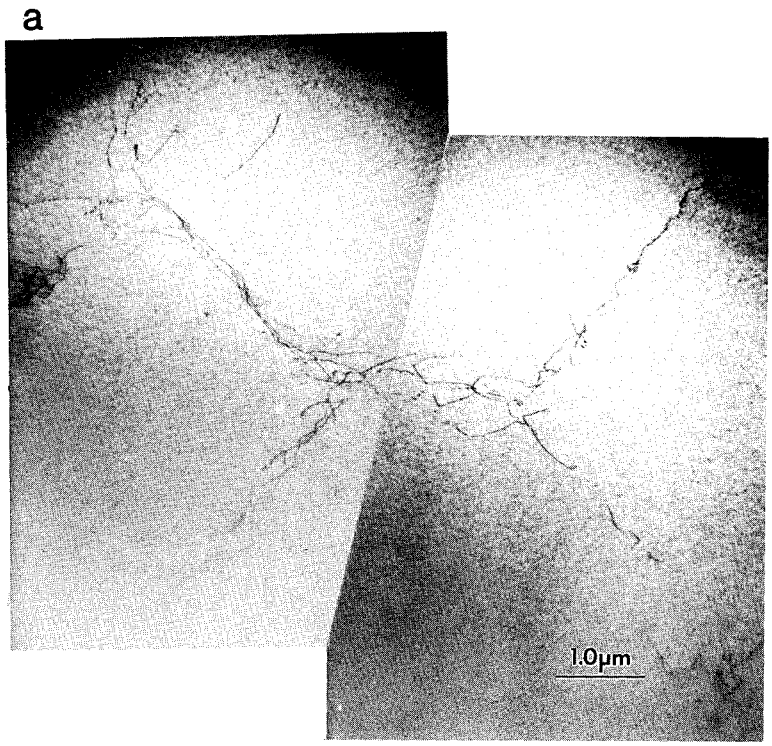

Figure 2 TEM micrograph showing dislocation structure (*a*) of the unreinforced control alloy; and (*b*) in the matrix of a 20 vol% SiC reinforced Al composite (from 31).

$$\Delta\sigma = \alpha\mu b\sqrt{\Delta\rho}, \qquad 2.$$

where μ is the shear modulus, and α is a material-dependent constant. Arsenault & Shi found that the agreement was good when the particle size is small (<1 μm) as shown in Figure 3. To experimentally correlate the strength increase and the matrix dislocation density, Arsenault et al (31) showed that a cold-rolled unreinforced 1100 Al may display a higher yield strength than that of a 20 vol% SiC_p/1100 Al composite, in which only 10% of the dislocation density was observed as compared with that in the composite.

Due to the potential role of the thermal mismatch-induced dislocations in the strengthening of DMMCs, the interest in the generation of mismatch dislocations was revived. Using the mean field method, Taya and co-workers (32, 33) studied the punching distance of the thermal mismatch dislocations by extending the misfit interface into the matrix to simulate the movement of the mismatch dislocation. The equilibrium punching

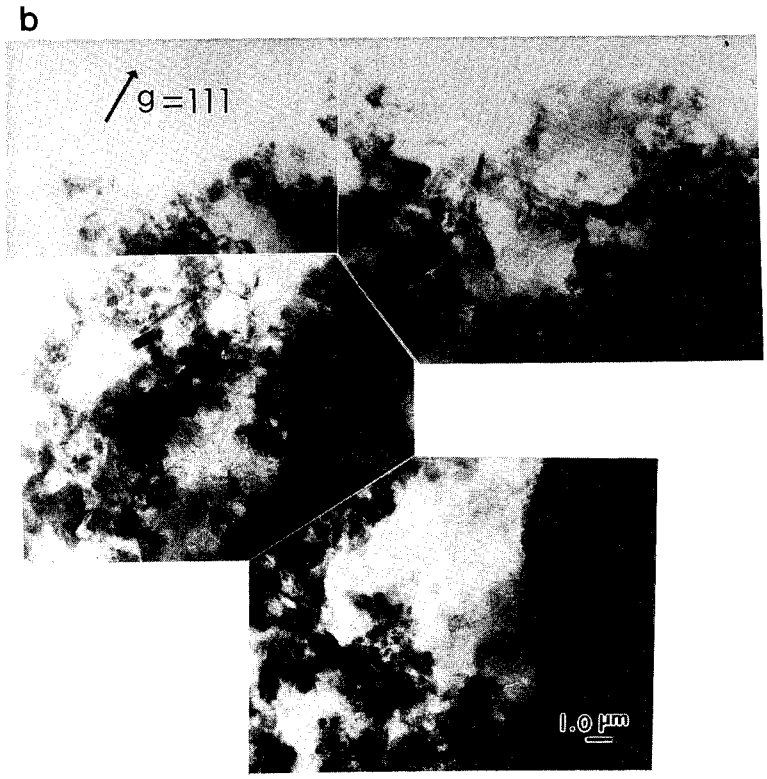

Figure 2—(continued).

distance was obtained by determining the minimum of the available total potential energy of the system comprised of the elastic strain energy less the work done by the dislocation motion. Flom & Arsenault (34) studied the generation of slip lines during thermal cycling of a SiC filament embedded in an Al cylinder. Dunand & Mortensen performed a comprehensive study of prismatic dislocation relaxation resulting from Al_2O_3 whiskers (35) or SiO_2 spheres (36) in a silver chloride matrix. To rationalize their experimental results from the whisker composite, they used the shear lag model to study the punching distance (35). For spherical particles (36), they employed an existing model by Hill (37), which predicts the plastic zone size from misfitting particles. The predicted plastic zone size was then corrected based on the work hardening resulting from thermal mismatch dislocations according to Equation 2. Kim et al (25) derived the thermal mismatch dislocation density from plastic energy density obtained from a continuum model. The results were consistent with TEM observations. Complimentary to prismatic punching, Shieu & Sass (38) observed that

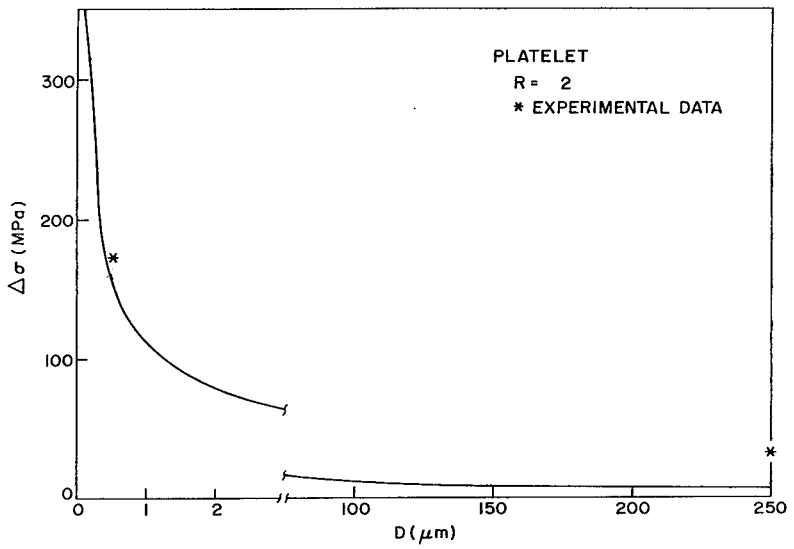

Figure 3 The calculated increase of yield strength of a 20 vol% SiC/Al composite over that of the unreinforced matrix resulting from prismatic dislocations punched from relaxation of thermal misfit (from 30). The $\Delta\sigma$ along the vertex represents the strengthening over the matrix ($\sigma_{yc} - \sigma_{ym}$). The aspect ratio (R) of the SiC platelets is 2.

thermal stresses in composites might be relieved by climb and glide of interfacial misfit dislocations. Albeit different approaches, the results from these investigations generally suggest that plastic relaxation of thermal stresses extend well into the matrix.

Although, in many cases, a high matrix dislocation density in SiC/Al due to ΔCTE has been confirmed, its role in the strengthening of DMMCs is still under debate. Christman et al (39) compared the peak microhardness of an artificially aged SiC_w/2124 Al composite with that of an unreinforced control alloy. They found that the difference was small and concluded (24, 39) that the thermally induced dislocations in the matrix played a minimal role in the strengthening of this composite. However, possible solute segregations near the particle-matrix interface, which have been confirmed in similar composites (40), may alter the chemistry of the matrix, and hence the in situ mechanical properties of the matrix (41). In a similar experiment, Derby & Walker (42) avoided this uncertainty by using a nominally pure, air-atomized Al matrix. They found that, upon quenching from different elevated temperatures, the matrix microhardness was always substantially higher than the unreinforced Al, and the matrix hardness increased with the quenching temperatures. Yang et al (43) also observed a 40% increase

Table 1 Comparison of composite matrix in situ microhardness and that of the unreinforced alloy

	Reference	Composite matrix	Unreinforced alloy
VHN	(43)	690	500
(MPa)	(42)	~640	~250
	(39)	~1048	~1009

in composite matrix in situ microhardness over the unreinforced alloy. The microhardnesses from these studies are listed in Table 1.

In addition to dislocation strengthening, Arsenault et al (31) further suggested that reduction of dislocation cell size also contributed to the strengthening of SiC/Al DMMCs. Using the McQueen & Jonas empirical relations (44, 45), Arsenault and co-workers (31, 46) estimated the contribution to strengthening from the refinement of the matrix dislocation cell size and found that the additional cell-strengthening was significant (Table 2). Kamat et al (47) found that the yield strength of Al_2O_3/Al DMMCs was proportional to the inverse of the interparticle spacing and therefore to that of dislocation cell size (48). They then suggested that it is the dislocation cell structure, formed by thermally and mechanically induced dislocations, that may be directly responsible for the strengthening.

To achieve good correlations with experiments, Pickard et al (26) found it necessary to invoke an in situ matrix reference strength in FEM calculations that is higher than that of the unreinforced alloy. Once the in situ matrix strength is empirically determined, good agreement can be

Table 2 Predicted increases in yield stress of 6061 Al alloy as a function of volume fraction of SiC_w from experimentally measured dislocation density, subgrain (dislocation cell) size, and residual stresses (31)

Vol%	$\Delta\sigma_p$ (MPa)	$\Delta\sigma_{SG}$ (MPa)	$\Delta\sigma_{res}$[a] (MPa)	$\Delta\sigma_{ypred}$[b] (MPa)	$\Delta\sigma_{yexp}$ (MPa)
1	37.7	0.0	1.7	36.0	6.9
5	56.6	7.0	8.6	55.0	52.0
20	70.0	48.3	34.5	83.8	100.0

[a] See text for effect of thermal residual stresses.

[b] $\Delta\sigma_{ypred} = \Delta\sigma_p + \Delta\sigma_{SG} - \Delta\sigma_{res}$, where $\Delta\sigma_p$, $\Delta\sigma_{SG}$ and $\Delta\sigma_{res}$ are strength differentials due to dislocations, subgrains, and thermal residual stresses, respectively.

obtained with the experiments for composites with different SiC volume fractions and cooling temperatures. This is consistent with the notion that variation of the matrix in situ strength induced by the thermally induced microstructural changes in the composite must be considered for composite strengthening.

Shi et al (17) realized that the matrix in situ strength increase resulting from thermally enhanced dislocation density, i.e. the ΔCTE effect, in DMMCs may be modeled through a phenomenological approach by accounting for the matrix work hardening during thermal loading from the cooling process. In a 20 vol%.SiC_w/Al composite, their FEM results indicated that the matrix in situ strength at the tip of the whisker was about twice that

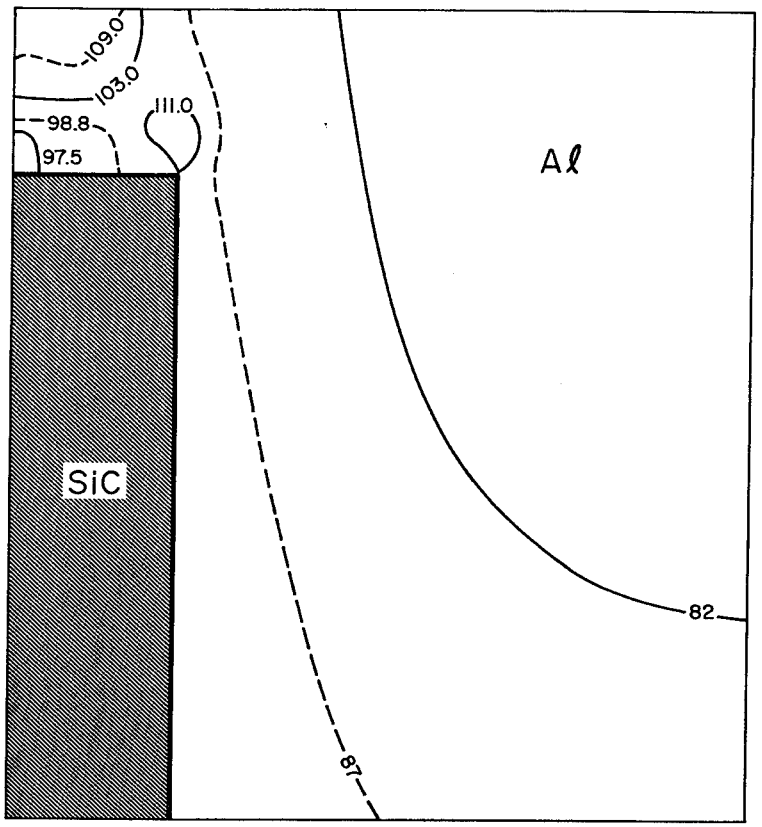

Figure 4 The in situ Von Mises yield stress contours (in MPa) predicted by FEM with cooling of 480°C in an annealed SiC_w 6061-Al (σ_y = 55.2 MPa) (from 17). The variation of the in situ matrix strength results from the ΔCTE-induced work hardening.

of the unreinforced alloy because of thermally induced work hardening as shown in Figure 4. They further pointed out that only those regions in the matrix contributed to the strengthening where the longitudinal TRS was of the opposite sense to the applied field. That is, the region where the movement of the dislocations due to applied field was opposed by the TRS. For tensile loading, this region has been identified at the tip of the whiskers (17). They also showed that by considering the cooling process the strength of the composite increased by 50% (Figure 5), which is consistent with Taya et al (33), who combined the strengthening from prismatic dislocations (32) and load partition from elasto-plastic misfit (20, 49). Similar numerical results as in (17) were also obtained by Nakamura & Suresh (50). However, they attributed this increase of strength to the TRS rather than to the thermally induced matrix work hardening, as suggested in (17). On the other hand, McHugh et al (51) showed via a physical slip model that the ΔCTE effect had little influence on the room temperature constitutive behavior.

To identify possible sources of thermally related strengthening, Shi et al (17), using FEM, studied the contributions from other previously proposed factors that could affect the composite flow behavior, e.g. the constraint to plastic flow and the TRS. They argued (17) that the constrained plastic

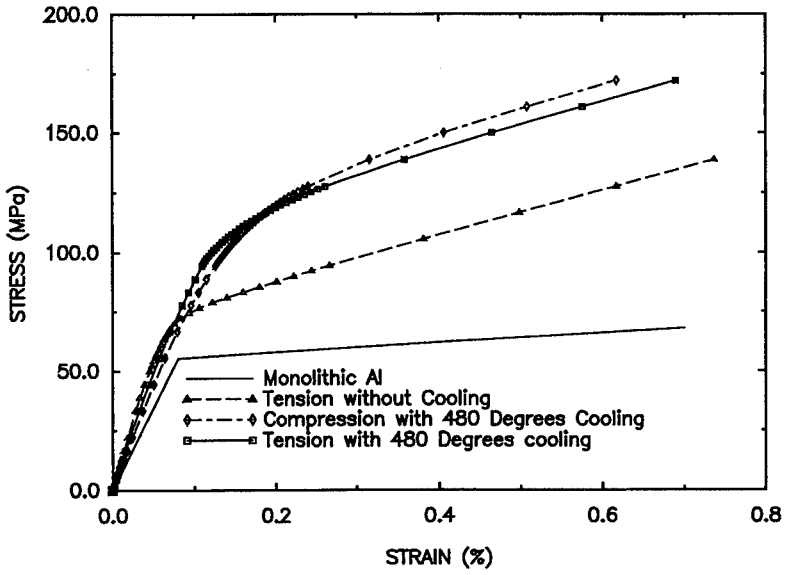

Figure 5 FEM predictions of the effect of ΔCTE on the stress–strain curves of 20 vol% SiC_w/Al composite. Both tensile and compressive curves are shown (from 17).

flow should not contribute to the thermally induced strengthening because of a decrease in matrix triaxial stresses from cooling [but this mechanism did make a contribution to the overall strengthening (13, 52)]. Within the context of mean field interaction, they suggested that the effect of TRS on the strength of a perfectly bonded composite should be related primarily to the difference between the tensile and compressive yield strengths (Figure 5), i.e. $\Delta\sigma_{res} = \frac{1}{2}|\sigma_y^c - \sigma_y^t|$. This comes from the fact that the tensile matrix TRS (53, 54) results in a reduction in the tensile yield stress and an increase in the compressive yield stress. Estimation from this method (17) led to about a 10% difference in the composite strength, which is consistent with estimations from dislocation mechanics (35). Therefore, they suggested that (17) contributions to the strength increase induced by cooling were small from these sources.

In summary, the strengthening of DMMCs can be attributed to two sources; while constrained-plastic flow and stress partition may be responsible for the composite strengthening in the absence of the ΔCTE effect, the contributions of the ΔCTE-induced matrix work hardening is significant to the strengthening.

THERMALLY INDUCED PLASTIC FLOW AND COMPOSITE ASYMMETRIC CONSTITUTIVE BEHAVIOR

For SiC/Al DMMCs, the stiffness and the yield strength are usually greater than that of the unreinforced matrix, and the ductility generally decreases (21). When a DMMC is exposed to a cyclic load, the constant stress-ratio fatigue life is noticeably better than the matrix (55, 56). In addition to these general trends, there are other intriguing characteristics that may lead to immediate insights into the deformation processes of DMMCs. For example, the proportional limit of DMMCs is usually very low (57) (much less than that of the unreinforced alloy) (see Table 3); the initial

Table 3 Selected tensile properties for 20 vol% SiC_w/2124 Al with different heat treatment (57)

Material	Condition	σ_{pl} (MPa)	$\sigma_{0.2}$ (MPa)	σ_{UTS} (MPa)
PM 2124	T4	386	414	587
PM 2124	T6	386	400	566
PM 2124	O	76	110	214
SiC/2124 Al	T4	352	497	890
SiC/2124 Al	T6	324	497	800
SiC/2124 Al	O	62	221	504

work hardening rate is high (57, 58), and it decreases when, for example, the 0.2% proof strain is reached. For composites tested in tension or compression, the tensile stiffness of the composite is higher than the compressive stiffness (59), while the compressive yield strength is higher than the tensile yield strength (49, 59) (Figure 6). If a Bauschinger test is conducted, softening in the reverse cycle (as characterized by the Bauschinger stress factor and the Bauschinger strain) is larger when the composite is tested in the compression-first loading scheme (59) (Figure 7).

Levy & Papazian (60), Shi et al (17) and, more recently, Davis & Allison (61) studied the influence of the thermally induced plasticity on the subsequent tensile behavior in a whisker composite. Their data indicated that matrix microplastic flow started near the longitudinal matrix-reinforcement interface upon initial loading. The plasticity went through a "plastic zone expansion and interconnection" process (17). It was shown that (17) with a 20 vol% SiC whiskers DMMC and a cooling of 480°C, the thermally induced plasticity spread over the entire matrix. Upon initial tensile loading, local unloading of TRS occurred at the tip of the whisker. Within this loading range, the stress–strain relationship remained approxi-

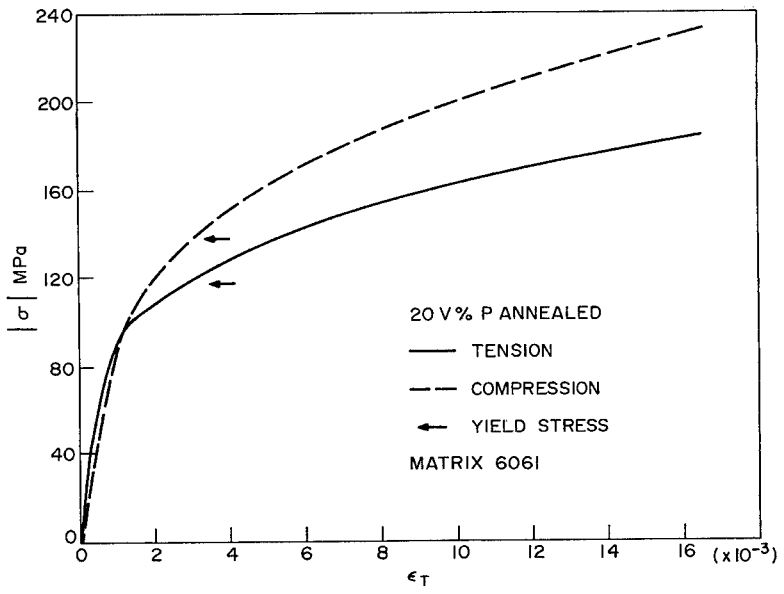

Figure 6 Experimental tensile and compressive stress–strain curves from an annealed 20 vol% SiC_p/6061 Al composite: *solid line*, sample tested in tension; *broken line*, sample tested in compression (59).

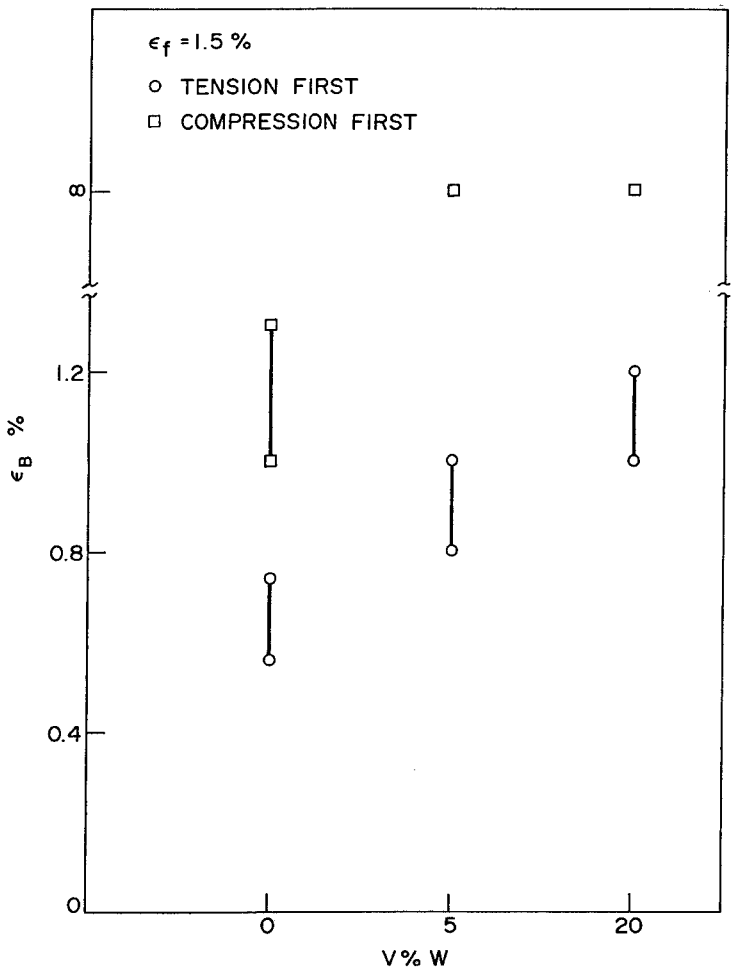

Figure 7 A plot of the experimental values of Bauschinger strain vs the volume fraction of whiskers in a composite with an Al alloy 6061 matrix for both tension-first (*circle*) and compression-first (*square*) tests (59) (the forward prestrain is 1.5%).

mately linear because the matrix plastic flow was unable to spread back into the unloading zone, halted by elastic unloading in the region, as shown in Figures 8 and 9. Because of the co-existence of the elastic and plastic matrices during loading, the stiffness measured from the stress–strain curve was an apparent Young's modulus (17, 50, 62), which was lower than the intrinsic value of the composite (17); the initial linear region should be

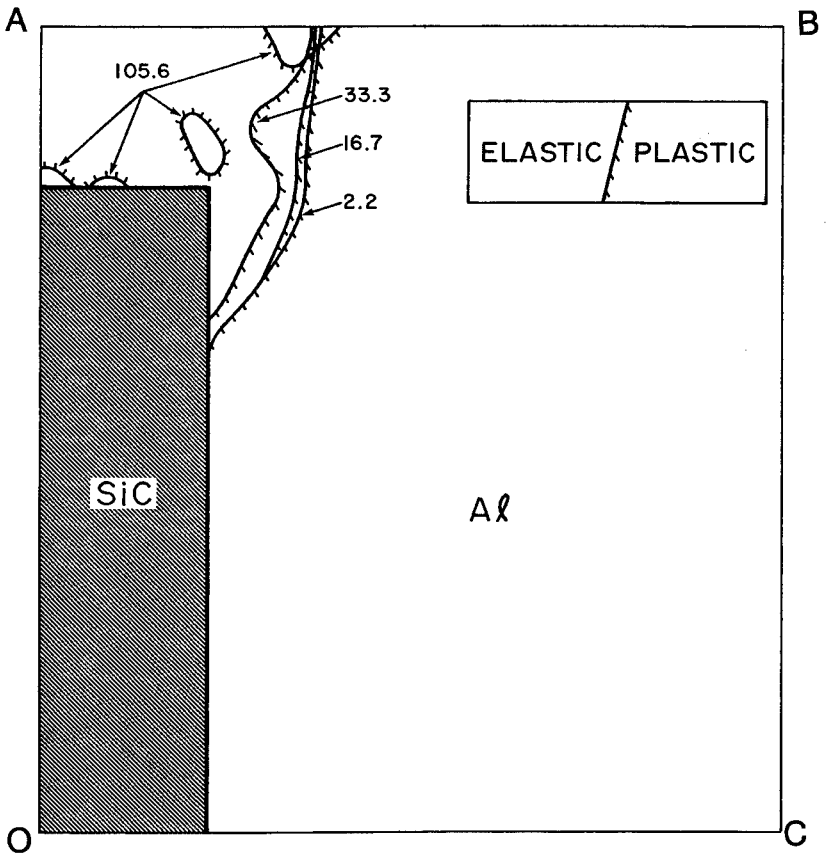

Figure 8 The process of plastic zone expansion and interconnection as revealed by FEM in the matrix of a 20 vol% SiC_w/Al composite with cooling of 480°C. The applied tensile stress (in MPa) is marked along the corresponding plastic zone boundaries, and the hatched side of the boundary corresponds to the plastic zone (17).

defined as an apparent proportional limit (17). The initial high work hardening rate (Figure 9) arises from the progressive consumption of elastic matrix at the tip of the whisker where the plastic flow is "blocked" by a continuous elastic matrix between reinforcements (17) (Figure 8). Once the elastic matrix is broken into isolated ligaments (e.g. 105.6 MPa), the work hardening rate is markedly reduced (Figures 8 and 9) through reductions of constraint to the plastic flow from the elastic matrix (17).

The thermally induced plastic flow has been shown to affect the initiation of the load-induced matrix plasticity. Levy & Papazian (63) showed from

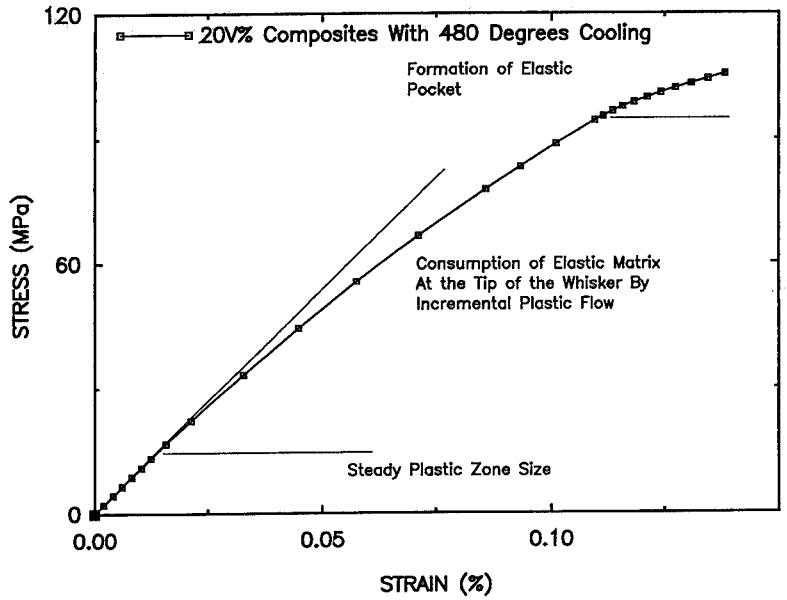

Figure 9 Different stages of plastic zone expansion and interconnection as in Figure 8 may be correlated to the stress–strain behavior of the composite (from 17). In the first stage in which the stress–strain response is approximately linear, the size of the plastic zone is steady because of local unloading of the TRS. In the second stage, in which a higher work hardening rate is observed, plasticity starts to develop at the tip of the whisker. In the third stage, in which global yielding takes place, only ligaments of elastic matrix remain.

an FEM study that without thermal misfit strain, the matrix plastic flow initiated at the tip of the whisker in a SiC_w/Al composite. With thermal misfit, the morphology of the evolution of the matrix plasticity changes depending on the loading direction (tension or compression) as shown in Figures 8 and 10 (64). Such changes of matrix plastic response inevitably affect the composite macroscopic mechanical behavior. Shi and co-workers (65, 66) have shown that by accounting for the thermal misfit the numerically predicted asymmetry in the composite tensile and compressive constitutive behavior (Figure 11) is consistent with that observed in experiments (Figures 6 and 7). This supports the suggestion that the TRS is responsible for the asymmetric composite constitutive behavior.

Hamann et al (67) and Levy & Papazian (60) studied the apparent stiffness differential between tensile and compressive loading in a whisker-reinforced composite. Their modeling results showed that the development of the longitudinal shear stress near whisker-matrix longitudinal interface was polarized by the TRS, and the development of shear stress was pref-

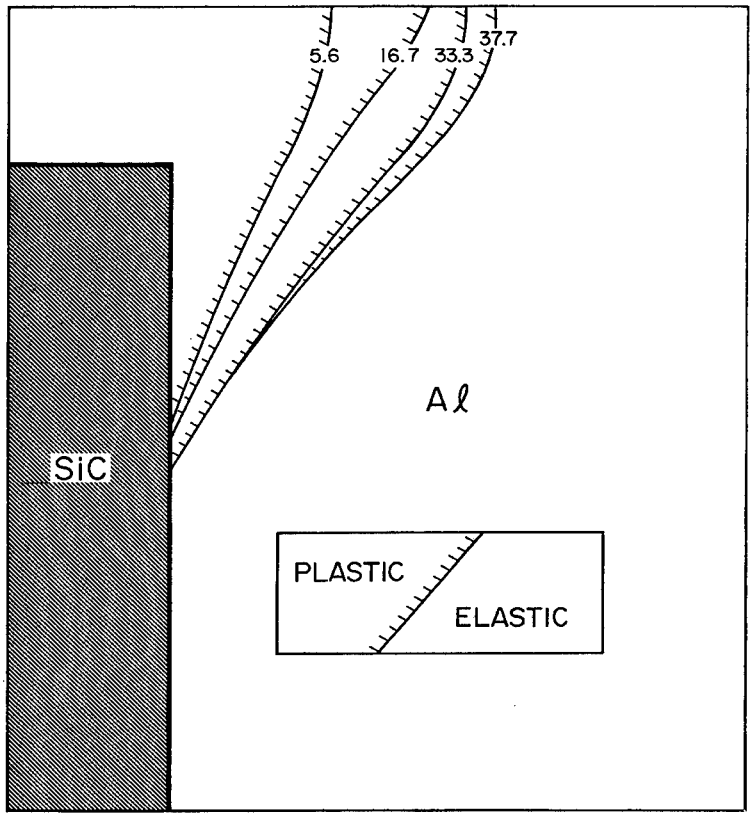

Figure 10 The process of plastic zone expansion of a 20 vol% SiC_w/Al composite (the same composite as in Figure 8) under compressive loading condition with cooling of 480°C (from 64).

erentially promoted during compression. Therefore, they suggested that early plastic flow due to shear stress accumulation was responsible for the observed lower compressive composite stiffness. However, this theory does not explain why the TRS induces a higher compressive yield strength. Shen et al (62) suggested that a higher tensile apparent stiffness resulted from an elevated matrix triaxial stress. This hypothesis is consistent with the FEM results by Nakamura & Suresh (50), who studied the influence of TRS on a transversely loaded continuous filament-reinforced composite. They found that the initial development of matrix plastic flow was more immense when under compressive loading, and therefore a more compliant global response. This result suggested that the volume fraction of the

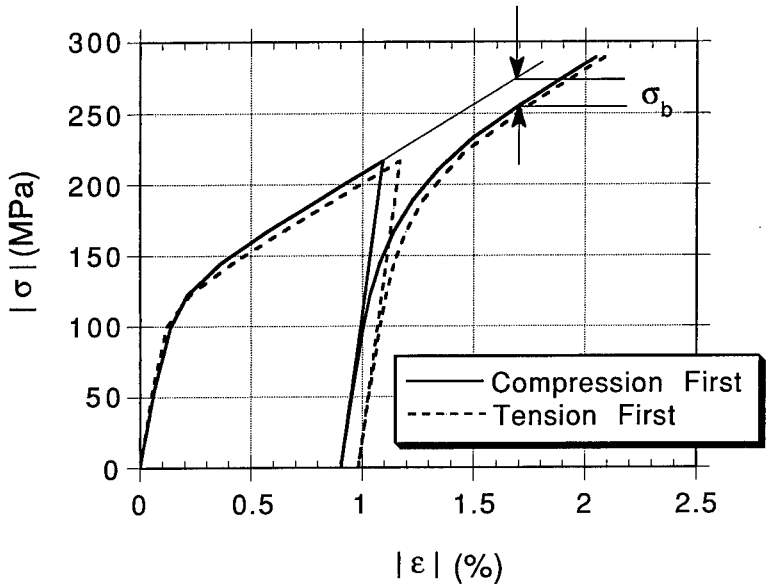

Figure 11 Stress–strain behavior predicted by FEM (66, 83). With cooling of $\Delta T = 480°C$, the tensile apparent stiffness is higher, while the compressive flow stress is higher. In the reverse loading cycle, the Bauschinger stress factor is larger for the compression-first loading scheme (more apparent in Figure 14).

plastic matrix was a major factor that dominated the variation of the composite apparent stiffness.

The correlation of the volume fraction of the plastic matrix for a whisker composite was also investigated by Shi & Arsenault (64). They found that, while the tensile apparent Young's modulus was higher, the volume fraction of the initial plastic zone from tensile loading was much larger than that from a comparable compressive loading (Figures 8 and 10). Furthermore, they noted that the morphology of the plastic zones under the two loading conditions was distinctly different. Because the apparent stiffness of the composite was related to the contribution to the far-field displacement from the local flow in the plastic zone, they suggested that the morphology of the plastic zone was important to the apparent modulus of the composite. By approximating the morphology of the plastic zone, as shown in Figure 12, they suggested that the contributions of the plastic zone were similar to those from isostress-type and isostrain-type deformation for compressive and tensile loading, respectively, when considered as separate entities, i.e. the more compliant plastic zone compared with the stiffer elastically deforming material (matrix and particle). They noted

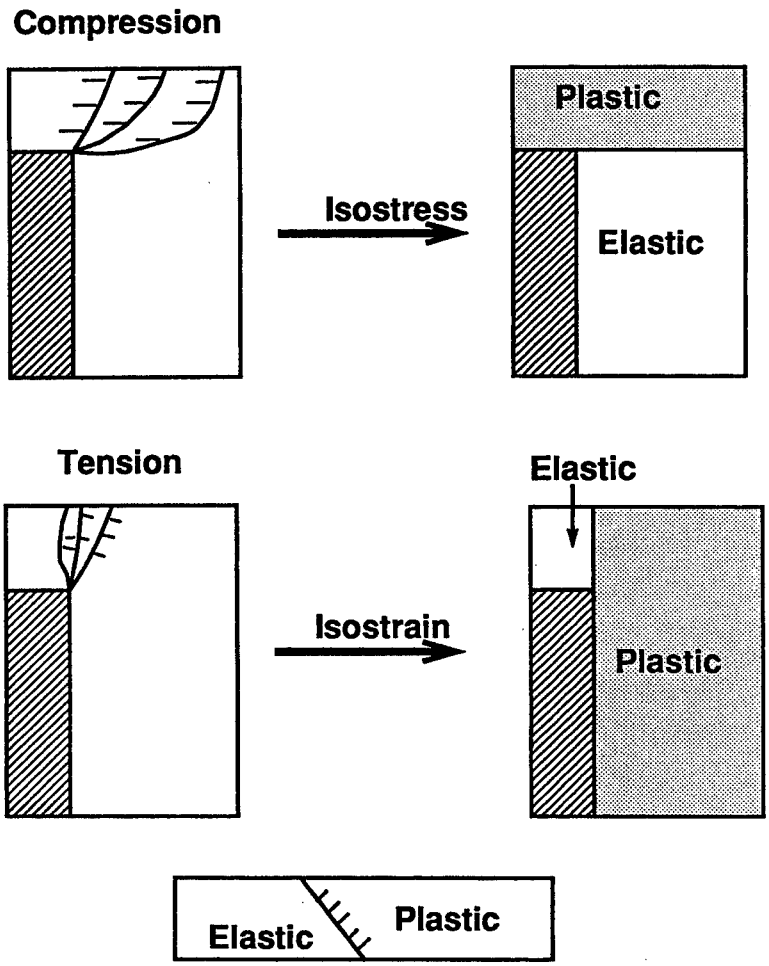

Figure 12 Schematics of the morphology of the plastic zones under different loading conditions, in which tensile loading produces a geometry that resembles an approximate isostrain condition and compressive loading resembles an approximate isostress condition (from 64).

that, even with a smaller volume fraction of plastic matrix as compared with that under tensile loading, the composite was more compliant during compressive loading because matrix plastic relaxation contributed more to the far-field displacement. Applying the same approximation to the composite lateral deformation, i.e. the Poisson's ratio, it is expected that the

Poisson's ratio in tension is greater than that in compression. Indeed, this trend has been verified by Davis & Allison (61) in their FEM calculations.

The TRS affects the composite performance by modifying the matrix-reinforcement plastic misfit and the stress partitions during deformation. Several investigators (49, 68) have used this fact to study the influence of the tensile and compressive composite flow behavior. Using the Eshelby-type mean field theory, a reasonable quantitative agreement has been obtained with experimental data (49) on the asymmetric composite flow stresses. The tensile matrix TRS appears to be responsible for the observed polarized yield strength (49, 68).

Premature reinforcement fracture has been suggested as another origin of the polarized yielding in DMMCs. The effect of particle fracture on the composite mechanical response has been illustrated through decreases of composite unloading stiffness after prestraining (69, 70). Further quantitative studies on the particle damage have been conducted (43, 71–73). From an Al_2O_3/Al composite, Klipfel et al (73) estimated the contributions to the asymmetric flow stress from both the TRS and the particle-fracture. They suggested that each source contributed about 50%. Based on experimental evidence that the composite apparent Young's modulus is larger in tension (59, 67), Shi & Arsenault (64) argued that particle fracture could only affect the post-yielding composite mechanical behavior. Otherwise, particle fracture would have resulted in a higher compressive stiffness in the pre-yielding regime. Experimental results obtained from acoustic emissions (74) showed that significant signals from particle fracture could be detected only after the onset of global yielding.

The asymmetric Bauschinger effect was initially investigated by Arsenault & Wu (59). Based on the assumption that the effects of TRS were not erased by the subsequent deformation (75), Arsenault and co-workers (59, 75) predicted that the asymmetric Bauschinger effect was caused by TRS. Taya et al (76) and Llorca et al (77) showed that without considering the matrix intrinsic Bauschinger effect (isotropic hardening), the composite reverse strain softening was significant. Therefore, they concluded that the Bauschinger effect in composites was driven by internal stresses. Taya et al (76) further indicated that the reverse strain softening increased with the magnitude of the prestrain.

Within the framework of mean field interaction, Withers (68) derived expressions using the mean field model in which

$$\bar{\boldsymbol{\sigma}}_M = -\mathbf{A}e^p + \mathbf{A}e^{th} + (\mathbf{I}+\mathbf{B})\boldsymbol{\sigma}^A; \qquad 3.$$

and the Bauschinger Stress Factor (σ_b):

$$\sigma_b = 2\frac{|\langle\sigma_3\rangle_M^p - \langle\sigma_1\rangle_M^p| \mp (\langle\sigma_3\rangle_M^{th} - \langle\sigma_2\rangle_M^{th})}{1+B_{33}-B_{13}}. \qquad 4.$$

In these expressions, the superscripts p and th represent plastically and thermally related quantities, respectively, subscript M denotes the matrix, and **A** and **B** are tensors that are related to the inclusion geometry and the material properties (68, 78). The sign $\mp$ corresponds to tensile and compressive prestrains, respectively. The predictions from the mean field theory (Equations 3 and 4) indicate a lasting TRS-effect during external deformation. On the other hand, several other individuals have shown, based on their FEM modeling, that the effect of TRS on the composite flow behavior is erased after a few percent of external strain (79, 80). Therefore, there may also be an argument that the residual stress state after unloading from prestraining has no memory of the initial TRS, and the observed asymmetric Bauschinger effect may not be a result of TRS.

To study the modifications of residual stresses by external deformation, Shi et al (81) performed a neutron diffraction study. They found that the morphology of deformation-induced changes of the residual stresses vs the applied strain was distinct for different loading directions, i.e. tension vs compression (Figure 13). When the applied total strain was small and within the nominal elastic region, modifications of residual stresses were controlled by the matrix plastic flow gradients induced by the local onset of plasticity. In this strain regime, both tensile and compressive deformation induced relaxation of matrix residual stresses. When the external deformation was large, e.g. beyond the 0.2% proof strain, the deformation-induced incompatibility between the matrix and the reinforcement, i.e. plastic misfit, became a major driving force for residual stress modifications. As a result, the matrix residual stresses decreased with the applied tensile deformation and increased with the applied compressive deformation. The changes of residual stresses are shown in Figure 13. Povirk et al (82) performed a similar study with emphasis on the effect of applied plastic strain. Similar modifications by the plastic misfit were captured, i.e. the average matrix residual stresses monotonically[1] changed with the applied plastic strain. Using FEM, they did a comprehensive parametric study of the influences on the residual stress generation from factors such as particle shape, reinforcement, and unit cell aspect ratios. Both studies (81, 82) seem to suggest that the effect of the TRS is not likely erased during modifications of residual stresses by the applied load.

The effect of the deformation-modified residual stresses on the reverse loading during Bauschinger tests has also been studied. A mean field approach (83) was employed to study the Bauschinger effect as a function of tensile and compressive prestrain. The deformation-induced residual stress was related to the back stress (3). In this study (83), Shi & Arsenault

[1] The study did not include the effect of the apparent elastic deformation.

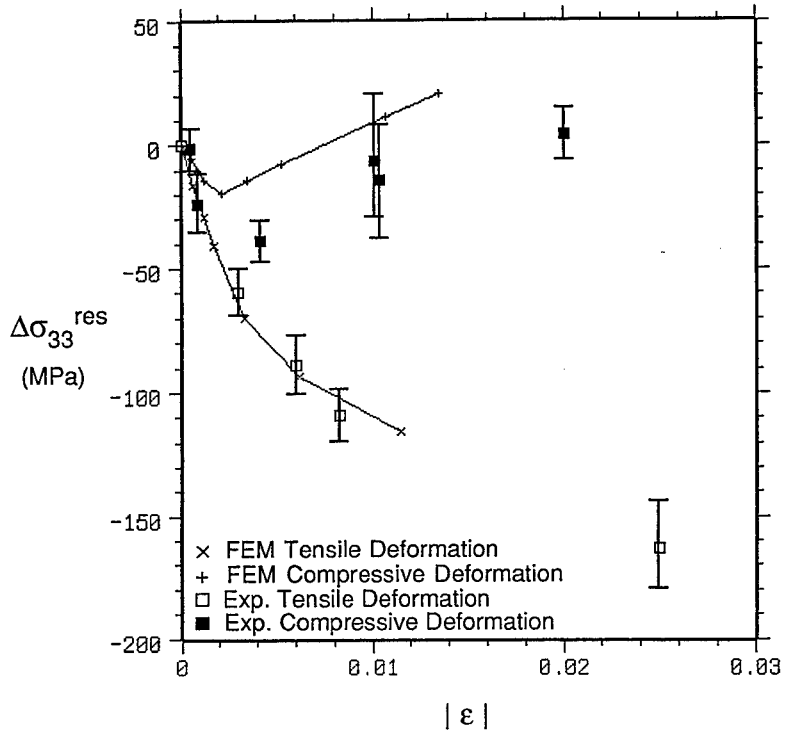

Figure 13 A comparison between the deformation-induced changes of residual stresses predicted by a three-dimensional FEM analysis and measured via neutron diffraction, where $|\varepsilon|$ is the magnitude of the total applied strain (from 81). Note that there is an initial residual stress relaxation in the apparent elastic loading regime.

suggested that the mean effect of the residual stress on the subsequent deformation, i.e. the back stress, should be determined based on energy equivalence rather than a simple volume average (81, 83). A result similar to Equation 4 was obtained,

$$\sigma_b = \beta(k\varepsilon_q^F \mp 2)\langle\tilde{\sigma}_m^{rT}\rangle, \qquad 5.$$

where β and k are constants, ε_p^F is the forward plastic strain, $\langle\tilde{\sigma}_m^{rT}\rangle$ is the average deviatoric matrix residual stress along the loading direction, and $\mp$ corresponds to tensile and compressive prestraining, respectively. Results from Equation 5 are comparable to FEM numerical predictions (Figure 14). Compared with the experimental data (84), the prediction by Shi & Arsenault followed a similar trend, but the observed parabolic relationship

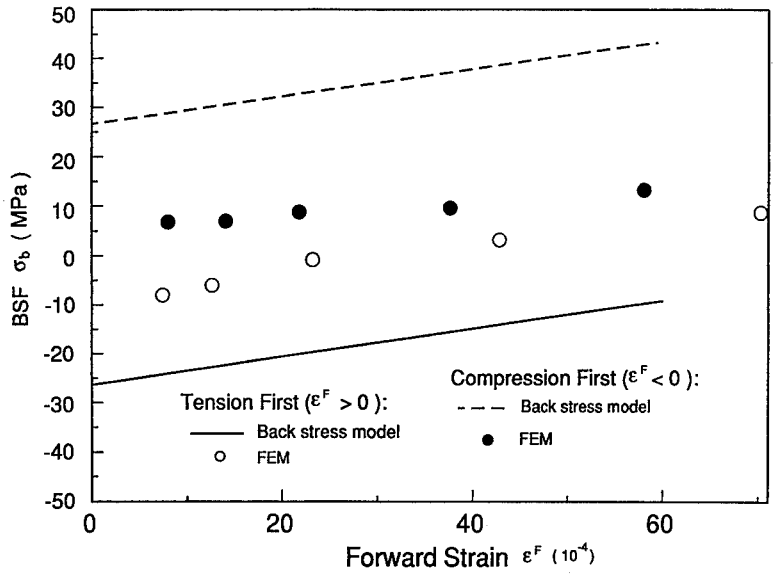

Figure 14 A comparison of the predictions from the back stress model and FEM. The two models give good agreement on the slopes and the general trends on the variations of the Bauschinger stress factor, while the back stress model predicts a larger asymmetry (from 83).

between the Bauschinger stress factor and the applied prestrain (84) was not predicted.

Bauschinger tests represent a simplified case for cyclic deformation since only one loading cycle is considered. Llorca et al (85) studied the accumulation of matrix plastic flow during cyclic loading both experimentally and numerically. The test results showed that saturation of cyclic flow could be reached after tens of cycles. They suggested that the saturation was a balance between matrix cyclic strain hardening and softening resulting from damage accumulation. Their numerical results also indicated that a significant stress redistribution occurred during the first several cycles, while damage accumulation such as matrix porosity, and hence redistribution of plastic strain, took place during deformation in higher cycles. In this study, the effect of TRS was not included.

All of the intriguing characteristics that have been discussed in this section are consistent with the effect of the plastic relaxation of the thermal misfit strain and to the TRS. Particle fracture during deformation is most likely to affect the post-yielding flow behavior of DMMCs.

COMPOSITE DUCTILITY—THE ROLE OF REINFORCEMENT AND MATRIX

Relatively low ductility is one of the major limitations of DMMCs. The total ductility, i.e. the energy required to rupture a ductile solid, is controlled by two factors: (*a*) the ability to withstand strain hardening before initiation of critical nuclei for final rupture (microcracks or voids); and (*b*) the resistance to crack extension. The experimental and theoretical efforts that have been undertaken to understand the low ductility of DMMCs can be divided into two main categories. The first group is related to the reinforcement; particle or whisker fracture, debonding and void nucleation, and growth at the reinforcement-matrix interface. The second group is related to the matrix; triaxials stress state in the matrix, the work hardened state of the matrix due to the ΔCTE effect, and localized matrix plastic flow. In this section, we concentrate on these aspects and discuss their contributions to the ductility of DMMCs.

The failure of SiC/Al DMMCs as revealed by fractography may be categorized into three modes; fracture of reinforcement and/or large intermetallics in the matrix, particle-matrix interfacial debonding, and ductile failure of matrix.

Clegg et al (58) and Llorca et al (86), while studying Al_2O_3 fiber- and SiC particulate-reinforced Al composites, respectively, observed that reinforcement fracture was the main failure mode for these composites. The damage process was found to follow Weibull statistics (86, 87). To identify critical factors that dictated the fracture of reinforcement particles in a composite, Llorca et al (86) studied the evolution of particle fracture in the composites with different heat treatments. They found that the number of fracturing particles correlated with the matrix strength. The higher the matrix strength, the higher proportions of fractured particles they could detect. From FEM modeling, they suggested that particle fracture was dominated by load transfer to the particle. With an increasing load-carrying ability for the matrix, the corresponding particle stress would also increase, which then increased the tendencies for particle fracture. The particle-stress model (86) is also consistent with experimental results by Lloyd (70), who observed in SiC/6061 Al composites more fractured particles along the fracture surface under the top-aged T6 temper than those in as-solution-treated T4 temper.

In another study, Wu & Arsenault (88) made an in situ SEM observation of crack propagation in a SiC/Al composite and found that cracks propagated through existing broken particles, which had existed prior to loading. It has also been reported that the composite failure is initiated by the fracture of large intermetallic inclusions in the matrix (89, 90).

Flom & Arsenault (91) studied the effect of particle size on the fracture of DMMCs. They found that reinforcement fracture is rarely observed when the particle size is small (<20 μm). They argued that for small particles the composite rupture process was dominated by matrix ductile failure. Christman et al (39) studied fractography of SiC_w/2124 Al composites. They noted that the fracture surfaces of both the reinforced and unreinforced alloys exhibited similar fine dimple structures. They suggested that the failure of the composite was predominantly through the matrix not along the matrix-reinforcement interfaces.

Yang et al (43) noted that with small particle size, debonding along interfaces was an accountable source for composite failure initiation. However, debonding was also seen as a less commonly observed phenomenon (92, 93). Li et al (94), using a quantum chemical approach, studied the interface between Al and SiC and concluded that the bonding strength was higher than the theoretical strength of Al (in the absence of interfacial chemical reactions). Arsenault & Pande (95) studied the surfaces of whiskers on the composite fracture surface with an Auger microprobe and found evidence that the surface of the whiskers was coated with Al. Therefore, they suggested that what appeared to be debonding was actually near-interface matrix failure. Nutt and co-workers (96, 97) observed that voids were being formed along the reinforcement-matrix interfaces and suggested that failure initiation at/near interfaces might take the form of void nucleation and growth, and coalescence, rather than a complete interfacial debonding.

Comparison of failure by void nucleation and growth at the particles drawn directly parallel from dispersion hardened alloys is often debatable because of the particle size scale difference. In DMMCs with well-bonded reinforcements, it may require a substantial amount of energy to form voids of size comparable to that of the reinforcements, and other failure mechanisms may be more favorable, including void nucleation and growth away from the interfaces (98).

The extent of void nucleation and growth (at the particles and/or in the matrix) can often be revealed through material uniaxial tensile behavior under a superimposed pressure (99). In a two-phase material, it has been shown that superimposed pressure may reduce the matrix tensile triaxial stresses by generations of misfit dislocations (100). Vasudevan et al (101) studied the effect of superimposed pressure on particulate- and whisker-reinforced composites. They found that pressure had a marked effect on both the composite flow behavior and ductility. The flow stress and ductility of the composites increased as a function of superimposed pressure, while no difference was observed for the unreinforced alloy. Tvergaard (102) noted that in a cavity-free composite, superimposed pressure should

not affect the flow stress of the composite. Therefore, the pressure-induced increases in flow stress in the composites (101) are probably a result of suppression of void accumulation. In another similar experiment with a nominally same composite, Mahon et al (92) noted that a superimposed pressure did not enhance the ductility of the composite. This result suggested that the composite failed by ductile tearing or shear localization (not by void nucleation and growth). Fractography by Davidson (103) revealed that in the composite he tested extensive tearing ridges appeared on the fracture surface, which suggested the possibility for ductile tearing.

Secondary processing is shown to affect the composite fracture process. Lewandowski and co-workers (104–106) studied the rupture of a SiC_p/7xxx Al composite. They showed that for composites of equivalent matrix microhardness and flow stress, i.e. the same load partition ratio, the fracture resistance could be altered by tailoring interfaces. In their experiments, an equivalent matrix was obtained by heat treatment to equivalent under-aged and over-aged conditions, respectively. In an under-aged condition, the interfaces were precipitate-free; whereas in an over-aged condition, solute segregation and precipitation preferentially occurred near the interfaces. The failure of the composite was found to be dominated by particle-fracture in the under-aged condition and matrix ductile rupture in the over-aged condition, respectively. Similar studies were also performed by Mahon et al (92) with a SiC_w/2124 Al composite. Contrary to Lewandowski's results (104, 105), they found that, while similar kinetics of precipitation was observed along the interface, fractured whiskers were much more frequently observed in the over-aged condition rather than in the under-aged condition. However, ductility of the composites decreased in both cases (92, 105) as a result of over-aging. Results from these two studies suggest that the role of interfacial precipitates is distinctly different in the two cases. It should be noted that the precipitates were suggested to be $MgZn_2$ in the former case (104) and CuMg in the latter (92). The ductility of the composites from both studies (92, 105) is summarized in Table 4.

The change of ductility due to under- and over-aging provides some insights into the role of the matrix in affecting the ductility of DMMCs. While the changes from matrix- to reinforcement-fracture dominated failure doubles the composite fracture-resistance (J_{IC}), only a fractional increase in strain-to-failure is obtained (see Table 4) (105). This points to the potential importance of the matrix strain hardening capacity in determining the ductility of DMMCs. The key role of the matrix in composite failure-resistance is further demonstrated by the ability to recover most of the ductility after prestraining by re-solutionizing the composite (70). That is, particle fracture induced by prestraining has a minimal role as compared

Table 4 Tensile ductility of under-aged (UA) and over-aged (OA) composites

Material (vol%)	Elongation (%)		J_{IC} (KJ/m^2)
	SiC/7xxx Al (105)	SiC/2124 Al[a] (92)	SiC/7xxx Al (105)
UA—0 unreinforced	20	~20	31.0
UA—13.5 SiC_w	—	~5	—
UA—15 SiC_p	4.9	—	16.3
UA—20 SiC_p	4.3	—	11.7
OA—0 unreinforced	19	~18	31.5
OA—13.5 SiC_w	—	~3	—
OA—15 SiC_p	3.5	—	7.4
OA—20 SiC_p	3.4	—	5.5

[a] With 0.1 MPa hydrostatic pressure.

with the matrix conditions in affecting the composite ductility. The matrix can affect the ductility of DMMCs in two ways: (*a*) the matrix in situ ductility is degraded by the addition of reinforcements, and (*b*) the matrix plastic flow preceding to the final failure is highly localized near the fracture path.

Arsenault (107) made an attempt to correlate the in situ matrix fracture toughness and ductility in a SiC/Al DMMC with those of a cold-worked unreinforced alloy. He argued that the matrix is in a highly cold-worked state due to ΔCTE. Therefore, the matrix in situ ductility and toughness should correspond to those in a cold-worked state. It is a general observation that ductility of a metal or alloy decreases with an increase in cold work. Since the microstructure of the matrix in 20 vol% SiC/Al composite is similar to that of an unreinforced alloy with 90% cold work (31), he suggested that the in situ matrix ductility of the composite should be comparable to the cold-worked unreinforced alloy. In a related experiment, it was shown (Table 5) that cold-rolling 6061 Al alloy to 69% resulted in

Table 5 Fracture toughness vs cold work

Material	Unreinforced Al (107)		20 vol% SiC/Al (110)
	Cold work (%)	K_{IC} (MPa·m$^{1/2}$)	K_{IC} (MPa·m$^{1/2}$)
6061 Al T6	0	43	—
6061 Al T6	15	31	22.4
6061 Al T6	69	27	—
6061 Al T6	139	~20	—

nearly a factor of two reduction in K_{IC}, and in the case of 139% cold-rolling there is further reduction in K_{IC}. At this level, the K_{IC} value of the cold-rolled matrix alloy is comparable to the 20 vol% SiC_p/6061 Al alloy composite (107).

In another investigation (89) in which correlations between K_{IC} and yield stress were determined, Hahn & Rosenfield showed that for 2000 and 7000 series Al alloys there was a substantial loss of fracture toughness with increasing yield strength (for the same volume fraction of inclusions). They further suggested that this was due to a reduction in the work needed to link the voids in the higher strength alloys. In the case of the cold-worked Al alloy and the Al matrix in a SiC/Al DMMC, this is related to the loss of strain-hardening capacity. Jagannadham & Wilsdorf (108) demonstrated that dislocation cell walls in metals and alloys could serve as microcrack nucleation sites and degraded the ability to resist crack propagation. Jones et al (109) calculated the fracture toughness of a SiC/Al DMMC by accounting for the strength increase from work hardening due to ΔCTE [Equations 1 and 2 (30)] and for the influence of the strength on the fracture toughness, i.e. $K_{IC} \propto (\sigma_y E)^{1/2}$ (110). They obtained a reasonable agreement with the existing experimental data.

The presence of a high matrix triaxial stress can also decrease the matrix in situ ductility of DMMCs. Embury (111) suggested that void nucleation might dominate the ductility since the subsequent stages of void growth and coalescence may be extremely rapid due to high matrix triaxiality. Rice & Tracey (112) predicted a spherical void dilatation under triaxial stresses. These predictions are consistent with the observations by Kamat et al (47), who revealed shallow dimples on the fracture surface by stereo pairs, and by Lewandowski et al (104) and Flom & Arsenault (91), who noted that no additional voids were observed immediately below the fracture surface of DMMCs. Although the concept of rapid void growth originated from void nucleation at the particles in dispersion-strengthened alloys, it also applies to other situations of void nucleation and growth under high triaxial stresses, for example, within the matrix. However, there is other experimental evidence that disputes the theory of void nucleation-controlled failure. Whitehouse & Clyne (113) measured the evolution of voids in DMMCs by monitoring the composite density. They showed a gradual accumulation of cavitations. This suggests that void nucleation may not be a catastrophic process.

Llorca et al (114) studied the void nucleation and growth process using FEM modeling. By assuming that the processes of void nucleation and void growth were controlled separately by the effective plastic strain and the dilatational stresses, respectively (115), they showed that for whisker-reinforced composites void nucleation at the tip of the whisker was

dominating. The void growth process is rapid because of the high matrix triaxial stresses; whereas for spherical composites substantial void growth could exist due to a smaller triaxial stress. This suggests that the void content should be higher in a spherical composite. However, this prediction is contrary to the experimental observations by Whitehouse & Clyne (113), who showed that more voids were detected at all strain levels in a whisker composite than those in a comparable spherical composite. These inconsistencies indicate that the triaxial stress-dominated mechanism cannot consistently predict composite ductility.

Localization of plastic deformation can further degrade the macroscopic ductility of DMMCs. The inherent origin for deformation localization in DMMCs attracts attention because of its importance in improving composite ductility. To assess the degree of matrix deformation localization, Arsenault et al (116) examined the dislocation density near the failure surface of a tensile sample. They found that the dislocation density was high near the fracture surface and decreased at a greater rate as a function of distance from the fracture surface in a composite with a higher SiC content. This suggested that plastic flow in a particle-reinforced metal was localized by the addition of SiC. Using stereoimaging, Davidson (103) noted that the maximum local strain near the fracture path is significantly in excess of the average strain-to-failure obtained by tensile tests.

To study plastic flow localization, McHugh et al (117, 118) developed a physical slip model that took into account crystallographic slip directions, and incorporated them into FEM. In their model, they formed an idealized composite by construction of a unit cell that consisted of an aggregate of hexagonal grains of matrix with different crystallographic orientations and elastic reinforcements. They found that slip is highly localized around the particles in the composite as compared to the unreinforced polycrystals, and the effect of the reinforcement on the flow pattern is much stronger than the effect of the crystallographic orientations. Their results seem to support the following view. For a given amount of applied load, the average matrix deformation increases when the reinforcements are added to accommodate the rigidity of the particle (the volume fraction effect, 117). However, additional local stresses are built up near the vicinity of the particles by the misfit generated during deformation. These stresses may be relieved by an onset of the localized plastic flow. Flow in the matrix provides a mechanism to relax the misfit and to prevent further build-up of local stresses. Local plastic relaxation and high matrix triaxiality then prevent further spread of plastic flow. This is also supported by Bolmaro et al (119), who showed in a transversely loaded continuously reinforced composite that while intense rotation took place in part of the matrix between particles, the rest of the matrix was

more in line with the far-field deformation mode. In the context of composite ductility, the localized plastic flow can lead to localized plastic rupture in the matrix where only limited ductility may be observed macroscopically.

Particle distribution is another factor that limits the ductility of the composites. With few exceptions, cracks are always initiated in the particle-rich region (103, 104) and follow a more random path when particle distribution is more uniform (93). Arsenault et al (116) studied localized plastic flow in a composite by in situ monitoring the development of slip lines in the matrix via an optical microscope. They found that slip lines were more prominent in the particle-rich region. A companion FEM analysis (116) on periodic clustering of four neighboring particles showed that inhomogeneous particle distribution led to a higher rate of effective plastic strain accumulation within/near reinforcement clusters. Therefore, aside from the deformation localization led by the additions of the reinforcement (117), particle clustering induces additional plastic flow localization.

Christman et al (13) performed a comprehensive FEM parametric study of the changes in plastic flow due to particle clustering by periodically clumping two neighboring particles in an infinite cubic particle array (Figure 15). By selecting different neighbors for clustering (vertical and horizontal clustering), they were able to show that clustering reduced the matrix triaxial stresses, and therefore the constraint to plastic flow, which was considered by these authors to be a main strengthening mechanism

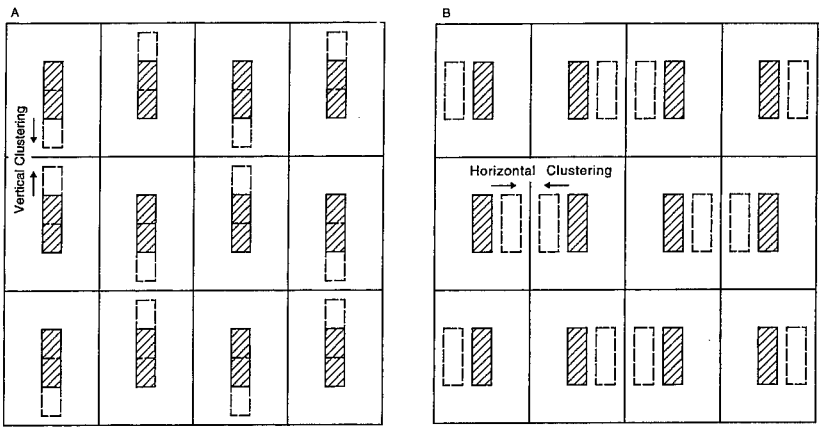

Figure 15 Schematics of the Christman-Llorca periodic clustering model (13, 114) for parametric study of the effect of reinforcement clustering, in which the effect is studied with respect to (*a*) vertical and (*b*) horizontal clustering.

(13). Similar FEM results were also reported by Dragone & Nix (120), who found that the time-dependent deformation rate decreased with an increase in the degree of particle overlap (decrease in vertical clustering, see Figure 15). Wang et al (121) performed another in situ slip line observation followed by FEM modeling. They found that an idealized periodic clustering model (13, 116) could qualitatively describe the evolution of field quantities in an actual geometry in which the FEM mesh was mapped directly from the optical images. It should be noted that the result of lower matrix triaxial stresses induced by particle clustering (13) are different from the perceptions that the matrix hydrostatic stresses are more intense in a particle cluster (70, 106, 122).

The periodic clustering approach (13) was also incorporated into ductility predictions (114). By assuming the same criteria that void nucleation and its subsequent growth were governed by the effective plastic strain and the triaxial stresses (115), respectively, it was shown that the void growth stage was extended in a clustered composite resulting from a lower matrix triaxiality, and therefore the composite ductility was enhanced. This result is contrary to the suggestions by many others that homogeneous reinforcement distributions would lead to improved composite ductility (e.g. 21, 70, 103).

The periodic clustering model (114) only accounted for the short-range interactions between particles in the cluster, long-range interactions between the clusters and the relatively homogeneous region could not be considered (17). To study this long-range interaction (i.e. a long-range fluctuation of the internal stresses), Shi et al (17) constructed an imaginary composite as shown in Figure 16, in which C_1 and C_2 represented the cluster and the uniform region, respectively. Because of a long-range interaction, they approximated this inhomogeneous composite by considering the smeared properties for C_1 and C_2, as if they were monolithic materials with equivalent properties from composites with predefined reinforcement volume fractions. From this approach, the short-range interactions between particles in C_is were approximated phenomenologically when the smeared material properties were assigned to each phase. Within the framework of mean field interactions, they obtained the following criterion (17):

$$\left(\frac{\sigma_y^{c2}}{\sigma_y^{c1}} - K_{12}^{-1}\frac{\mu^{c2}}{\mu^{c1}}\right)\begin{cases} >0 & C_1 \text{ yields first;} \\ =0 & C_1 \text{ and } C_2 \text{ yield simultaneously;} \\ <0 & C_2 \text{ yields first,} \end{cases} \qquad 6.$$

where σ_y is the yield stress for the constituents, K_{12} is the ratio between the average elastic strains in C_1 and C_2, and μ is the stiffness that resists shear.

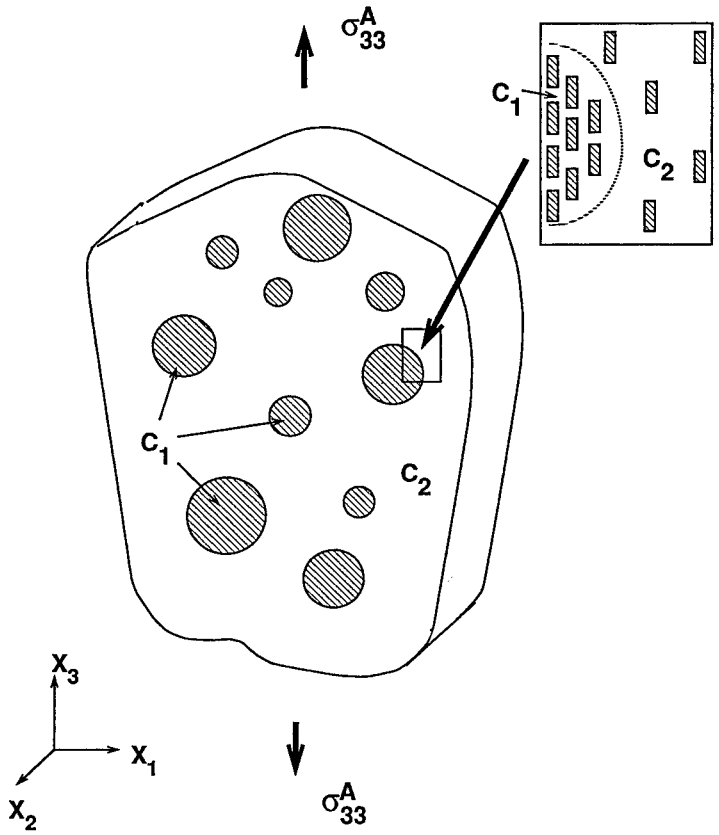

Figure 16 Schematics of mean field approximation of a composite with inhomogeneous particle distribution, where shaded spheres stand for reinforcement clusters, C_1, embedded in a uniform composite, C_2. An imaginary boundary between clustered and unclustered regions is shown on the right upper corner (from 17).

The predictions from Equation 6 may be compared with experimental results. Experimentally, strain localization in a reinforcement cluster generally initiates within an early stage of deformation (103). Lloyd (70) recently showed that the strain distribution may be controlled by heat treatment. In a SiC-reinforced 6061 Al composite, a T4 temper led to a rather uniform deformation until final fracture, whereas strain localization initiated at a relatively early stage of deformation in a T6 condition. While this variation cannot be predicted by the periodic cluster unit cell model (114), it is consistent with Equation 6. If the degree of deformation localization induced from different heat treatments (70) is dictated by the

changes of matrix strength, then Equation 6 predicts the same trend as the experimental observation (70). That is, compared with a T6 condition, reduction in matrix strength from T4 has more effect on C_2 than that on C_1, i.e. a larger reduction in σ_y^{c2} while no changes in K_{12} and μ. This promotes yielding in C_2, i.e. localized plastic flow in the clusters. Therefore, while clustering of particles tends to increase tendency for plastic flow (13, 114, 116, 121), fluctuation of local particle density may cause long-range perturbations of the mean stresses, which may either promote or suppress plastic flow in the reinforcement-rich region (Equation 6). In this case, the long-range interactions dominate.

Although particle clusters may exhibit a ductile nature (114), their contribution to the global composite ductility may be offset by an early onset of local plastic flow, as noted by Davidson (103), who estimated 50% local strain within clusters and yet the composite still suffered low ductility (1.6 to 2.4% strain-to-failure) because of excessive local plastic flow in the clusters. In addition, increase in the loss of strain-hardening capacity from the ΔCTE effect (107) may also offset the predicted increase in local ductility in the particle cluster (114).

From a consideration of the data and the explanation presented above, the following summary can be drawn: the lack of strain-hardening capacity of the matrix is the major contributing factor to the low ductility of DMMCs. This may be attributed intrinsically to the exhaustion of the strain-hardening capacity from ΔCTE-induced work hardening and/or extrinsically to the high matrix triaxial stresses, which induce rapid void growth. Further study is needed to evaluate the magnitude of the contributions of these two sources. The other contributing factors are localized plastic flow and reinforcement clustering.

CLOSING REMARKS

In DMMCs, several strengthening mechanisms are operating. The presence of the second-phase plastically non-deformable inclusions in a ductile plastic matrix may (*a*) reduce the stresses in the matrix by transferring load to the reinforcement, (*b*) increase the resistance for activation of dislocation glide or plastic flow, and (*c*) modify matrix microstructure to enhance matrix load-carrying ability. Each strengthening mechanism may operate independently, and their contributions are material-dependent.

Relief of the matrix stress that is commonly known as load transfer is strongly influenced by the reinforcement morphology; for DMMCs, load transfer is expected to be a minor strengthening mechanism. For inclusions of micron size such as those in DMMCs, the resistance to dislocation glide may be represented phenomenologically by changing the deformation mode

from shear distortion to forced volumetric dilatation resulting from matrix plastic flow constraint, i.e. increase in hydrostatic stress component. Load transfer and constrained plastic flow are expected to be responsible for the non-thermally related strengthening.

Matrix microstructural modifications herein are referred to as dislocation generation due to the ΔCTE effect and the subsequent formation of dislocation substructures. The strengthening from thermally generated dislocations and refined dislocation substructures depends on the amount of work hardening that has been achieved during the course of dislocation generation. The magnitude of this strengthening can be determined by experimentally measuring the increase in dislocation density, $\Delta\rho$, and the decrease in the subgrain size. The strengthening due to the $\Delta\rho$ can be found by a simple expression that has been obtained both experimentally and theoretically, i.e. $\Delta\sigma = \alpha\mu b\sqrt{\Delta\rho}$. The contribution from subgrain size reduction can be obtained from the experimental empirical relations from McQueen & Hackett (44). Sufficient evidence has been generated that clearly demonstrates the strengthening by thermally induced microstructural changes is significant.

Plastic relaxation of thermal matrix stresses affects the development of internal stresses and therefore alters the composite constitutive response. This relaxation-induced plastic flow lowers the composite proportional limit and the stiffness. These nominal values are different from their intrinsic counterparts because of the existence of pre-loading matrix plasticity—thermally induced plastic flow. The thermally induced plastic flow also polarizes the composite tensile and compressive constitutive behavior. Evidence from numerical and analytical modeling has demonstrated that the asymmetry in the composite constitutive response can be best described by the influence of TRS. Strong evidence also shows that damage to the reinforcement accumulates in the composite during the course of tensile deformation. The effects of these damages on the asymmetry of the composite constitutive response are still unclear, but it is expected that they affect the post-yielding behavior the most.

The final rupture of DMMCs may be characterized as particle-, interface-, or matrix-controlled processes. The failure mode is dominated by the bulk matrix and reinforcement properties, and the interfacial precipitation conditions. However, no matter what the final failure mode is, the ductility of the composite seems to be controlled by the flow pattern and the in situ ductility of the matrix. There are two factors that limit the ductility of the composite: (*a*) degraded in situ matrix ductility from thermally induced work hardening and/or the high matrix triaxial stresses, and (*b*) localized plastic flow. A major factor affecting the ductility of DMMCs is that the matrix is in a work-hardened condition prior to actual testing. The

exhaustion of matrix in situ ductility prior to loading may affect the micromechanisms of failure, for example, by limiting the ability of strain hardening. High triaxial stresses, at the same time, have similar effects. They increase the driving force for void growth and degrade microductility. With localized flow, much of the local ductility is exhausted with little contribution to the far-field displacement.

Particle clustering usually further enhances the localization of plastic flow. Although the clustering of particles is shown to elevate ductility of clusters, in an actual composite the long-range fluctuation of the internal stresses promotes highly localized flow in the cluster, which reduces global ductility. In addition, work hardening induced by ΔCTE, which is expected to be more severe in a particle-rich region, may also counterbalance the enhanced ductility in the clusters.

ACKNOWLEDGMENTS

NS would like to acknowledge the support of the US Department of Energy, Office of Basic Energy Science under contracts W7405-ENG-36, and to express his gratitude to Drs. JA Goldstone and RB Schwarz for their encouragement during the preparation of this manuscript; RJA would like to acknowledge the support from Office of Naval Research under contract N00014–91-J-1353 under the auspice of Dr. SG Fishman.

Literature Cited

1. Orowan E. 1959. *Internal Stresses and Fatigue in Metals*, ed. GM Rassweiler, WL Grube, pp. 59–80. New York: Elsevier
2. Ashby MF. 1970. *Philos. Mag.* 21: 399–424
3. Brown LM, Stobbs, WM. 1971. *Philos. Mag.* 23: 1185–99; 1201–33
3a. Atkinson JD, Brown LM, Stobbs WM. 1974. *Philos. Mag.* 30: 1247–80
3b. Atkinson JD, Brown LM. 1976. *Philos. Mag.* 34: 351–72
4. Tanaka K, Mori T. 1970. *Acta Metall.* 18: 931–41
5. Eshelby JD. 1957. *Proc. R. Soc. London Ser. A* 241A: 376–96
5a. Eshelby JD. 1959. *Proc. R. Soc London Ser. A* 252A: 561–69
6. Taya M, Arsenault RJ. 1989. *Metal Matrix Composites—Thermomechanical Behavior*. Oxford: Pergamon
7. Clyne TW, Withers PJ. 1993. *An Introduction to Metal Matrix Composites*. Cambridge: Cambridge Univ. Press
8. Arsenault RJ, Fishman S, Taya M. 1994. *Prog. Mater. Sci.* In press
9. Suresh S, Mortensen A, Needleman A, eds. 1993. *Fundamentals of Metal-Matrix Composites*. Stoneham: Butterworth-Heinemann
10. Lederich RJ, Sastry ML. 1982. *Mater. Sci. Eng.* 55: 143–46
11. Miller WS, Humphreys FJ. 1991. *Scripta Metall.* 25: 33–38
12. Arsenault RJ. 1991. *Scripta Metall. Mater.* 25: 2617–21

13. Christman T, Needleman A, Suresh S. 1989. *Acta Metall.* 37: 3029–50
14. Brockenbrough JR, Suresh S, Wieneck HA. 1991. *Acta Metall. Mater.* 39: 735–52
15. Drucker DC. 1966. *J. Mater.* 1: 873–910
16. McHugh PE, Asaro RJ, Shih CF. 1993. *Acta Metall. Mater.* 41: 1477–88; see also Ref. 51, 117, 118
17. Shi N, Wilner B, Arsenault RJ. 1992. *Acta Metall. Mater.* 40: 2841–54
18. Cox HC. 1952. *Brit. J. Appl. Phys.* 3: 72–79
19. Nardone VC, Prewo KM. 1986. *Scripta Metall.* 20: 43–48
20. Taya M, Arsenault RJ. 1987. *Scripta Metall.* 21: 349–54
21. McDanels DL. 1985. *Metall. Trans.* 16A: 1105–15
22. Arsenault RJ, Fisher RM. 1983. *Scripta Metall.* 17: 67–71
23. Vogelsang M, Arsenault RJ, Fisher RM. 1986. *Metall. Trans.* 17A: 379–89
24. Christman T, Suresh S. 1988. *Acta Metall.* 36: 1691–704
25. Kim CT, Lee JK, Plichta MR. 1990. *Metall. Trans.* 21A: 673–82
26. Pickard SM, Schmauder S, Zahl DB, Evans AG. 1992. *Acta Metall. Mater.* 40: 3113–19
27. Yang J, Pickard SM, Cady C, Evans AG, Mehrabian R. 1991. *Acta Metall. Mater.* 39: 1863–69
28. Barlow CY, Hansen N. 1991. *Acta Metall. Mater.* 39: 1971–79
29. Arsenault RJ. 1984. *Mater. Sci. Eng.* 64: 171–81
30. Arsenault RJ, Shi N. 1986. *Mater. Sci. Eng.* 81: 175–87
31. Arsenault RJ, Wang L, Feng CR. 1991. *Acta Metall. Mater.* 39: 47–57
32. Taya M, Mori T. 1987. *Acta Metall.* 35: 155–62
33. Taya M, Lulay KE, Lloyd DJ. 1991. *Acta Metall. Mater.* 39: 73–87
34. Flom Y, Arsenault RJ. 1985. *Mater. Sci. Eng.* 75: 151–67
35. Dunand DC, Mortensen A. 1991. *Acta Metall. Mater.* 39: 1405–16; 1417–29
36. Dunand DC, Mortensen A. 1991. *Acta Metall. Mater.* 39: 127–39
37. Hill R. 1950. *The Mathematical Theory of Plasticity*. Oxford: Oxford Univ. Press
38. Shieu F-S, Sass SL. 1991. *Acta Metall. Mater.* 39: 539–47
39. Christman T, Needleman A, Nutt S, Suresh S. 1989. *Mater. Sci. Eng.* A107: 49–61
40. Dutta I, Bourell DL. 1989. *Mater. Sci. Eng.* A112: 67–77
41. Hong SI, Gray GT III. 1992. *Acta Metall. Mater.* 40: 3299–315
42. Derby B, Walker JR. 1988. *Scripta Metall.* 22: 529–32
43. Yang J, Cady C, Hu MS, Zok F, Mehrabian R, Evans AG. 1990. *Acta Metall. Mater.* 38: 2613–19
44. McQueen HJ, Hackett JE. 1970. *Metall. Trans.* 1: 2997–3004
45. Jonas JJ, Axelrad DR, Uvira JL. 1968. *Trans. Jpn Inst. Metal Suppl.* 9: 257–67
46. Wang L, Shi N, Arsenault RJ. 1990. *Proc. Morris E. Fine Symp.*, ed. PK Liaw, JR Weertman, HL Marcus, LS Santer, pp. 129–42. PA: TMS-AIME
47. Kamat SV, Hirth JP, Mehrabian R. 1989. *Acta Metall.* 37: 2395–402
48. Hansen N, Kuhlmann-Wilsdorf D. 1986. *Mater. Sci. Eng.* 81: 141–61
49. Arsenault RJ, Taya M. 1987. *Acta Metall.* 35: 651–59
50. Nakamura T, Suresh S. 1993. *Acta Metall. Mater.* 41: 1665–81
51. McHugh PE, Asaro RJ, Shih CF. 1993. *Acta Metall. Mater.* 41: 1501–10; see also Ref. 16, 117, 118
52. Bao G, Hutchinson JW, McMeeking RM. 1991. *Acta Metall. Mater.* 39: 1871–82
53. Ledbetter HM, Austin MW. 1989. *Mater. Sci. Eng.* 89: 53–61
54. Smith LF, Krawitz AD, Clarke P, Saimoto S, Shi N, Arsenault RJ. 1992. *Mater. Sci. Eng.* A159: L13–15
55. Nair SV, Tien JK, Bates RC. 1985. *Int. Metall. Rev.* 30: 275–90
56. Bonnen JJ, Allison JE, Jones JW. 1991. *Metall. Trans.* 22A: 1007–19
57. Papazian JM, Adler PN. 1990. *Metall. Trans.* 21A: 401–10
58. Clegg WJ, Horsfall I, Mason JF, Edwards L. 1988. *Acta Metall.* 36: 2151–59
59. Arsenault RJ, Wu SB. 1987. *Mater. Sci. Eng.* 96: 77–88
60. Levy A, Papazian JM. 1991. *Acta Metall. Mater.* 39: 2255–66
61. Davis LC, Allison JE. 1993. *Metall. Trans.* 24A: 2487–96
62. Shen Y-L, Finot M, Needleman A, Suresh S. 1994. *Acta Metall. Mater.* 42: 77–98
63. Levy A, Papazian JM. 1990. *Metall. Trans.* 21A: 411–20
64. Shi N, Arsenault RJ. 1993. *Scripta Metall. Mater.* 28: 623–28
65. Shi N, Sarfarazi MP, Arsenault RJ. 1989. *Proc. Plasticity '89 Symposium—2nd Int. Symp. Plasticity and Current Applications*, ed. AS Khan, M Tokuda, pp. 133–36. Oxford: Pergamon
66. Shi N, Arsenault RJ. 1991. *J. Comp. Tech. Res.* 13: 211–26

67. Hamann R, Gobin PF, Fougeres R. 1990. *Scripta Metall. Mater.* 24: 1789–94
68. Withers PJ, Stobbs WM, Pedersen OB. 1989. *Acta Metall.* 37: 3061–84
69. Hunt WH Jr, Brockenbrough JR, Magnusen PE. 1991. *Scripta Metall. Mater.* 25: 15–20
70. Lloyd DJ. 1991. *Acta Metall. Mater.* 39: 59–71
71. Taggart DG, Bassani JL. 1991. *Mech. Mater.* 12: 63–80
72. Bao G. 1992. *Acta Metall. Mater.* 40: 2547–55
73. Klipfel YL, He MY, McMeeking RM, Evans AG, Mehrabian R. 1990. *Acta Metall. Mater.* 38: 1063–74
74. Mummery PM, Derby B, Scruby CB. 1993. *Acta Metall. Mater.* 41: 1431–45
75. Arsenault RJ, Taya M. 1989. *Mater. Sci. Eng.* A108: 285–88
76. Taya M, Lulay K, Wakashima K, Lloyd DJ. 1990. *Mater. Sci. Eng.* A124: 103–11
77. Llorca J, Needleman A, Suresh S. 1990. *Scripta Metall. Mater.* 24: 1203–8
78. Pedersen OB. 1990. *Acta Metall. Mater.* 38: 1201–19
79. Zahl DB, McMeeking RM. 1991. *Acta Metall. Mater.* 39: 1117–22
80. Povirk GL, Needleman A, Nutt SR. 1991. *Mater. Sci. Eng.* A132: 31–38
81. Shi N, Arsenault RJ, Krawitz AD, Smith LF. 1993. *Metall. Trans.* 24A: 187–96
82. Povirk CL, Stout MG, Bourke M, Goldstone JA, Lawson AC, et al. 1992. *Acta Metall. Mater.* 40: 2391–412
83. Shi N, Arsenault RJ. 1993. *Metall. Trans.* 24A: 1879–82
84. Wang Z, Zhang RJ. 1991. *Metall. Trans.* 22A: 1585–93
85. Llorca J, Suresh S, Needleman A. 1992. *Metall. Trans.* 23A: 919–34
86. Llorca J, Martin A, Ruiz J, Elices M. 1993. *Metall. Trans.* 24A: 1575–88
87. Brechet Y, Embury JD, Tao S, Luo L. 1991. *Acta Metall. Mater.* 39: 1781–86
88. Wu SB, Arsenault RJ. 1991. *Mater. Sci. Eng.* A138: 227–35
89. Hahn GT, Rosenfield AR. 1975. *Metall. Trans.* 6A: 653–68
90. Kim Y-H, Lee S, Kim N. 1992. *Metall. Trans.* 23A: 2589–96
91. Flom Y, Arsenault RJ. 1989. *Acta Metall.* 37: 2413–23
92. Mahon GJ, Howe JM, Vasudevan AK. 1990. *Acta Metall. Mater.* 38: 1503–12
93. You CP, Thompson AW, Bernstein IM. 1987. *Scripta Metall. Mater.* 21: 181–85
94. Li S, Arsenault RJ, Jena P. 1988. *J. Appl. Phys.* 64: 6246–53
95. Arsenault RJ, Pande CS. 1984. *Scripta Metall.* 18: 1131–34
96. Nutt SR, Duva JM. 1986. *Scripta Metall.* 20: 1055–58
97. Nutt SR, Needleman A. 1987. *Scripta Metall.* 21: 705–10
98. Wilner B. 1988. *J. Mech. Phys. Solids* 36: 141–65
99. Auger JP, Francois D. 1977. *Int. J. Fract.* 13: 431–41
100. Margevicius RW, Lewandowski JJ. 1993. *Acta Metall. Mater.* 41: 485–96
101. Vasudevan AK, Richmond O, Zok F, Embury JD. 1989. *Mater. Sci. Eng.* A107: 63–69
102. Tvergaard V. 1990. *Acta Metall.* 38: 185–94
103. Davidson DL. 1991. *Metall. Trans.* 22A: 113–23
104. Lewandowski JJ, Liu C, Hunt WH Jr. 1989. *Mater. Sci. Eng.* A107: 241–55
105. Manoharan M, Lewandowski JJ. 1990. *Acta Metall. Mater.* 38: 489–96
106. Singh PM, Lewandowski JJ. 1993. *Metall. Trans.* 24A: 2531–43
107. Arsenault RJ. 1993. *Composite Materials Studies in Applied Mechanics*, ed. GZ Voyiadjis, 34: 219. Amsterdam: Elsevier
108. Jagannadham K, Wilsdorf HGF. 1986. *Mater. Sci. Eng.* 81: 273–92
109. Jones RH, Lavender CA, Smith MT. 1987. *Scripta Metall.* 21: 1565–70
110. Crowe CR, Gray RA, Hasson DF. 1985. *Proc. 5th Int. Conf. Composite Materials (ICCM V)*, ed. WC Harrigan, J Strife, AK Dhingra, pp. 843–66. PA: TMS-AIME
111. Embury JD. 1985. *Metall. Trans.* 16A: 2191–200
112. Rice JR, Tracey DM. 1969. *J. Mech. Phys. Solids* 17: 201–17
113. Whitehouse AF, Clyne TW. 1993. *Acta Metall. Mater.* 41: 1701–11
114. Llorca J, Needleman A, Suresh S. 1991. *Acta Metall. Mater.* 39: 2317–35
115. Gurson AL. 1977. *J. Eng. Mater. Tech.* 99: 2–15
116. Arsenault RJ, Shi N, Feng CR, Wang L. 1991. *Mater. Sci. Eng.* A131: 55–68
117. McHugh PE, Asaro RJ, Shih CF. 1993. *Acta Metall. Mater.* 41: 1461–76
118. McHugh PE, Asaro RJ, Shih CF. 1993. *Acta Metall. Mater.* 41: 1489–99; see also Ref. 16, 51, 117
119. Bolmaro RE, Guerra FM, Kocks UF, Browning RV, Dawson PR, Embury JD, Poole WJ. 1993. *Acta Metall. Mater.* 41: 1893–905
120. Dragone TL, Nix WD. 1991. *Acta Metall. Mater.* 38: 1941–53
121. Wang Z, Chen T-K, Lloyd DJ. 1993. *Metall. Trans.* 24A: 197–207
122. Argon AS, Im J. 1975. *Metall. Trans.* 6A: 825–37

UNIVERSITY OF MARYLAND AT COLLEGE PARK

DEPARTMENT OF MATERIALS AND NUCLEAR ENGINEERING
MATERIALS ENGINEERING

Nov. 30, 1994

Dr. George R. Yoder
Contract No. N00014-94-10118
Office of Naval Research
800 N. Quincy Street
Arlington, VA 22217

Dear Dr. Yoder:

In accordance with the applicable requirements of the contract, we herewith submit two (2) copies of our annual report.

Sincerely,

R.J. Arsenault
Professor and Director
Metallurgical Materials
Laboratory

RJA:wc
cc:
Administrative Contract Officer (1 copy)
Office of Naval Research
800 North Quincy Street
Arlington, VA 22217-5000

Director (1 copy)
Naval Research Laboratory
Code 2627
Washington, DC 20375-5000

Defense Technical Information Center (12 copies)
Bldg. 5, Cameron Station
Alexandria, VA 22314

Ms. E. Crierie (1 copy)
Office of Research Admin. & Advancement
University of Maryland

BUILDING 090 • COLLEGE PARK, MARYLAND 20742-2115 • (301) 405-5211 • FAX: (301) 314-9467